THREE-PHASE GENERATION USING REACTIVE NETWORKS

A Thesis

presented to

the Faculty of California Polytechnic State University

San Luis Obispo

In Partial Fulfillment

of the Requirements for the Degree

Master of Science in Electrical Engineering

by

Tattiana Karina Coleman Davenport

March 2015

COMMITTEE MEMBERSHIP

TITLE:	Three-Phase Generation Using Reactive Networks
AUTHOR:	Tattiana Karina Coleman Davenport
DATE SUBMITTED:	March 2015
COMMITTEE CHAIR:	Vladimir Prodanov, PhD Assistant Professor of Electrical Engineering
COMMITTEE MEMBER:	Dale Dolan, PhD Associate Professor of Electrical Engineering
COMMITTEE MEMBER:	Taufik, PhD Professor of Electrical Engineering

ABSTRACT

Three-Phase Generation Using Reactive Networks

Tattiana Karina Coleman Davenport

Household appliances utilize single-phase motors to perform everyday jobs whether it is to run a fan in an air conditioner or the compressor in a refrigerator. With the movement of the world going "green" and trying to make everything more efficient, it is a logical step to start with the items that we use every day. This can be done by replacing single-phase motors with three-phase motors in household appliances. Three-phase motors are 14% more efficient than single-phase motors when running at full load and typically cost less over a large range of sizes [1]. One major downside of incorporating three-phase motors in household appliance is that three-phase power is not readily available in homes. With the motor replacement, a single to three-phase converter is necessary to convert the single-phase wall power into the required three-phase input of the motor. One option is active conversion, which uses switches and introduces different stages that produce power loss [2]. An alternative solution is passive conversion that utilizes the resistances within the motor windings along with additional capacitors and inductors, which in theory are lossless. This study focuses on three different single to three-phase passive converters to run both wye and delta-connected three-phase induction motors, and a possible third winding configuration that utilizes one of the three converters. There will be an emphasis on proving the equivalency of two converters, one proposed by Stuart Marinus and Michel Malengret [11] and the other by Otto Smith [12]. Sensitivity analysis is performed to study the effects of variation of torque and converter component tolerances on the system.

Keywords: Three-phase, power conversion, reactive networks, single to three-phase conversion

ACKNOWLEDGMENTS

I would like to thank my advisors, Dr. Vladimir Prodanov and Dr. Dale Dolan, who have provided so much support and guidance, not only for my thesis, but in other academic and career related areas. Thank you for starting me off on the right foot into the rest of my life.

This thesis is dedicated to my mother and father, Sherry and James Davenport, of whom I owe all my achievements. Because of their unconditional love and support I have been able to achieve everything that I had my heart set out for. I will never be able to thank you enough.

TABLE OF CONTENTS

Page

LIST OF TABLES

Page

LIST OF FIGURES

Page

Chapter 1: Introduction

Many household appliances utilize single-phase motors to perform their everyday functions, one example being an air conditioner. The output of the single-phase motor can be connected to one of two things: 1) a compressor that pumps coolant through coils that cool the surrounding air or 2) the fan used to circulate the cooled air. With the shift of society becoming more environmentally friendly, a logical solution is to increase the efficiency on appliances that are being used every day. This paper suggests the replacement of single-phase motors with three-phase motors. Three-phase motors are proven to be 14% more efficient than single phase motors when running at full load and typically cost less over a large range of sizes [1].

In current household appliances, the single-phase motors are powered by $120V_{rms}$ AC voltage which can be found in any residence. Three-phase motors require a three-phase power source, of which residences are not furnished with. To successfully perform the motor replacement, a single to three-phase conversion network would need to be included to convert the $120V_{rms}$ single-phase power into the required three-phase power of the motor. Typically this process is done by using active converters which utilize switches and diodes to perform the conversion.

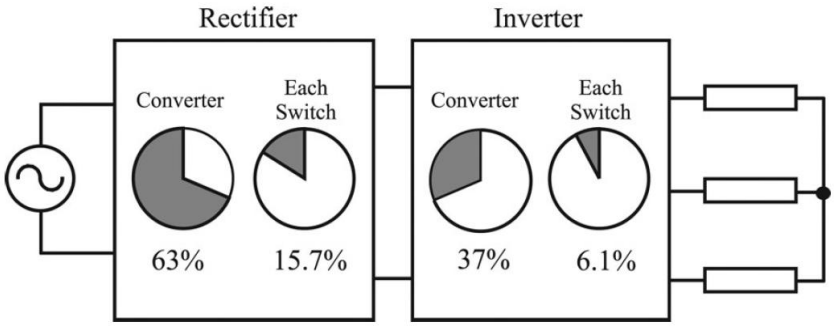

Figure 1: Block diagram of active single to three-phase converter power losses [2]

An active converter, shown in Figure 1, consists of two stages: a rectifying stage and a three-phase inverting stage. The rectifying stage, consisting of diodes, converts the single-phase AC signal into a DC signal. From there, a three-phase inverting stage, consisting of switches, converts the DC signal into a three-phase AC signal. Each stage of the converter exhibits a power loss, 63% for the rectifying stage and 37% for the inverting stage, decreasing the overall efficiency of the system [2].

An alternative solution would be to create a passive converter by using inductors and capacitors along with the resistance within the motor windings to implement the three-phase conversion. If the dynamic components are chosen with high quality factor ratings, then high efficiency can be achieved. The quality factor of dynamic components is the ratio of its reactance over its internal resistance. The lower the resistance is, the higher the quality factor will be. Power loss is due to the internal resistance. Therefore, with increasing quality factor of the dynamic components, the lower the reduction in efficiency on the system. This study focuses on three different single to three-phase passive converters to run both wye and delta-connected three-phase induction motors, and a possible third winding configuration which utilizes one of the three converters. There will be an emphasis on proving the equivalency of two converters, one proposed by Stuart Marinus and Michel Malengret [11] and the other by Otto Smith [12]. Sensitivity analysis is performed to study the effects of variation of torque and converter component tolerances on the system.

1.1 Induction Motors

Before performing the derivation of the converters, here is some background information on the equipment and concepts used to construct and test the passive converters, starting with the induction motor [4]. An induction motor is an AC electric motor that converts electrical power into mechanical power and is made up of two parts, a stator and a rotor, shown in Figure 2. The exterior part of the motor is called the stator. The stator is an iron core of a cylindrical shape that is laminated with slots where the three-phase windings are placed. The ends of the windings are then connected in either a wye or delta configurations. The input AC current creates a rotating magnetic field within the stator inducing currents in the conductor of the rotor. The rotor, in this case, is a squirrel-cage winding consisting of bars embedded in the rotor slots and shorted at both ends by end rings. The interaction between the induced current and the rotating magnetic field produces a torque that causes the rotor to turn, producing a mechanical output power in terms of speed and torque.

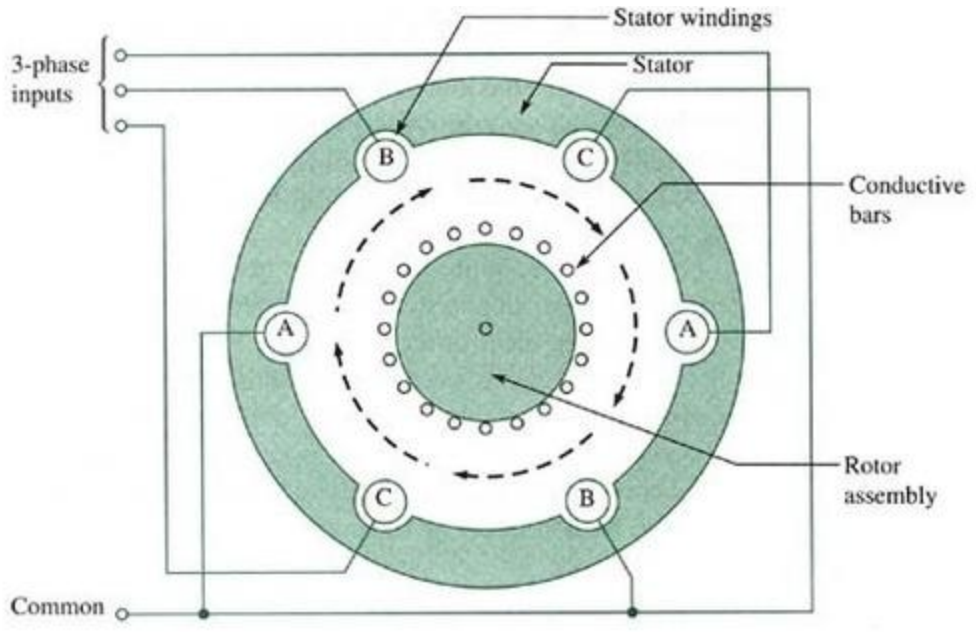

Figure 2: Cross-sectional diagram of a three-phase induction motor with 2-poles [3]

Induction motors come in two different phase modes: single-phase and three-phase. Single-phase motors use a single alternating current and voltage whereas three-phase motors use three alternating currents and voltages that are all out of phase by 120˚. Within the three-phase motor, there are three separate windings that are electrically spaced apart by 120˚. This induces a torque in the rotor that causes the rotor to constantly "chase" the stator magnetic field to try and align with it. With three-phase power, the supply is never able to drop to zero. This makes it possible to provide a more constant power, whereas the single phase the power is at zero three different times during one cycle [5]. Due to the more constant of power, three-phase power makes it easier to start the motor and provide a better starting torque.

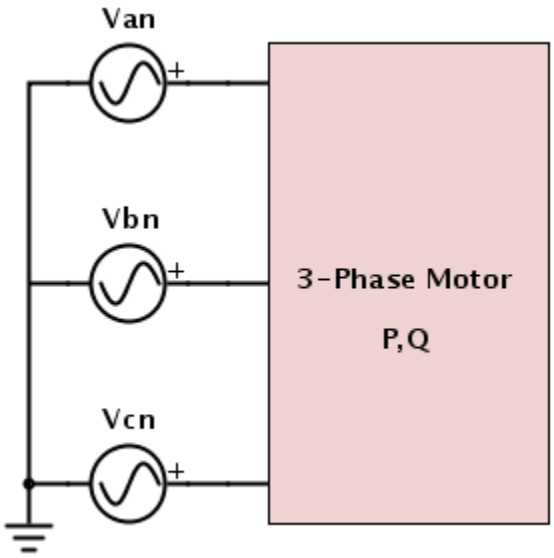

Figure 3: Block diagram of three-phase induction motor

The top level diagram of a three-phase system is shown in Figure 3. The three-phase input consists of three voltages, V_{an}, V_{bn} and V_{cn}, all with the same amplitude value but each out of phase by 120˚. Looking at the system at a lower level, there are two possible winding configurations. The most common is the wye configuration, shown in

Figure 4. There are three lines connected from the source to the motor, and a neutral point where the windings are connected to each other. The three-phase input voltages are applied to the three windings and cause a flow of current. The summation of the three phase currents should equal zero if they are equal in magnitude and perfectly separated by 120˚. If there is any imbalance, the summation of the current will not equal zero and the neutral provides a return path to the source for the extra current. As the torque of the motor changes within the motor, the impedance and the current of each winding changes.

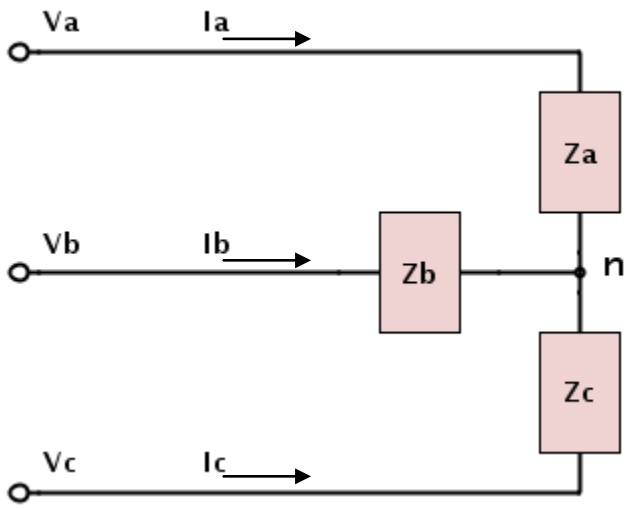

Figure 4: Block diagram of wye-connected three-phase induction motor windings

There are two forms of three-phase voltage and current for a wye-connected motor. The first form is phase voltage, having a magnitude of the voltage across the winding impedance, which is the source voltage in reference to the neutral point of the motor. The reference voltage has a phase of 0˚, and the other two voltages are out of phase by ±120˚. This relationship can be seen in Figure 5, plotting the voltage vectors on an imaginary versus phase plot.

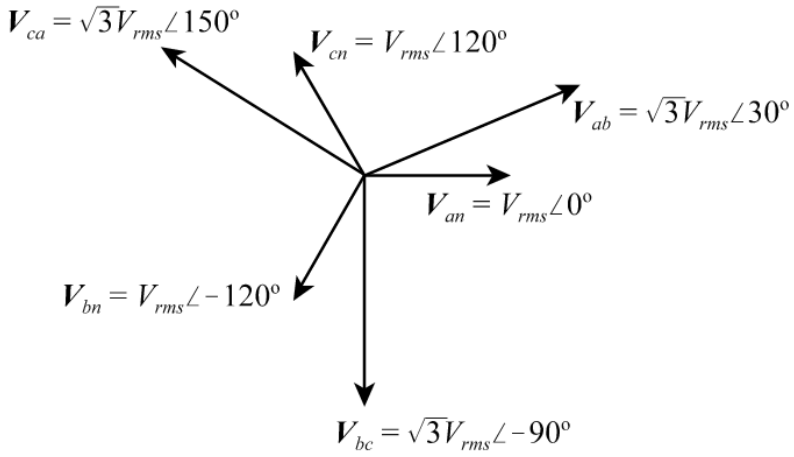

Figure 5: Phase and line voltage phasor diagram of a wye-connected three-phase induction motor [6]

The second form of voltage is in terms of line-to-line which is the difference between two phase voltages. By subtracting V_{bn} from V_{an}, the resulting voltage, V_{ab}, is $\sqrt{3}$ times larger in magnitude than the phase voltage. The same method is used to calculate the V_{bc} and V_{ca} line-to-line voltages. The line current of the wye-connected system is equal to the phase current.

The second winding configuration of the motor is the delta connection shown in Figure 6. This system also uses the phase and line form of the voltage and current. In this case, the line voltage is equivalent to the phase voltage, because the line-to-line voltage, V_{ab}, is equal to the phase voltage across the winding. The line and phase currents, on the other hand, are not equivalent.

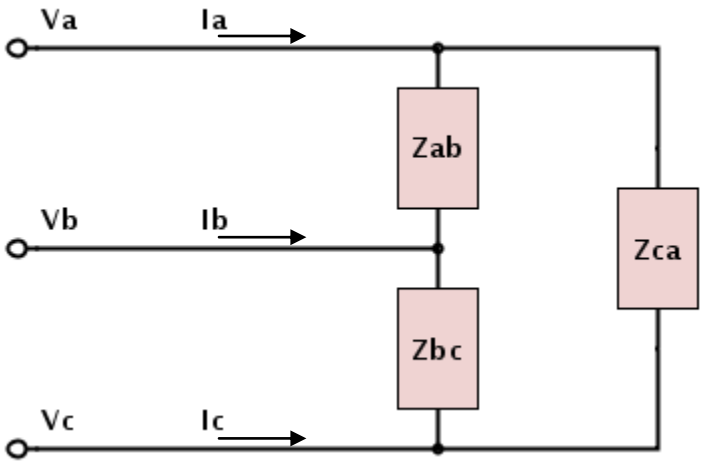

Figure 6: Block diagram of delta-connected three-phase induction motor windings

The line current entering into the motor has the magnitude of the source current, out of phase by 120˚. When it enters the motor, it splits into the two directions creating the phase current, flowing through the windings. The magnitude of the phase current is √3 times smaller and leads the line current by 30˚, shown in Figure 7.

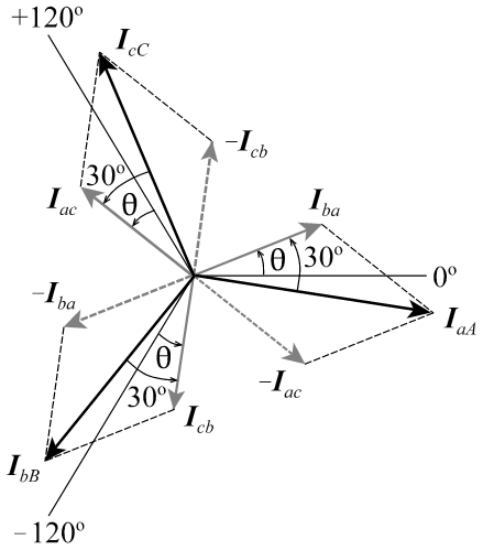

Figure 7: Phase and line voltage phasor diagram of delta-connected three-phase induction motor [6]

The entire system of an induction motor can be characterized by its input voltage (V_{in}), input current (I_{in}), real input power (P_{in}), reactive input power (Q_{in}), power factor (pf), speed (n), and torque (T). The reactive power is due to the imaginary impedance element in the load, which is this case is the inductance of the winding. The real power is due to the real component of the load, which is the resistance of the motor winding.

Figure 8 displays the characteristics of the real and reactive input power for an induction motor in reference of the torque that is introduced to the system. This is the experimental data for a 1/3hp, three-phase induction motor with full load properties of $208V_{LL}$, 1725rpm and 1.4A. The relationship in Figure 8 shows that as the torque increases from no load, the reactive power stays relatively constant whereas the real power increases linearly. The dip is due to experimental error and should be in line with the linear relationship.

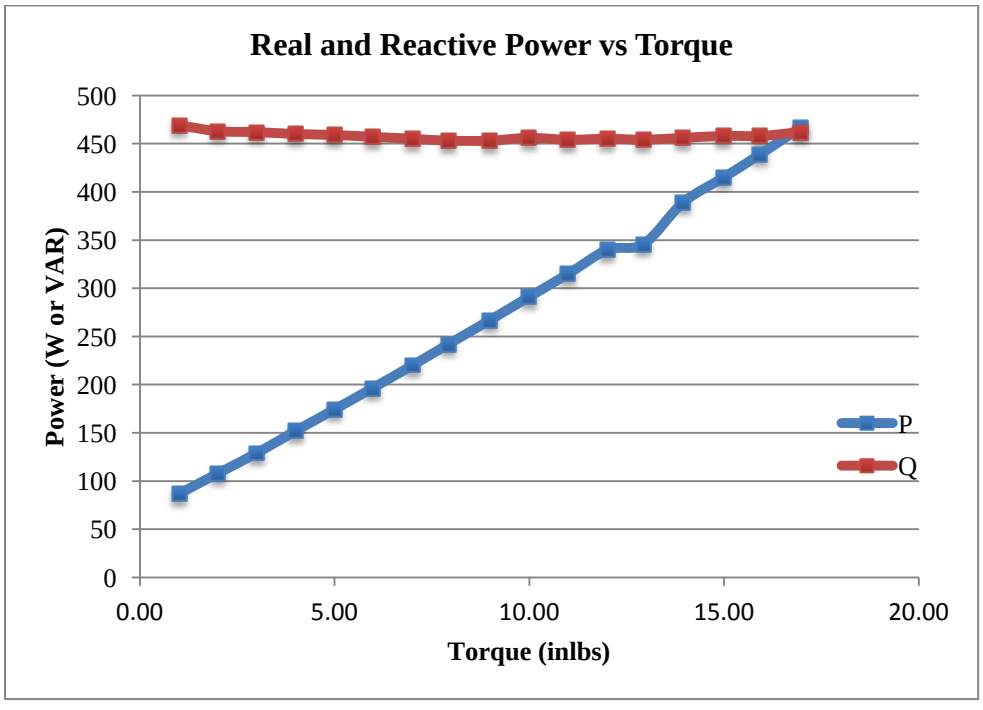

Figure 8: Real (P) and reactive (Q) power versus torque of a 1/3HP three-phase induction motor

1.1.1 Winding Models

The equivalent circuit model for an induction motor, shown in Figure 9, follows the IEEE Standard 112 [7]. The stator resistance and reactance correspond with R_1 and X_1, and the rotor resistance and reactance correspond with R_2 and X_2. The mutual inductance of the stator and the rotor is depicted as X_m. The core resistance, R_c, can typically be neglected when it is much larger than the mutual inductance, causing the parallel combination equal the mutual reactance.

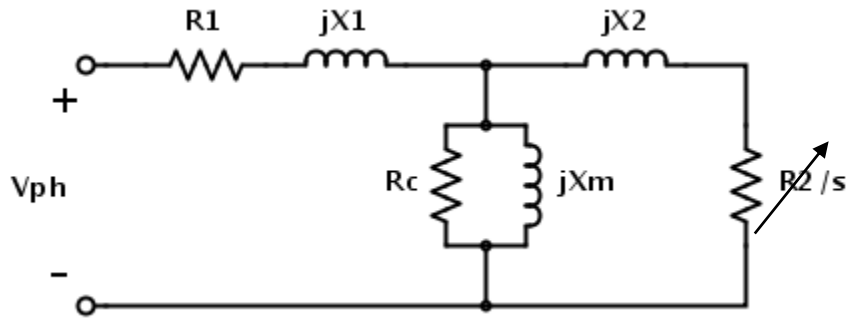

Figure 9: IEEE standard equivalent circuit of a three-phase induction motor winding

The "s" in the denominator of the rotor resistance corresponds to relative motion between the rotor and the stator called the slip. To understand the affect of the slip on the equivalent circuit it is important to know how the torque changes with the loading of the motor. At first the motor is operating at no load, running close to the speed of the magnetic field called the synchronous speed. The net magnetic field in the machine is produced by the magnetization current flowing through the motors equivalent circuit. The magnetization current and field is proportional to the induced voltage on the rotor side of the air gap between the stator and the rotor. If the induced voltage is held constant then the magnetic field is held constant. As the load varies on the motor, the induced voltage changes because of the stator impedances cause varying voltage drops with the load.

Since the voltage drops are relatively small, the rotor induced voltage remains almost constant with varying loads.

At no load, the rotor slip is very small so the relative motion of the rotor and the magnetic fields, and rotor frequency is also small. Due to the slow relative motion, the induced voltage in the rotor's cage and resulting current is very small. Since the rotor's reactance is also small, the maximum rotor current is almost in phase with the rotor's induced voltage, producing a very small rotor magnetic field with a phase slightly greater than the 90˚ behind the total magnetic field of the system. This means that the magnetic field on the stator side must be very large to be able to supply the full magnetic field. Since the current is directly related to the magnetic field, the stator current is very large at no load. The induced torque of the rotor is the cross product between the total and rotor's magnetic field, resulting in a very small torque due to the small magnetic field in the rotor but it is large enough to overcome the rotational losses and turn the rotor.

As the load on the motor increases the motor speed falls. Since the motor speed decreases, there is more relative motion between the rotor and the stator, increasing the slip. The greater relative motion also produces a stronger rotor voltage and in turn increases the rotor current. With a larger rotor current, the magnetic field of the rotor increases, increasing the induced torque of the rotor. This is why it is suggested that the slip of the motor to stay under 5%, otherwise the increase in current will be too high causing power loss and heating of the windings possibly damaging the system.

To obtain the equivalent circuit components three tests must be performed: No Load, DC and Locked Rotor. The no load test measures the rotational losses of the motor

and provides information about the magnetization current when the motor is not loaded. The equivalent circuit reduces to R_1, X_1 and X_m in series. This test solves for X_m because R_1 and X_1 can be found in the other two tests. The DC test is used to measure R_1. A DC voltage is applied to the stator windings of the induction motor and because the current is DC, there is not induced voltage on the rotor, resulting in no current flow into the rotor. The reactance of the motor is also zero at direct current. Therefore, the current will nice flow through the stator resistor.

The locked rotor test locks the rotor so it can't move. An AC voltage is applied to the stator and the current is adjusted to be approximately full-load. At this point the voltage, current and power is measured. The slip is set equal to 1, preventing the rotor from turning. R_2 and X_2 are so small that almost all the input current is flowing through them instead of through X_m. Therefore, the equivalent circuit under this test looks like R_1, X_1, R_2 and X_2 in series. Since R_1 is measured in the DC test and X_1 is equivalent to X_2 for Class A induction motor, this concludes the equivalent circuit derivation.

Figure 10 is the fully reduced equivalent circuit model of Figure 9 for a wye-connected motor following the IEEE standard.

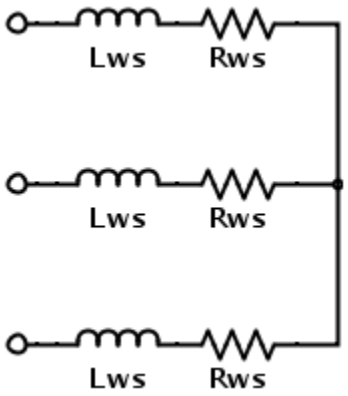

Figure 10: Reduced equivalent circuit of a wye-connected three-phase induction motor winding

Another method to calculate the fully reduced equivalent circuit is from the measured real and reactive input power of the motor. Each motor winding has equivalent properties leading to even distribution of real and reactive powers through each winding from the total input power. To obtain the real and reactive input power for each winding, divide each total input power by three.

$$Q_A = Q_B = Q_C = \frac{1}{3} Q_{IN_{TOTAL}}$$

$$P_A = P_B = P_C = \frac{1}{3} P_{IN_{TOTAL}}$$

By using the input phase voltage or line current, the reactance (X_{LWS}) and resistance (R_{WS}) of each winding can be calculated by using the equations below.

$$X_{LWS} = \frac{Q}{I_{RMS}^2} = \frac{V_{RMS}^2}{Q}$$

$$R_{WS} = \frac{P}{I_{RMS}^2} = \frac{V_{RMS}^2}{P}$$

1.1.2 Series-to-Parallel Winding Component Transformation

As discussed previously, the current through each winding changes as the torque is increased. Therefore, when solving for the impedances for the series winding components, both the inductance and resistance values change with the varying current.

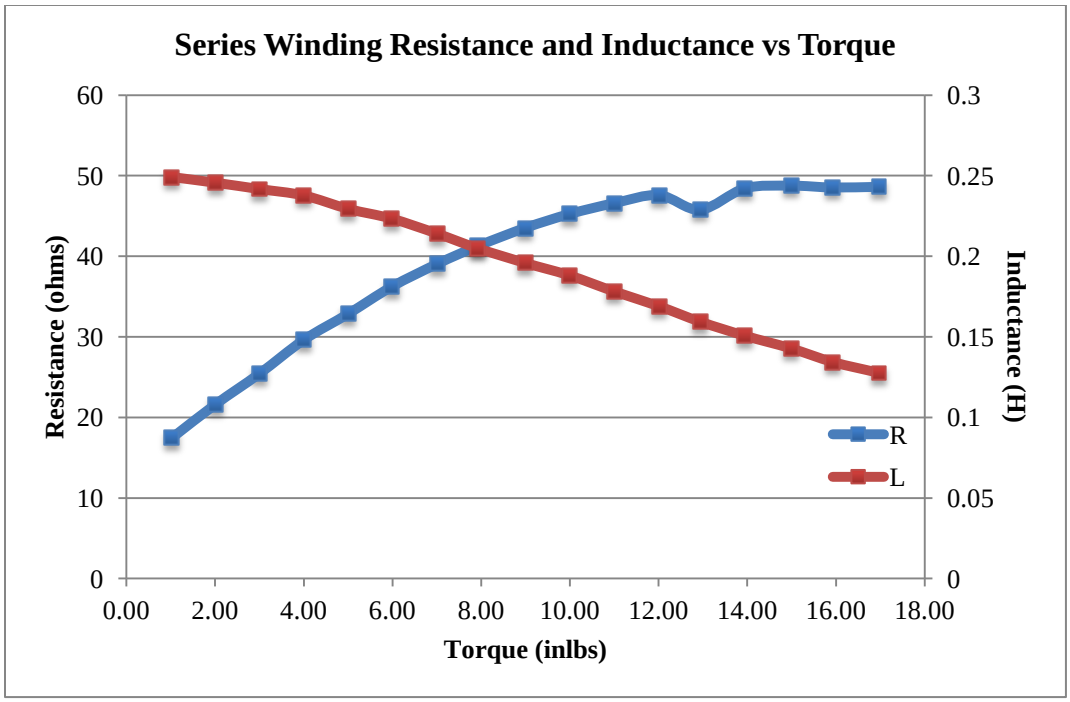

Figure 11: Series winding resistance and inductance vs torque of 1/3HP three-phase induction motor

In referencing the previous equations, if the reactive power remains constants in Figure 8 and the torque increases while the current increases, then the reactance value will in turn decrease at somewhat of a linear rate. Figure 11 displays this relationship. Now, when analyzing the resistance equation on the previous page, as the torque increases due to the increasing current, the input power also increases. But the power will increase at such a higher rate, so the resistance will also increase. This relationship is verified in the experimental data shown in Figure 11. Another way to model the inductance and reactance within each winding is in parallel, shown in Figure 12.

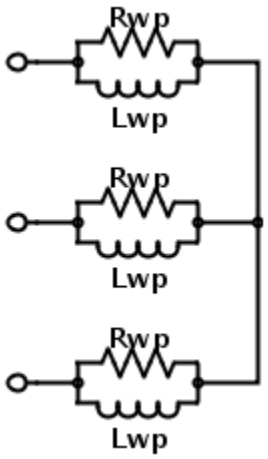

Figure 12: Wye-connected motor with parallel resistive and inductive windings

The following equations perform the series-to-parallel transformation using the series quality factor (Q_s) and the series component values:

$$R_{WP} = (1 + Q_S^2)R_{WS}$$
$$L_{WP} = \left(1 + \frac{1}{Q_S^2}\right)L_{WS}$$

Where,

$$Q_S = \frac{2\pi f L_{WS}}{R_{WS}}$$

Since the relationship between the torque and inductance are inversely proportional, the quality factor decreases due to the change in resistance being larger than the change in inductance. Referencing the parallel winding resistance (R_{WP}) in the equation above, as the quality factor decreases, the resulting winding resistance will also decrease. For the parallel winding inductance (L_{WP}) equation, the quality factor is decreasing, increasing the scaling term of the series winding inductance at the same rate as the winding inductance decreases. This keeps the parallel winding inductance almost constant. This is understandable because as the resistance decreases, it pulls more current

through its branch, leaving a constant current to go through the inductor. This relationship is verified using the experimental data shown in Figure 13.

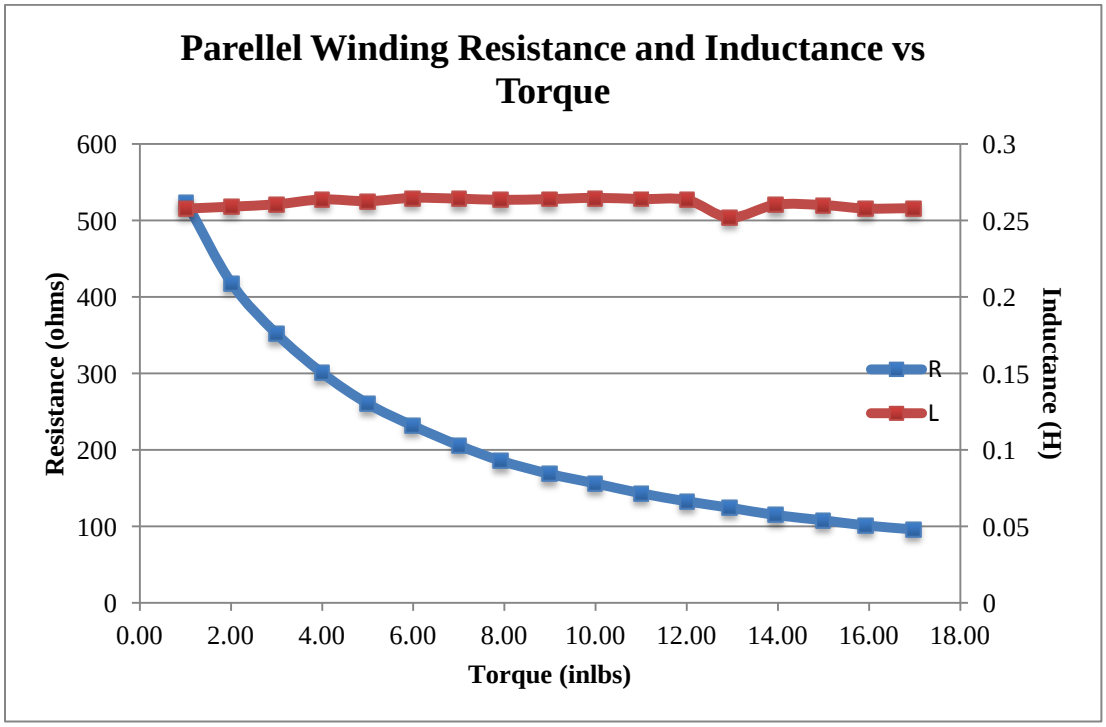

Figure 13: Parallel winding resistance and inductance vs torque of 1/3HP three-phase motor

This proves to be a good spice modeling technique to analyze the change in torque of the motor since there is only one component value that is varying. With the parallel winding model, the change in torque of the motor can be related with the change in resistance, creating a user friendly model for computer simulation of an induction motor. With the series component motor winding, both components would need to vary simultaneously making the model of the motor more complex.

1.1.3 Wye-to-Delta Motor Winding Transformation

An alternate way of modeling an induction motor is the orientation in which each of the windings is connected with the other two windings. This is referred to as a delta

configuration. Below are the equations used to transform a wye-connected motor into a delta-connected motor.

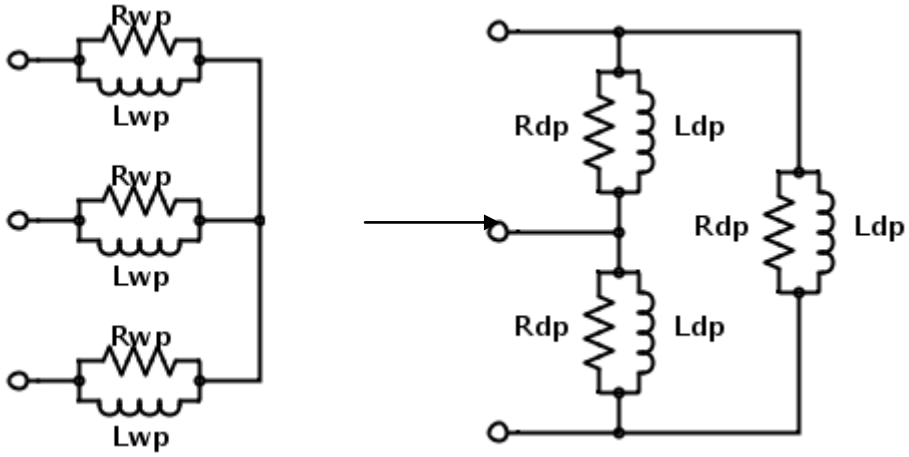

Figure 14: Wye-to-delta transformation of parallel resistive and inductive induction motor windings

$$X_{\mathrm{DP}} = \frac{X_{WP1}X_{WP2} + X_{WP1}X_{WP3} + X_{WP2}X_{WP3}}{X_{WP1}}$$

$$X_{\mathrm{DP}} = 3X_{WP}$$

$$X_{\mathrm{DP}} = 3(R_{WP} + jX_{LWP})$$

By using the delta configuration, it is easier to power factor correct the motor. In power factor correction, capacitors are added in parallel to each winding. Since capacitors are opposite in polarity with inductors it reduces the inductance of the winding down to zero and in turn reduces the reactive power down to zero. This is valuable because it will require less power from the source, only transferring real power to the load.

1.2 Passive Single to Three-Phase Conversion Topologies

There are three passive single to three-phase conversion topologies that will be analyzed in this study. They are referenced as the Cal Poly (CP) converter, Marinus/Malengret converter and the Smith converter. The first two were discovered for

a previous study to design a high efficiency portable air conditioner, which was sponsored by Lawrence Berkeley National Labs and the Department of Energy [8]. The third conversion network, proposed by an inventor Otto Smith, shows similarities in voltage characteristics and motor connections to the Marinus/Malengret converter. Due to these similarities, this thesis will attempt to prove the equivalency of the two motors.

1.2.1 Cal Poly Converter

The first single to three-phase conversion network is called the Cal Poly converter and is named after California Polytechnic State University in San Luis Obipso, where the design was developed [8]. The network consists of four conversion components for a wye-connected three-phase induction motor, shown in Figure 15. One of the windings is connected straight to single-phase input and acts as the reference voltage with the 0˚ phase shift. The next two branches contain a reactive phase shifting network that are opposite in polarity, producing the +120˚ and -120˚ phase shift. Since the phase shifting networks utilizes the resistance within the motor windings, the motor modeled in Figure 15 is power factor corrected, leaving the windings purely resistive (R_{Load}).

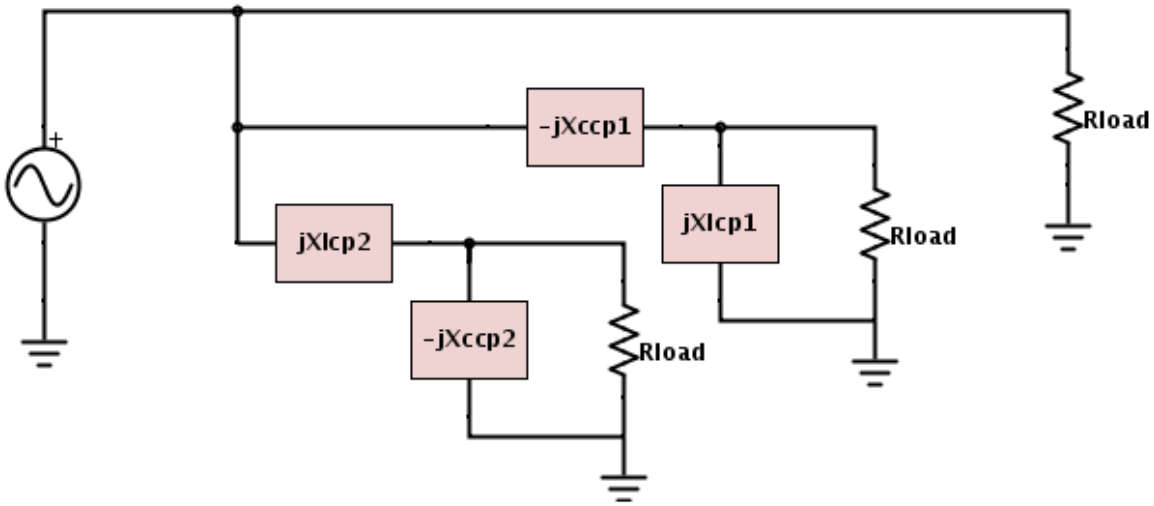

Figure 15: Cal Poly single to three-phase power converter diagram

When LC networks are present on their own, they introduce a phase shift of 180˚ as demonstrated by the below transfer function. The LC network behaves as a voltage divider and inverter if the magnitude of the capacitor's reactance is larger than the inductor's.

$$V_{out} = -\frac{jX_C}{jX_L - jX_C}V_{in} = -\frac{jX_C}{j(X_L - X_C)}V_{in} = -\frac{X_C}{X_L - X_C}V_{in}$$

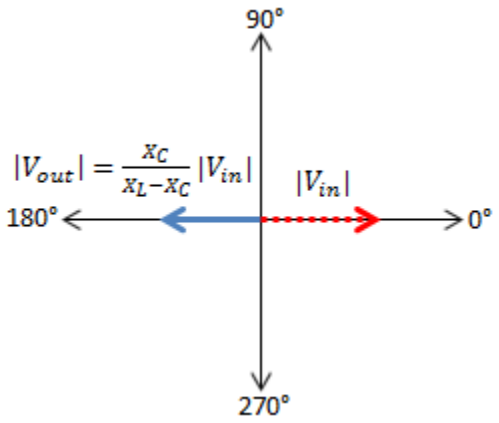

Figure 16: Phase conversion results of LC network

Each branch of the conversion network is derived individually and utilizes its transfer function to derive the components. Figure 17 displays the top branch, which introduces the +120˚ phase shift.

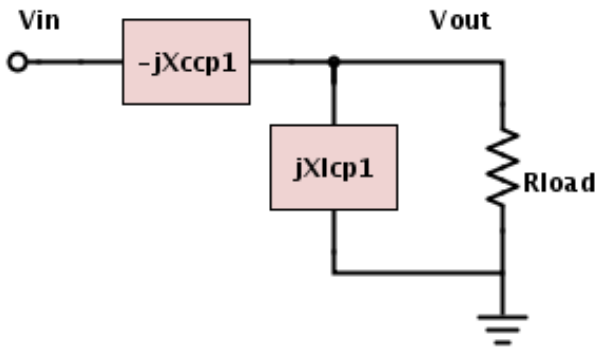

Figure 17: +120˚ phase shifting branch of Cal Poly converter

The transfer function of the Figure 17 consists of the output voltage over the input voltage of the branch. Since the current going through the capacitor is the same as the current going through the parallel combination of the inductor and resistor, we can reduce the transfer function in terms of the output impedance over the total impedance of the circuit.

$$V_{out} = \frac{\frac{(R_{Load})(jX_{LCP1})}{R_{Load}+jX_{LCP1}}}{\frac{(R_{Load})(jX_{LCP1})}{R_{Load}+jX_{LCP1}} - jX_{CCP1}} V_{in} = \frac{jX_{LCP1}R_{Load}}{X_{LCP1}X_{CCP1} + jR_{Load}(X_{LCP1} - X_{CCP1})} V_{in}$$

$$= \frac{j}{\frac{X_{CCP1}}{R_{Load}} + j\left(1 - \frac{X_{CCP1}}{X_{LCP1}}\right)} V_{in}$$

By reducing the equation further, a "j" component is left in the numerator and a complex relationship in the denominator. The "j" component in the numerator introduces a +90˚ phase shift, therefore to achieve the full +120˚ phase shift the denominator needs to experience a -30˚ phase shift. By setting the denominator equal to the complex rectangular form of -30˚ and matching the real and imaginary coefficients from both sides of the equation, we can derive the value of each conversion component in terms of the resistance within the motor winding.

$$\frac{X_{CCP1}}{R_{Load}} + j\left(1 - \frac{X_{CCP1}}{X_{LCP1}}\right) = \cos(30°) - \mathrm{j}\sin(30°) = \frac{\sqrt{3}}{2} - j\frac{1}{2}$$

$$X_{CCP1} = \frac{\sqrt{3}}{2} R_{Load}$$

$$X_{LCP1} = \frac{1}{\sqrt{3}} R_{Load}$$

The same method is performed on Figure 18, the bottom branch of the conversion network which introduces the -120˚.

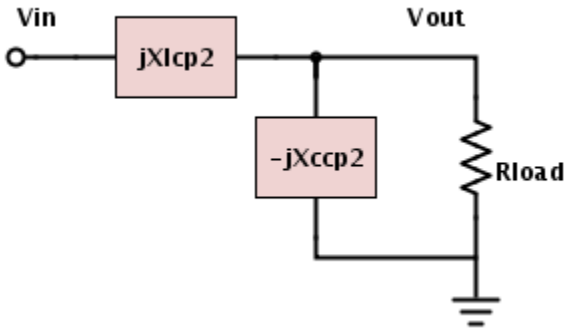

Figure 18: -120˚ phase shifting branch of Cal Poly Converter

$$V_{out} = \frac{\frac{(R_{Load})(-jX_{CCP2})}{R_{Load} - jX_{CCP2}}}{\frac{(R_{Load})(-jX_{CCP2})}{R_{Load} - jX_{CCP2}} + jX_{LCP2}} V_{in} = \frac{-jX_{CCP2}R_{Load}}{X_{LCP2}X_{CCP2} + jR_{Load}(X_{LCP2} - X_{CCP2})} V_{in}$$

$$= \frac{-j}{\frac{X_{LCP2}}{R_{Load}} + j\left(\frac{X_{LCP2}}{X_{CCP2}} - 1\right)} V_{in}$$

In this case, the reduced equation contains a "-j" component in the numerator, introducing a -90˚ phase shift. To achieve the full -120˚ phase shift for the branch, it is necessary for the complex relationship in the denominator to have a +30˚ phase shift. By setting the denominator equal to the complex rectangular form of +30˚ and matching the real and imaginary coefficients from both sides of the equation, each conversion component can be derived in terms of the resistance within the motor winding.

$$X_{LCP2} = \frac{\sqrt{3}}{2} R_{Load}$$

$$X_{CCP2} = \frac{1}{\sqrt{3}} R_{Load}$$

1.2.2 Marinus/Malengret Converter

The second single to three-phase conversion network is called the Marinus/Malengret (MM) converter. It is referenced after the authors of an IEEE article in which Stuart Marinus and Michel Malangret proposed the design [11]. The network

uses a delta connected induction motor with two conversion components, one capacitor and one inductor. Referencing the network displayed Figure 19, both of the conversion components are placed across the main winding and supply, with each individual component connected in parallel with the other two windings. The motor is power factor corrected, leaving the windings purely resistive. The conversion network is displayed on the left hand side of Figure 19 and the power factor corrected motor is on the right hand side.

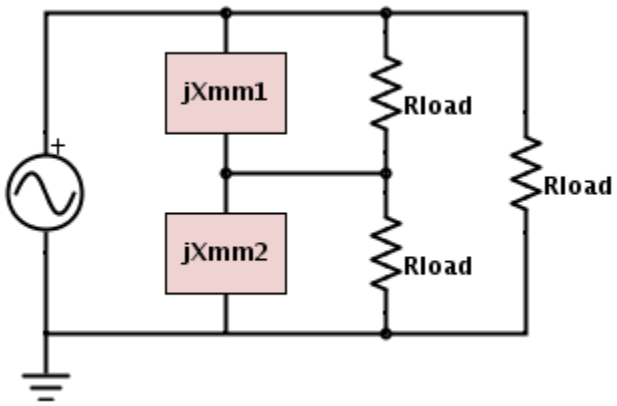

Figure 19: Block diagram of Marinus/Malengret converter and power factor corrected motor

The approach to derive the Marinus/Malengret converter components involves combining the inductor and capacitor with their parallel winding resistance and using the current relationship through that line. The combined impedance is displayed below in Figure 20.

$$Z_{TMM1} = \frac{R_{Load} \cdot jX_{MM1}}{R_{Load} + jX_{MM1}}$$

$$Z_{TMM2} = \frac{R_{Load} \cdot jX_{MM2}}{R_{Load} + jX_{MM2}}$$

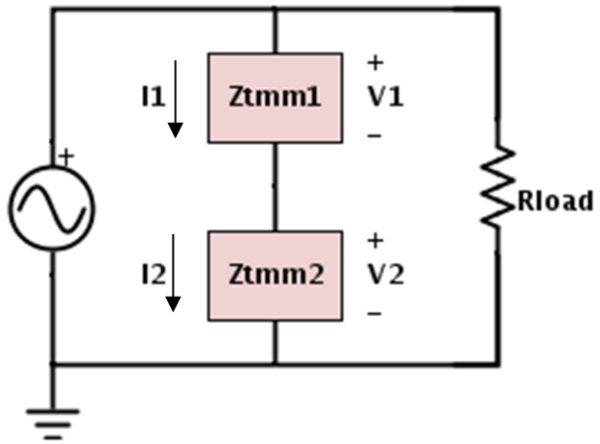

Figure 20: Reduced Marinus/Malengret converter and power factor corrected motor

The voltage across the bottom impedance (V_2) is 120˚ out phase with the top voltage (V_1). For derivation purposes the voltages have unity amplitude, since the phase shift should take place no matter the value of the amplitude of the signal.

$$V_1 = 1\angle 0^\circ = 1 + j0$$

$$V_2 = 1\angle 120^\circ = \cos(120^\circ) + jsin(120^\circ) = -\frac{1}{2} + j\frac{\sqrt{3}}{2}$$

Using the relationship that the current through the top impedance is equivalent to the current going through the bottom impedance, we can substitute the above equations into the equations below to derive the conversion component values.

$$i_1 = i_2$$

$$\frac{V_1}{Z_{TMM1}} = \frac{V_2}{Z_{TMM2}}$$

$$(1 + j0)\left(\frac{R_{Load} + jX_{MM1}}{R_{Load} \cdot jX_{MM1}}\right) = \left(-\frac{1}{2} + j\frac{\sqrt{3}}{2}\right)\left(\frac{R_{Load} + jX_{MM2}}{R_{Load} \cdot jX_{MM2}}\right)$$

This equation can be further reduced, producing an equation that contains the inverse of each component. By recognizing that the inverse of resistance is conductance

(G) and the inverse of reactance is susceptance (B), we can make those substitutions and more easily derive the conversion components.

$$(1 + j0)\left(\frac{1}{R_{Load}} + \frac{1}{jX_{MM1}}\right) = \left(-\frac{1}{2} + j\frac{\sqrt{3}}{2}\right)\left(\frac{1}{R_{Load}} + \frac{1}{jX_{MM2}}\right)$$

$$(1 + j0)(G_{Load} - jB_{MM1}) = \left(-\frac{1}{2} + j\frac{\sqrt{3}}{2}\right)(G_{Load} - jB_{MM2})$$

By matching the real and imaginary parts of each side, the two following equations are produced:

$$\sqrt{3}G_{Load} - B_{MM2} = 0$$

$$2B_{MM1} + B_{MM2} + \sqrt{3}G_{Load} = 0$$

By adding the two equations together, we get the equation below, which can be fully reduced into terms of the conductance.

$$2B_{MM1} + 2\sqrt{3}G_{Load} = 0$$

$$\therefore B_{MM1} = -\sqrt{3}G_{Load}$$

The same can be done by subtracting the equations. This time it is reduced down to a relationship between the susceptances, and then a relationship between the conversion component reactances. The resulting relationship shows that the two reactances are opposite in polarity verifying the use of a capacitor and an inductor in the conversion network.

$$-2B_{MM1} - 2B_{MM2} = 0$$

$$\therefore B_{MM1} = -B_{MM2}$$

$$X_{MM2} = -X_{MM1}$$

By converting the suspectance and conductance back into reactance and resistance and making the substitutions into the above equation, the final derivation of the conversion component values is possible. The values are shown in the equations below.

$$X_{MM1} = \frac{1}{\sqrt{3}} R_{Load}$$

$$X_{MM2} = -\frac{1}{\sqrt{3}} R_{Load}$$

1.3 Otto Smith Converter

The third conversion circuit is called the Smith converter. This converter is named after its inventor Otto Smith and he received a patent for this design in 1994 [12]. Smith has done extensive research related to solar generators, wind generators and high efficiency motors. He has received 15 patents for devices that generate or conserve energy. The Smith converter was designed for a standard three-phase induction motor. Two of the motor windings are connected across a single phase power supply, and a center-tapped autotransformer is connected between the second and third motor winding. A diagram of the Smith conversion network with a three-phase motor is shown in Figure 21.

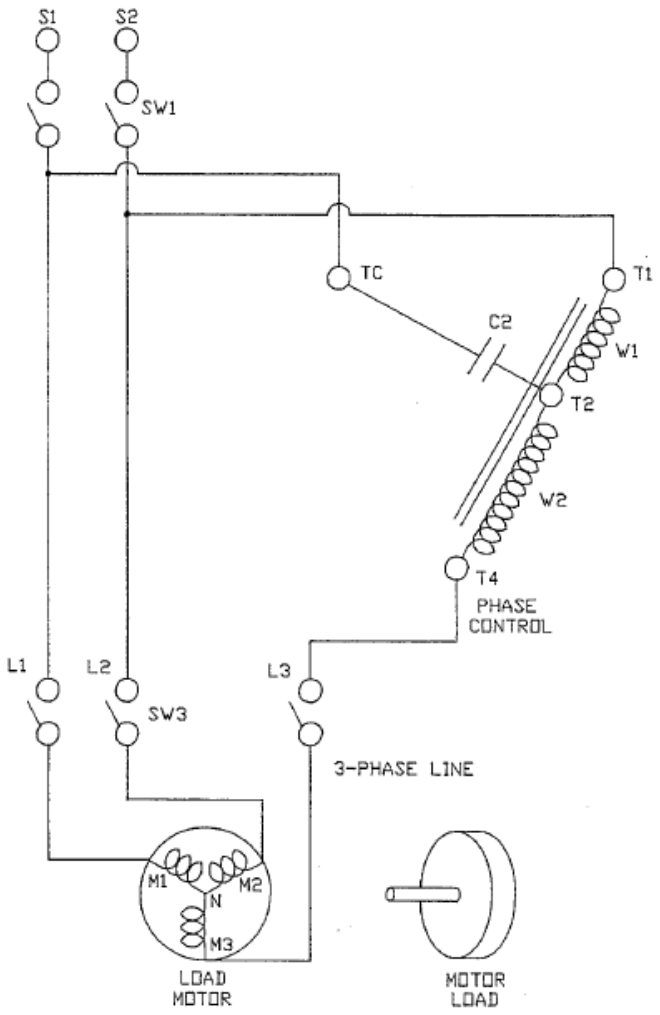

Figure 21: Single to three-phase power converter proposed by Otto Smith with a three-phase induction motor [12]

The capacitor (C2) provides a current consisting of a suitable phase angle for the third motor winding by being between the center tap and the first motor winding (M1). The value of it is chosen such that at a preselected full load, the magnitude of the voltage between the second motor winding (M2) and the third motor winding (M3) across the transformer from points T1 to T4, is approximately equal to the absolute value of the supply voltage.

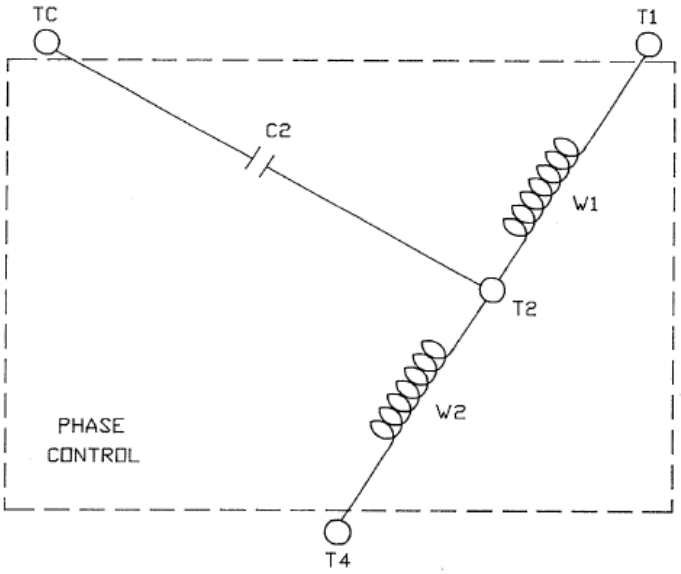

Figure 22: Single to three-phase power converter proposed by Otto Smith [12]

The voltage from TC to T1 is the applied voltage with magnitude of the supply and reference angle of 0˚. The voltage from T1 to T2 is the voltage across the top side of the tapped auto-transformer (W1), lagging the reference voltage by 120˚. The voltage from T2 to T4, the bottom side of the auto-transformer (W2), also lags the reference voltage by 120˚. Each voltage magnitude is half of the supply and after the addition of the phasors the resulting phase shift is -120˚. The voltage across C2 lags the reference voltage by 30˚ when the autotransformer is center-tapped, meaning the step-down turns ratio (R=1/N) is one-half, with N being the step-down turns ratio of the transformer winding. The phase of the capacitance voltage is calculated from the following equation:

$$\theta = \tan^{-1}\left(\frac{R\sqrt{3}}{2-R}\right)$$

Capacitors cause current to lead voltage by 90˚ therefore the current through C2 is going to lead the voltage by 60˚. These relationships are shown in the bode plot in

Figure 23. By closing the triangle in the bode plot, the resulting phasor of T4 to TC is leading the input by 120˚, providing the third phase of +120˚.

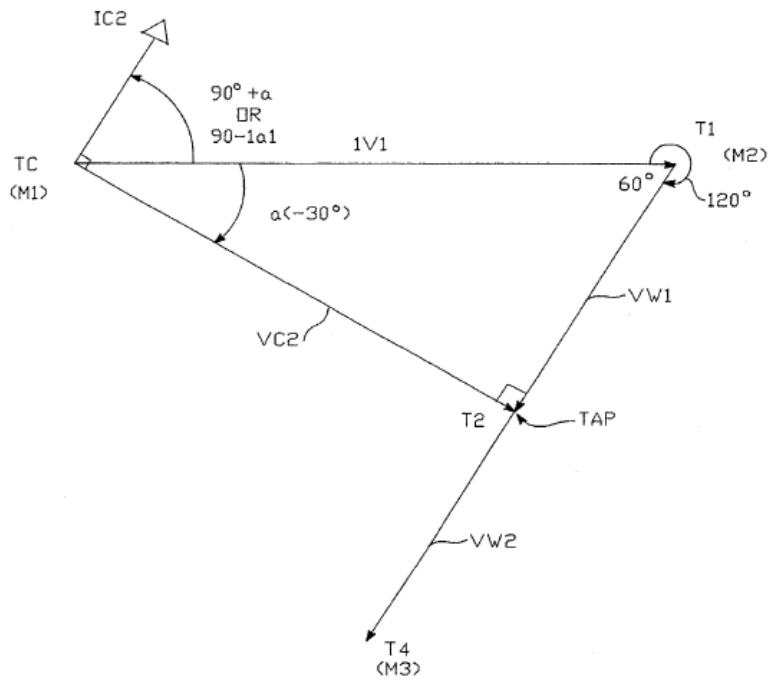

Figure 23: Current and Voltage phasor diagram of Otto Smith's conversion network [12]

This conversion can also be performed using a two winding or multiple winding transformer in place of the center-tapped autotransformer, shown in Figure 24. The winding between T2 and T1 has the same voltage as W1 and the same current from C2, as in the auto-transformer design. The voltage of the secondary winding, from T1 to T4, has the same magnitude as the input voltage with a lagging phase angle of 120˚, same as W2 from the previous design. The step-down ratio still equals the inverse of the step-down ratio of the transformer winding, thus the two winding transformer has an effective center-tap or, in more general terms, an intermediate tap as in an autotransformer.

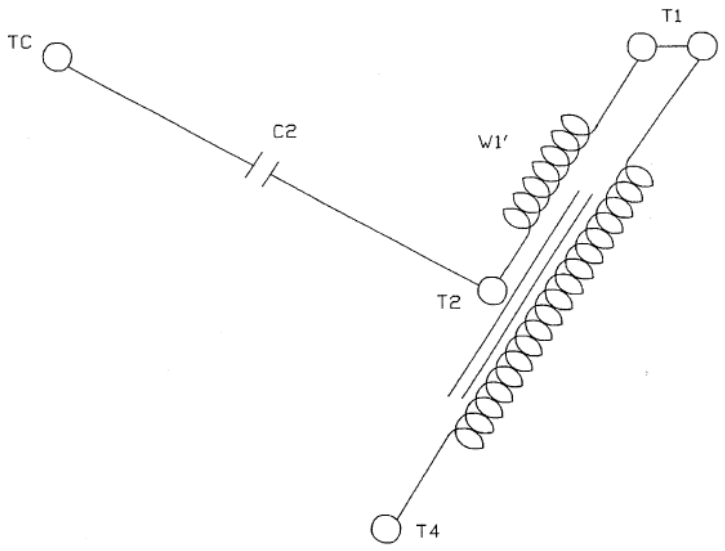

Figure 24: Alternate conversion network proposed by Otto Smith utilizing a two winding transformer [12]

1.4 Derivation of Marinus/Malengret Converter from Induction Motor

To begin the derivation of the values of the Marinus/Malengret converter components, the motor characteristics at the operating load is needed.

Table 1 is the data from a motor loading test from no load to full load. The rotor's speed (n_r), input line-to-line RMS voltage ($V_{L\text{-}L}$), RMS line current (I_L), input real power (P_{in}) and input reactive power (Q_{in}) were collected as the torque (T) increased from 1 in-lbs to 17 in-lbs for a 1/3 HP three-phase induction motor. The 12in-lbs operating torque is calculated by using the equation below.

$$T_{inlbs} = \frac{P_{HP} \cdot 63024}{n_{RPM}}$$

Table 1: Measurement results of 1/3HP three-phase induction motor

T [inlbs]	n_r [RPM]	V_{L-L} [V]	I_L [A]	P_{in}[W]	Q_{in} [VAR]
0.00	1797	210.6	1.290	77.8	471
1.02	1795	210.7	1.290	87.1	469
2.01	1791	210.7	1.291	108.2	463
3.00	1788	210.6	1.300	129.0	462
4.00	1784	210.6	1.308	152.1	460
5.00	1781	210.7	1.330	174.4	459
5.98	1777	210.6	1.345	196.6	457
7.01	1772	210.4	1.371	220.3	455
7.92	1769	210.6	1.398	242.0	453
8.99	1764	210.3	1.430	267.0	453
9.99	1760	210.4	1.464	291.0	456
11.00	1755	210.3	1.501	315.0	454
12.01	1751	210.2	1.543	340.0	455
12.94	1747	210.1	1.587	346.0	454
13.95	1741	210.0	1.636	389.0	456
14.99	1736	210.0	1.684	415.0	458
15.93	1732	210.1	1.736	439.0	458
16.97	1726	210.0	1.789	467.0	462

Figure 25 is the layout of the non-reduced Marinus/Malengret converter. On the right side of the figure is the delta-connected three-phase motor utilizing the parallel model for the non-power factor corrected windings. To the left of the motor are the power factor (PF) correction capacitors. Due to the choice in motor winding connection, the value of these components can be read directly from the schematic. Since the PF components are in parallel with the winding inductances, reactance of the PF components are equivalent to the negative reactance of the winding inductance (L_{DP}). This will eliminate the effects of the inductance, leaving the windings completely resistive and eliminate the reactive power. On the left side of Figure 25, is the single to three-phase conversion network and its components were derived in Section 1.2.2.

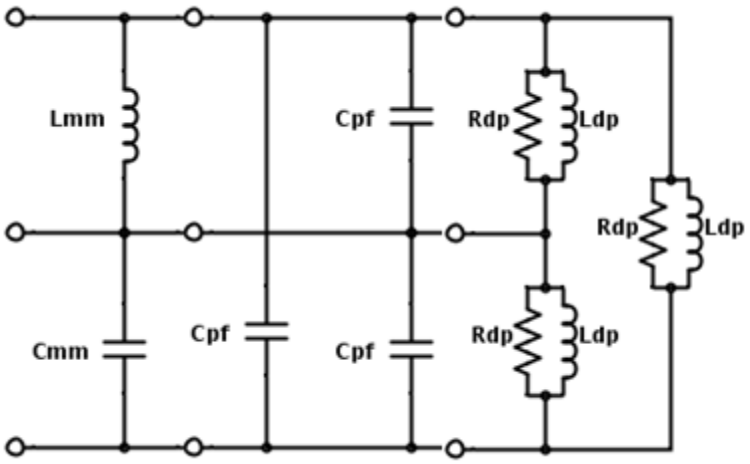

Figure 25: Marinus/Malengret converter with delta-connected motor and power factor correction network

Below are the equations for the previously derived reactances of conversion network and PF components, in terms of the motor resistance and reactance at the point of operation.

$$X_{LMM} = \frac{1}{\sqrt{3}} R_{DP}$$

$$X_{CMM} = -\frac{1}{\sqrt{3}} R_{DP}$$

$$X_{CPF} = -X_{LDP}$$

Now that the values have been derived, the circuit can be simplified to reduce the number of components being used. Due to the parallel connection of the inductor of the conversion network and a PF capacitor, an equivalent converter inductance is derived.

$$X_{LMMeq} = \frac{X_{LMM} X_{CPF}}{X_{LMM} + X_{CPF}}$$

$$L_{MMeq} = \frac{X_{LMMeq}}{2\pi f}$$

Due to the parallel connection of the capacitor of the conversion network and another PF capacitor, an equivalent converter capacitance is derived.

$$X_{CMMeq} = \frac{X_{CMM}X_{CPF}}{X_{CMM} + X_{CPF}}$$

$$C_{MMeq} = \frac{1}{2\pi f X_{CMMeq}}$$

To verify that the calculations are correct, LTspice simulations were performed using a sinusoidal voltage input with and amplitude of 170_{pk} at 60Hz. Figure 26 displays the schematic with the calculated numerical values. From left to right is single-phase source, the delta-connected motor and the converter.

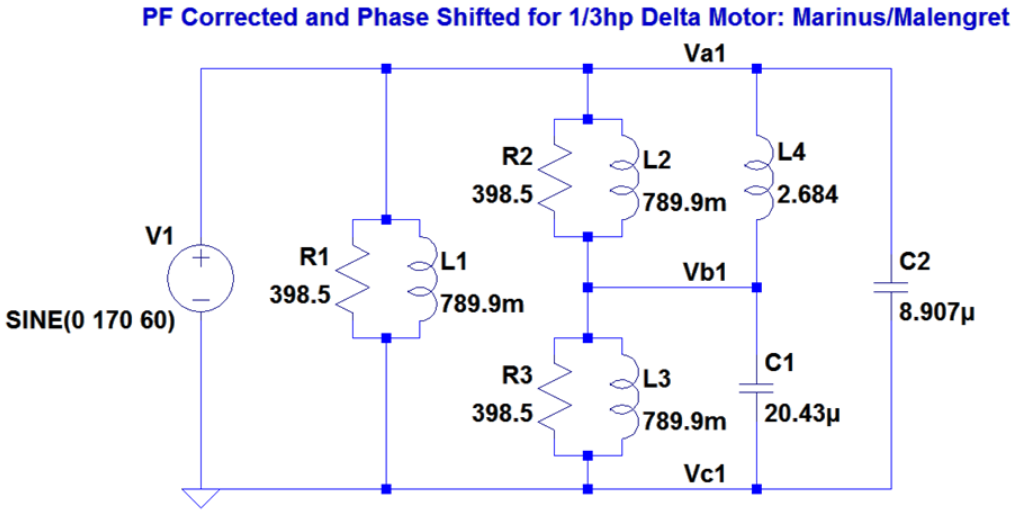

Figure 26: LTspice model of reduced MM converter with 1/3HP delta-connected motor

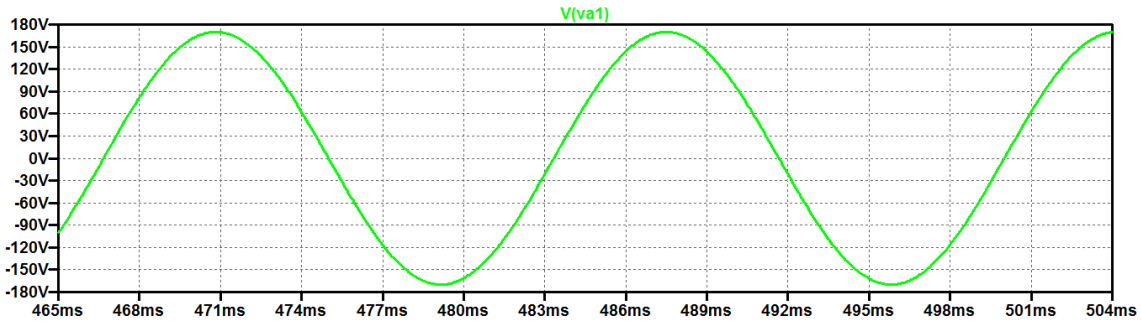

Figure 27: Single-phase source voltage with MM converter and 1/3HP delta-connected motor

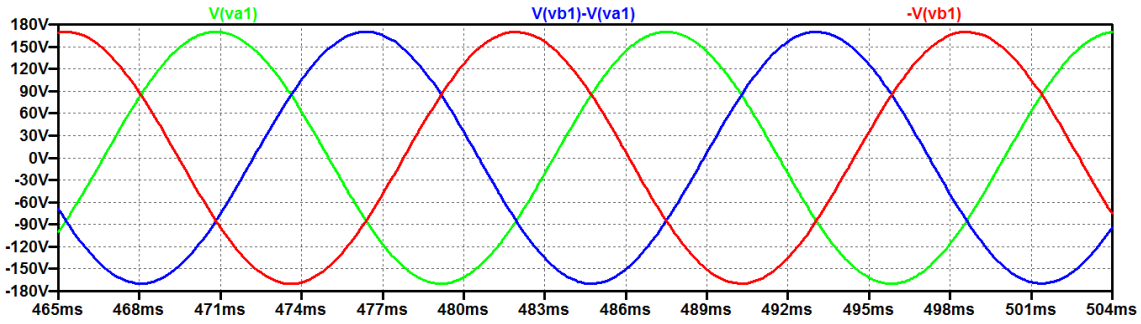

Figure 28: Three-phase voltage delivered from MM converter to 1/3HP delta-connected motor

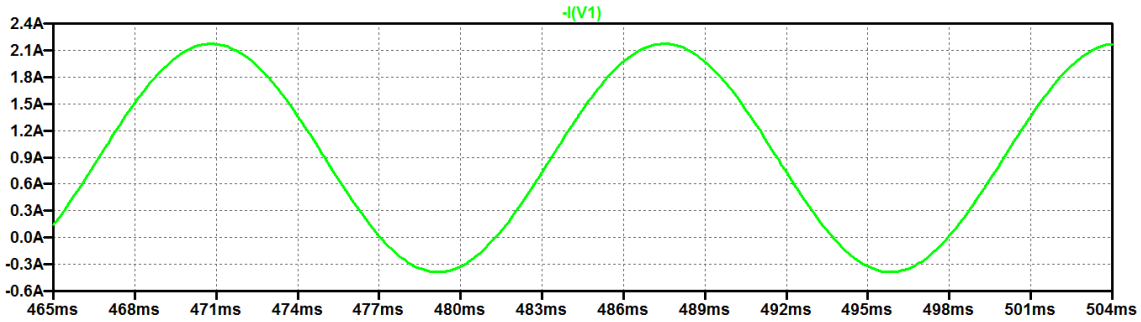

Figure 29: Single-phase source current with MM converter and 1/3HP delta-connected motor

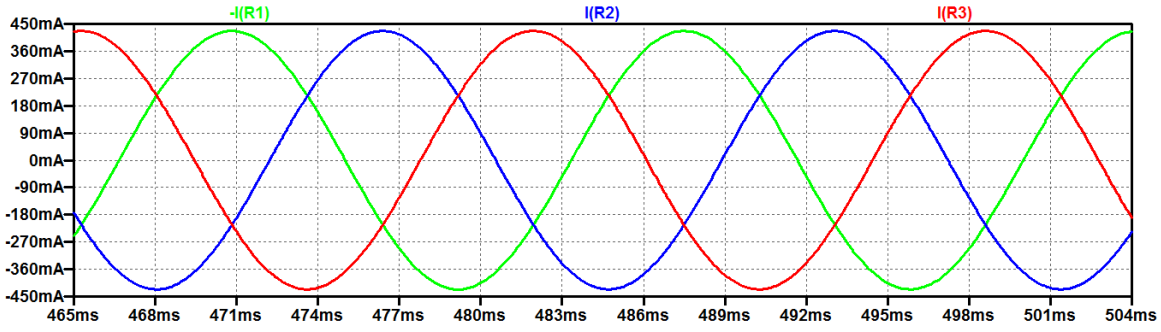

Figure 30: Three-phase current delivered from MM converter to 1/3HP delta-connected motor

Figure 27 displays the voltage from the single-phase source driving the Marinus/Malengret converter and the 1/3HP delta-connected motor. This waveform is also the reference voltage in Figure 28 with peak amplitude of 170V. Figure 28 displays the three-phase voltage delivered from the converter to the motor in Figure 26. The green waveform is the reference voltage with a phase of 0˚, the blue waveform is the voltage between the top and middle line of the system shifted by +120˚, and the red waveform is the voltage between the middle and bottom line shifted by -120˚, all with the amplitude of 170V.

Figure 29 displays the current from the single-phase source driving the Marinus/Malengret converter and the 1/3HP delta-connected motor. Its amplitude is 1.28A with an offset of 0.89A, increasing the peak current to 2.17A. This offset is due to the simulation parameters set by LTspice. Without the current initialized to zero, this circuit experiences a DC offset in the source current. Therefore, by placing a voltage controlled variable resistor, called a varistor, between the single-phase source and the remaining components in the system, the voltage will gradually increase from zero, initializing both the voltage and current to zero.

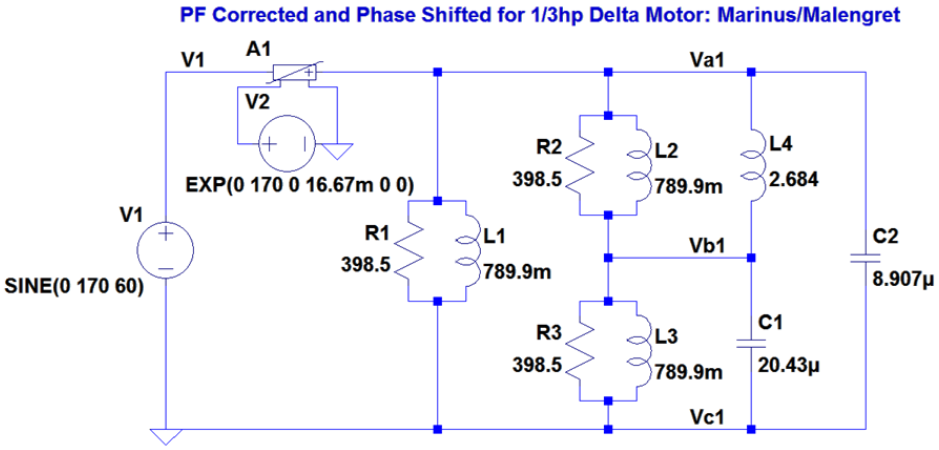

Figure 31: Model of reduced MM converter with 1/3HP delta-connected motor with varistor

The updated system with the varistor is shown in Figure 31. The voltage controlling the varistor is an exponential function that starts the voltage at zero, initializing the voltage and current to zero, and increases it to the set maximum voltage at an exponential rate. In this case the exponential peak voltage is equal to the source at 170V with the time constant set to 16.67ms corresponding to one period of the input voltage. The addition of the varistor results in a source current shown in Figure 32 below, and is equivalent to the waveform from the original circuit but with a reference of 0A. The amplitude balance and phase shift of the three-phase current through the motor remains unaffected by the varistor as well.

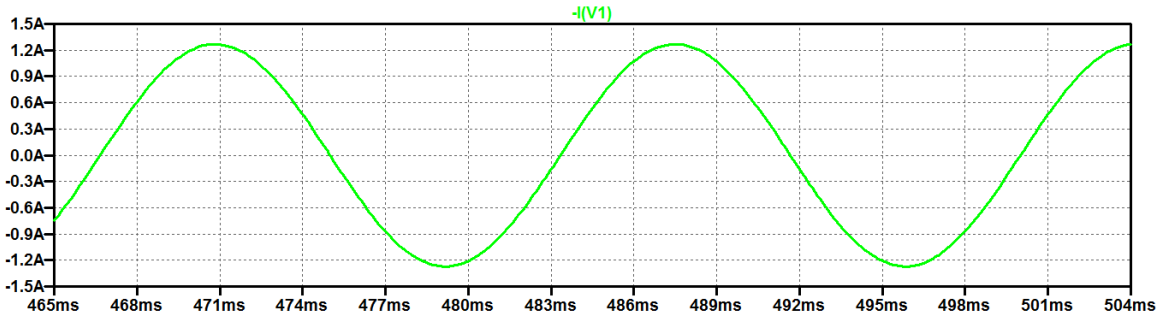

Figure 32: Source current with MM converter and 1/3HP delta-connected motor with varistor

Figure 30 displays the three-phase current delivered from the converter to the motor. The green waveform is the current through resistor R1, the blue waveform is the current through resistor R2, and the red waveform is the current through resistor R3, all with the amplitude of 426.6mA. The nominal current through the motor without the conversion network ran by a three-phase source, like in Figure 3, is approximately 739mA. The single-phase voltage source connected to the converter creates a three-phase delta-connected source. The converter equally divides the single-phase source current into three currents with amplitudes of 426.6mA and shifts them out of phase by 120˚.

Next, a simulation is performed to examine the effect of replacing the delta-connected motor with a wye-connected motor. The phase shifting properties in theory should remain the same since the wye and delta-connected representations of the motor are equivalent models, just a transformation of the other. The voltages should remain the same with the on difference being that the current amplitude is larger by a factor of $\sqrt{3}$.

This is because the current for the wye-connected load is the line current and the current of the delta-connected load is the phase current. Line current is $\sqrt{3}$ times larger than phase current. This relationship is shown previously in Figure 5 from Section 1.1. The voltage should remain the same because the line-to-line voltage of a wye-connected motor is equivalent to the phase voltage of a delta-connected motor, since phase voltage for delta connection is line-to-line of the input three-phase voltage.

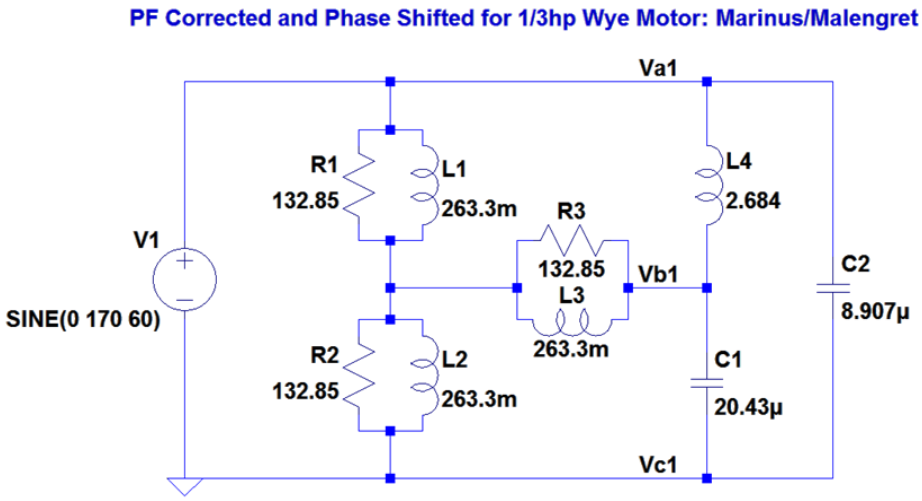

Figure 33: LTspice model of reduced Marinus/Malengret converter and 1/3hp wye-connected motor

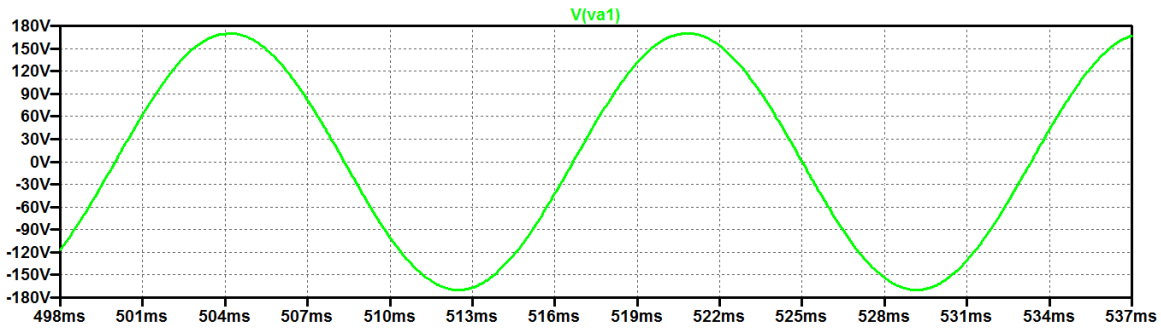

Figure 34: Single-phase source voltage with MM converter and 1/3HP wye-connected motor

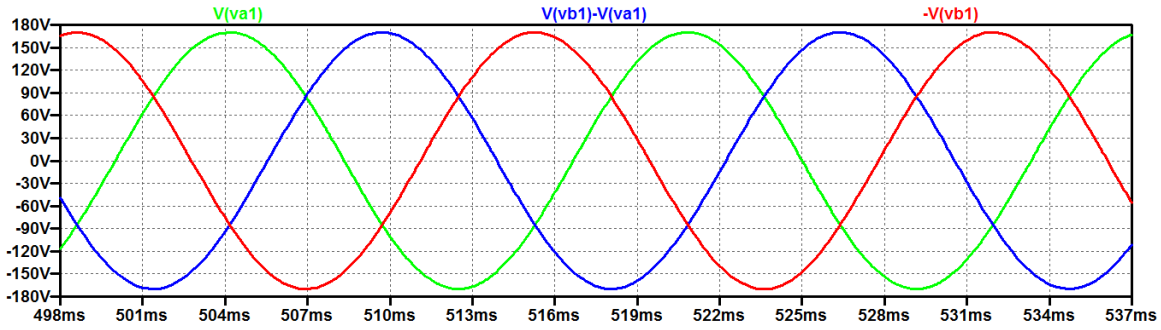

Figure 35: Three-phase voltage delivered from MM converter to 1/3HP wye-connected motor

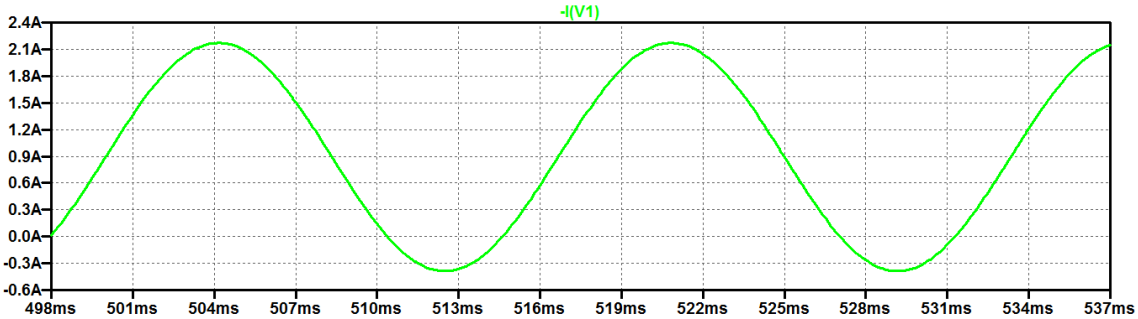

Figure 36: Single-phase source current with MM converter and 1/3HP wye-connected motor

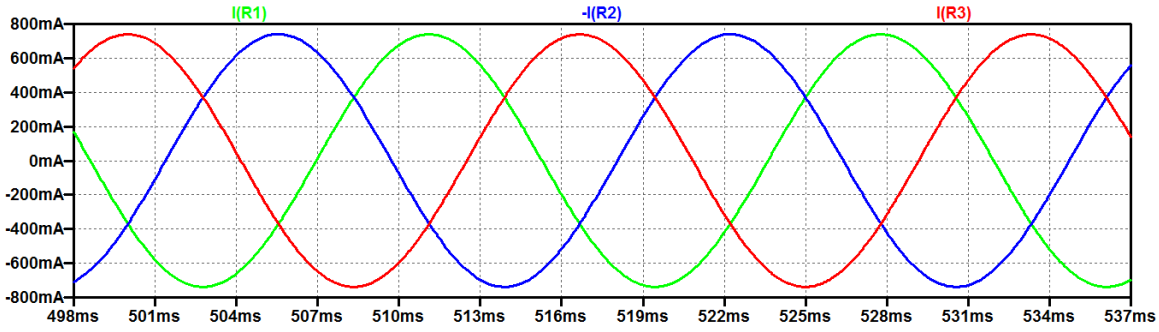

Figure 37: Three-phase current delivered from MM converter to 1/3HP wye-connected motor

Figure 34 displays the voltage from the single-phase source driving the Marinus/Malengret converter and the 1/3HP wye-connected motor. This waveform is also the reference voltage in Figure 35 with peak amplitude of 170V. Figure 35 displays the three-phase voltage delivered from the converter to the motor in Figure 33. The green waveform is the reference voltage with a phase of 0˚, the blue waveform is the voltage between the top and middle line of the system shifted by +120˚, and the red waveform is the voltage between the middle and bottom line shifted by -120˚, all with the amplitude of 170V.

Figure 36 displays the current from the single-phase source driving the Marinus/Malengret converter and the 1/3HP wye-connected motor. Its amplitude is 1.28A with an offset of 0.89A, increasing the peak current to 2.17A. This is due to the same reason as the system with delta-connected motor. The current is not initialized to zero by the simulation settings. Therefore, we will incorporate the varistor into the network to initialize the voltage and the current. This is shown in Figure 38, below.

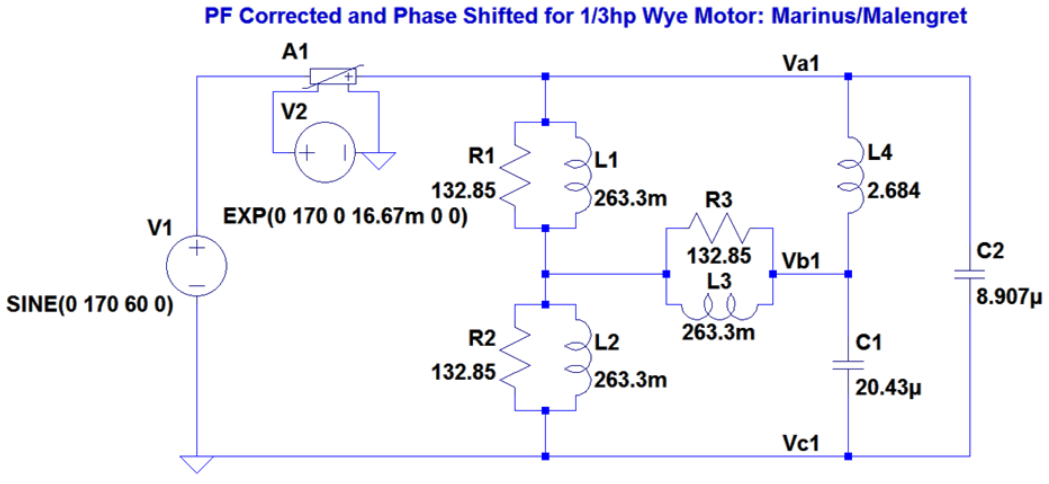

Figure 38: LTspice model of reduced MM converter and 1/3hp wye-connected motor with varistor

The exponential peak voltage controlling the varistor is equal to the source at 170V and the time constant it set to 16.67ms corresponding to one period of the input voltage. The addition of the varistor produces the source current waveform shown in Figure 39 below, and is equivalent to the waveform from the original circuit, but with the reference set at 0A. The amplitude balance and phase shift of the three-phase current in the motor remains unaffected by the varistor.

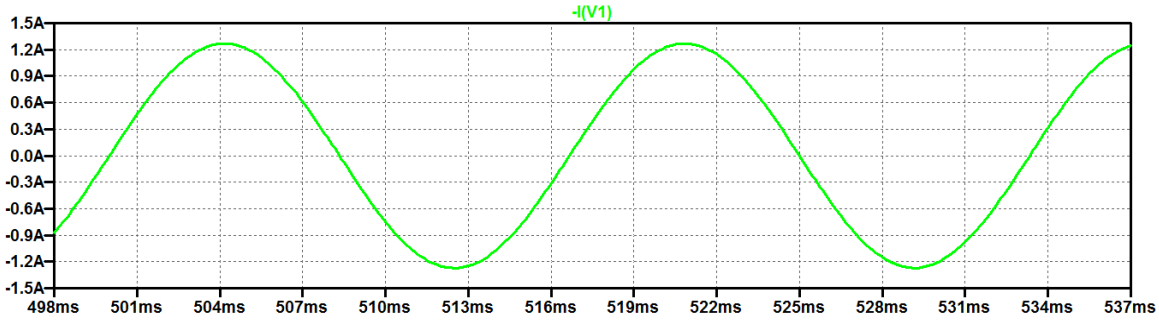

Figure 39: Source current with MM converter and 1/3HP wye-connected motor with varistor

The theory of the current holds true and is shown in Figure 37, displaying the current simulation of the motor of Figure 33. The green waveform is the current through resistor R1, the blue waveform is the current through resistor R2, and the red waveform is the current through resistor R3, all with the amplitude of 738.6mA. These peak currents equate to about √3 times the peak currents of the delta connected motor, which is correct since a delta to wye transformation is being performed. The single-phase voltage source connected to the converter creates a three-phase delta-connected source. The converter equally divides the single-phase source current into three currents with amplitudes of 426.6mA, equivalent to 738.6mA line current for the motor, and shifts them out of phase by 120˚. The waveforms extracted from the wye and delta-connected motors exhibit the same phase shift and balance in waveform amplitudes. From that we can conclude that the conversion network can be used for both motor configurations.

Chapter 2: Marinus/Malengret to Smith Transformation

From a top level block diagram perspective, the three conversion networks can be separated into two categories. The converter either has three or four connection lines between itself and the motor. The two converters that fall under the three connection line category are the Marinus/Malengret converter and the Smith converter. Another detail to notice from Figure 40 is that the output of the converters would need to be equivalent to properly supply the required power to the motor. To achieve the same output, there should be a correlation between the two converters. This next step is to prove the equivalency of the two converters that were proposed by Stuart Marinus and Michel Malengret, and Otto Smith.

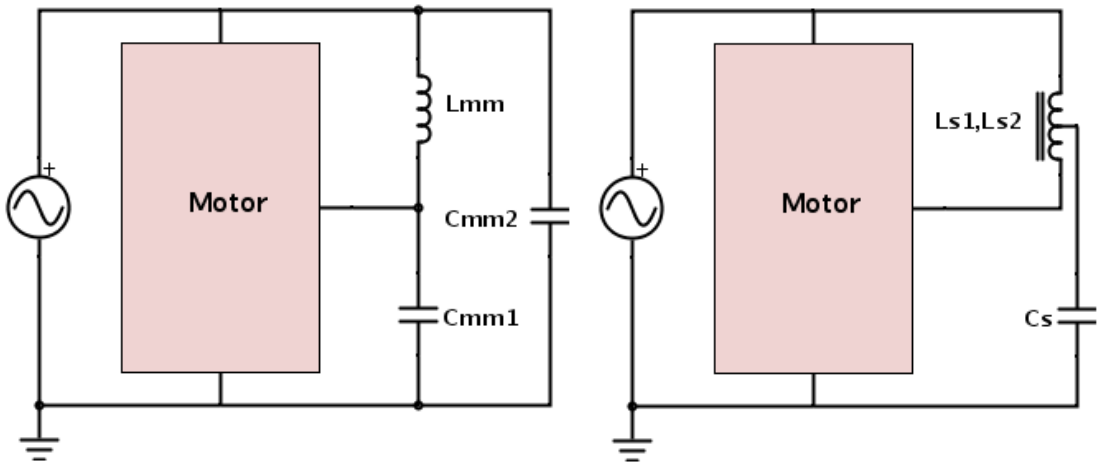

Figure 40: Marinus/Malengret and Smith conversion network comparison

The Marinus/Malengret converter utilizes a delta network for its components and the Smith converter utilizes a wye network. The wye configuration of the Smith converter might not be immediately apparent, but the tapped auto-transformer can be thought of as two coupled inductors creating a two winding transformer, as discussed earlier in Section

1.3. Therefore, if the delta-to-wye transformation shown in Figure 41 is performed on the Marinus/Malengret converter, a wye network is created.

Figure 41: Delta-to-wye transformation of Marinus/Malengret converter

To prove the proposed theory, the desired result is two inductors and one capacitor, as shown in Figure 42. An additional step of coupling the two inductors will then create a two winding transformer.

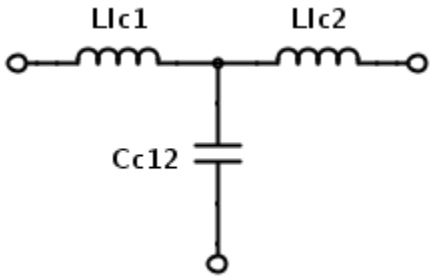

Figure 42: Desired result of delta-to-wye transformation of Marinus/Malengret converter

The equations below are used to perform the above delta-to-wye transformation. The equations are in terms of the reactance of the conversion components.

$$X_{LC1} = \frac{X_{LMM}X_{CMM1}}{X_{LMM} + X_{CMM1} + X_{CMM2}}$$

$$X_{LC2} = \frac{X_{LMM}X_{CMM2}}{X_{LMM} + X_{CMM1} + X_{CMM2}}$$

$$X_{C12} = \frac{X_{CMM1}X_{CMM2}}{X_{LMM} + X_{CMM1} + X_{CMM2}}$$

Table 2 displays the calculated wye-network reactances from the above equations for the components in Figure 41. Also included are the corresponding torques and power factors of the 1/3hp three-phase induction motor, used previously to derive the Marinus/Malengret converter. When the motor is operating at its rated torque of 12 in-lbs, the resulting component reactances include two negative and one positive value.

Table 2: Component results of uncoupled Smith converter with 1/3hp motor

Smith (uncoupled)				
T [inlbs]	**PF**	**$X_{LC1}(\Omega)$**	**$X_{LC2}(\Omega)$**	**$X_{C12}(\Omega)$**
1.02	0.185	-100.656	-133.034	-68.279
2.01	0.230	-103.298	-145.109	-61.486
3.00	0.272	-106.535	-158.057	-55.012
4.00	0.318	-111.626	-175.555	-47.697
5.00	0.361	-115.682	-191.813	-39.551
5.98	0.400	-122.454	-213.698	-31.211
7.01	0.439	-130.105	-239.213	-20.997
7.92	0.473	-138.971	-267.560	-10.383
8.99	0.511	-152.458	-308.100	3.183
9.99	0.546	-168.367	-354.466	17.733
11.00	0.574	-191.874	-422.460	38.711
12.01	0.605	-224.797	-515.748	66.153
12.94	0.598	-226.600	-525.718	72.517
13.95	0.654	-360.372	-892.843	172.099
14.99	0.677	-547.808	-1407.556	311.941
15.93	0.697	-1196.323	-3182.455	789.809
16.97	0.717	4470.214	12296.647	-3356.219

These reactances translate into two capacitors and one inductor, shown in Figure 43, which is the opposite of what is desired. The only row on the table that delivers the desired two inductors and one capacitor has a torque of 16.97in-lbs and has a power factor of 0.717. From this data, two theories are formulated. Either the motor needs to have a higher rated torque or it needs to have a higher rated power factor.

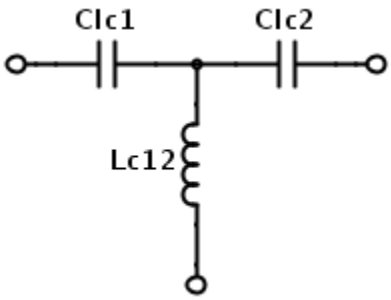

Figure 43: Actual result of delta-to-wye transformation of Marinus/Malengret converter

To test the first theory, a motor with a higher rated torque was chosen. Due to lack of access to motors larger than 1hp, Example 6.3 was chosen from "Electric Machinery Fundamentals" that provided the equivalent circuit for a 25hp three-phase induction motor, shown in Figure 44 [4].

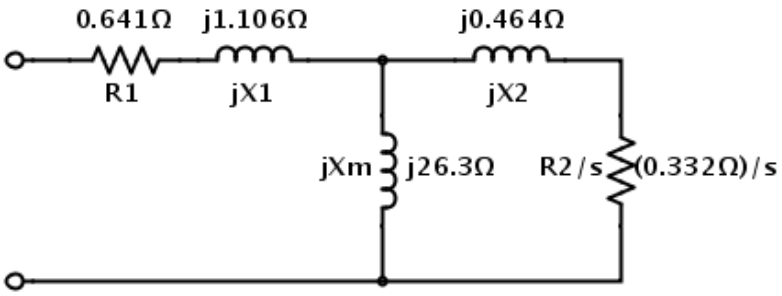

Figure 44: IEEE standard equivalent circuit of 25hp three-phase induction motor

The equivalent circuit can be reduced into two components, an inductor and a resistor which varies with slip (s). To calculate the component values of the reduced equivalent circuit, the maximum slip allowed on the system must be calculated using the equation below.

$$s_{max} = \frac{R_2}{\sqrt{R_{th}^2 + (X_{th} + X_2)^2}}$$

Where,

$$Z_{th} = R_{th} + jX_{th} = \frac{jX_m(R_1 + jX_1)}{R_1 + j(X_1 + X_m)}$$

With the range of slip, the winding reactance values are calculated and transformed into Marinus/Malengret and Smith converter components, recorded in Table 3. The list provides values up to 5% slip because it is highly suggested to stay under that range. Anything higher will introduce too much current into the system causing a greater power loss and could possibly damage the motor due to excess heat. The power factor is also included for each slip value by taking the cosine of the negative phase of the total impedance of the winding.

Table 3: Component results of Marinus/Malengret and uncoupled Smith converter with 25hp motor

		Marinus/Malengret			Smith (Uncoupled)		
s	**PF**	**$X_{Lmm}(\Omega)$**	**$X_{Cmm1}(\Omega)$**	**$X_{Cmm2}(\Omega)$**	**$X_{LC1}(\Omega)$**	**$X_{LC2}(\Omega)$**	**$X_{C12}(\Omega)$**
0.010	0.610	246.431	-35.276	-82.340	-67.486	-157.521	22.549
0.015	0.742	87.854	-27.581	-80.404	120.368	350.897	-110.161
0.020	0.813	54.517	-22.641	-77.448	27.086	92.650	-38.478
0.022	0.840	46.564	-21.279	-78.377	18.662	68.738	-31.413
0.025	0.854	40.100	-19.212	-73.764	14.570	55.941	-26.801
0.030	0.878	32.084	-16.699	-69.644	9.874	41.182	-21.434
0.035	0.892	27.000	-14.782	-65.336	7.514	33.210	-18.183
0.040	0.901	23.502	-13.277	-61.033	6.141	28.231	-15.949
0.045	0.906	20.958	-12.065	-56.871	5.271	24.843	-14.302
0.050	0.909	19.034	-11.072	-52.935	4.686	22.404	-13.032

The results in the above table provide the desired two inductors and one capacitor for the Smith converter, starting at a slip of 1.5%. The component values at 2.2% slip are chosen since that is what was suggested by the example in the textbook. The next step is to couple the inductors into a two winding transformer. When coupling inductors, a negative mutual inductance is introduced to the rest of the network and can be drawn as the connection on the right in Figure 45. By combining the negative mutual inductance ($-L_{mutual}$) and the capacitance (C_{C12}) we get the capacitor in the Smith converter.

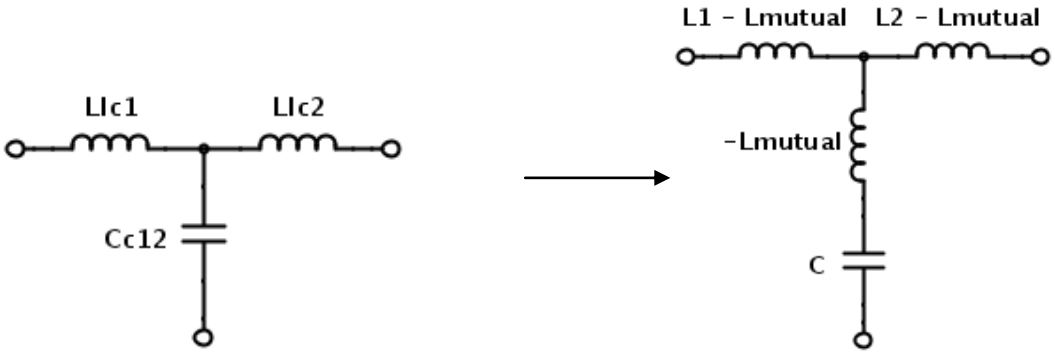

Figure 45: Uncoupled-to-coupled inductor model of Smith converter

To calculate the coupled inductances, L_{S1} and L_{S2}, and the mutual inductance, L_m, the following equations are used, in terms of reactance.

$$X_{LS1} = X_{LC1} - X_M$$

$$X_{LS2} = X_{LC2} - X_M$$

$$X_M = \sqrt{X_{LS1} X_{LS2}}$$

The next step is to solve for the impedance of the first winding of the coupled inductor, X_{LS1}. The following equation is produced by isolating the mutual inductance in the top two equations above, setting those resulting equations equal to each other and then isolating the reactance of the first winding.

$$X_{LS1} = X_{LS2} - (X_{LC2} - X_{LC1})$$

The next equation is derived by substituting X_{LS1} into the original X_{LS2}.

$$X_{LS2} = X_{LC2} - \sqrt{\left(X_{LS2} - (X_{LC2} - X_{LC1})\right) X_{LS2}}$$

Now we can solve for mutual reactance, X_M.

$$X_M = \sqrt{X_{L1} X_{L2}}$$

The last step is to solve for the capacitance of the converter. This is done by adding the negative mutual reactance with the reactance of the capacitor.

$$X_{CS} = X_{C12} - X_M$$

The following equations calculate the component values for Figure 46.

$$L_{S1} = \frac{X_{LS1}}{2\pi f}$$

$$L_{S2} = \frac{X_{LS2}}{2\pi f}$$

$$C_S = \frac{1}{2\pi f X_{CS}}$$

The components L_4, L_5 and C_1 in the LTspice schematic correspond to L_{S1}, L_{S2} and C_S, respectively. With these component values, Figure 46 is ready to simulate to verify the calculations.

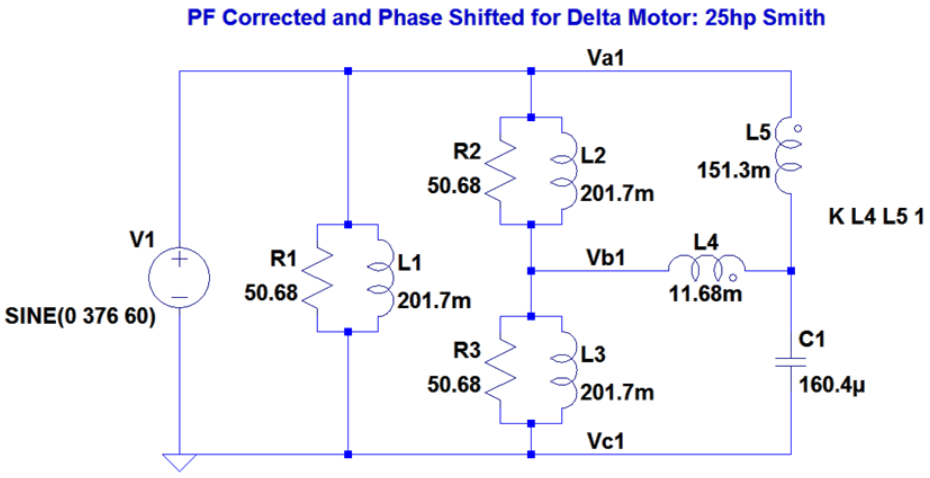

Figure 46: LTspice model of Smith converter with 25hp delta-connected motor

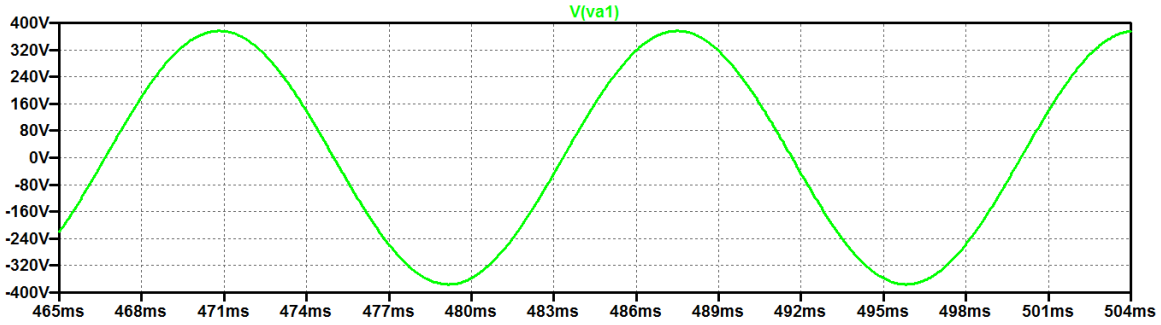

Figure 47: Single-phase source voltage with Smith converter and 25HP delta-connected motor

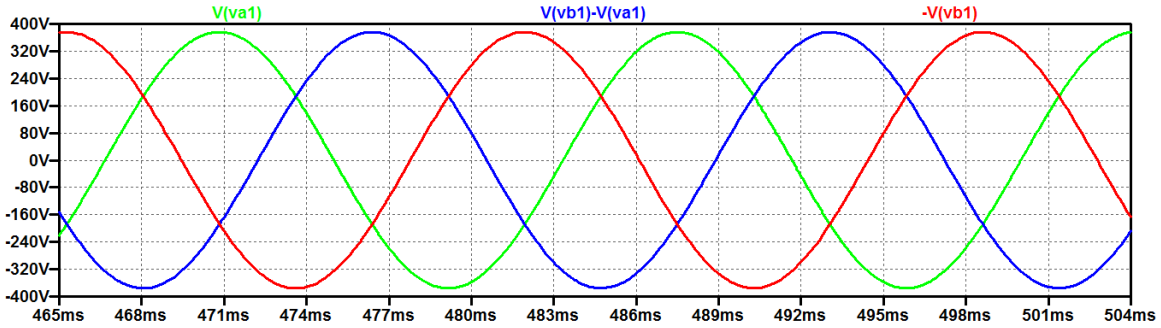

Figure 48: Three-phase voltage delivered from Smith converter to 25HP delta-connected motor

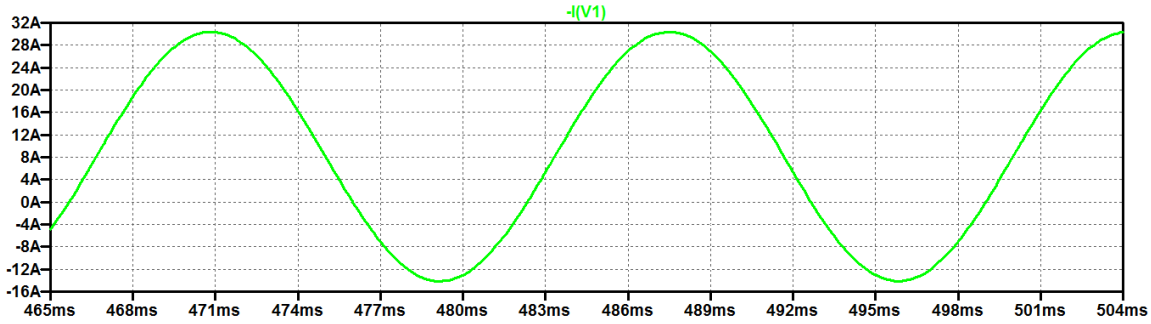

Figure 49: Single-phase source current with Smith converter and 25HP delta-connected motor

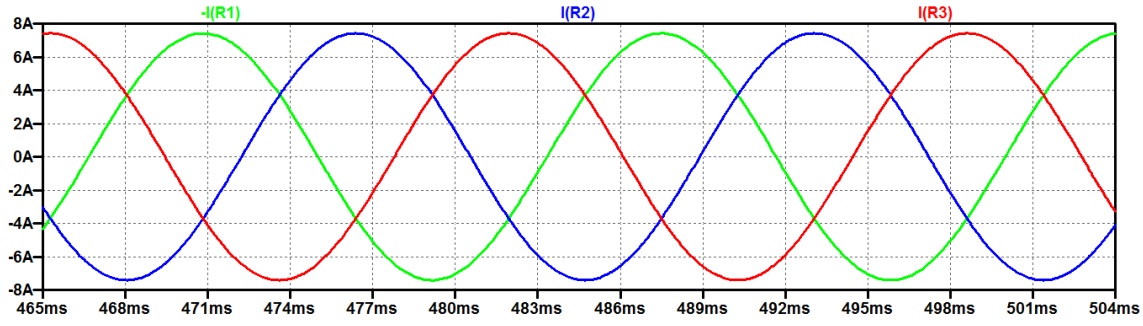

Figure 50: Three-phase current delivered from Smith converter to 25HP delta-connected motor

Figure 47 displays the voltage from the single-phase source driving the Smith converter and the 25HP delta-connected motor. This waveform is also the reference voltage in Figure 48 with peak amplitude of 376V. Figure 48 displays the three-phase voltage delivered from the converter to the motor in Figure 46. The green waveform is the reference voltage with a phase of 0˚, the blue waveform is the voltage between the top and middle line of the system shifted by +120˚, and the red waveform is the voltage between the middle and bottom line shifted by -120˚, all with the amplitude of 376V.

Figure 49 displays the current from the single-phase source driving the Smith converter and the 25HP delta-connected motor. Its amplitude is 22.26A with an offset of 8.11A, increasing the peak current to 30.37A. This is due to the same reason as the systems with the Marinus/Malengret converter. The current is not initialized to zero by the simulation settings. Therefore, we will incorporate a varistor into the network to initialize the voltage and the current. This is shown in Figure 51, below.

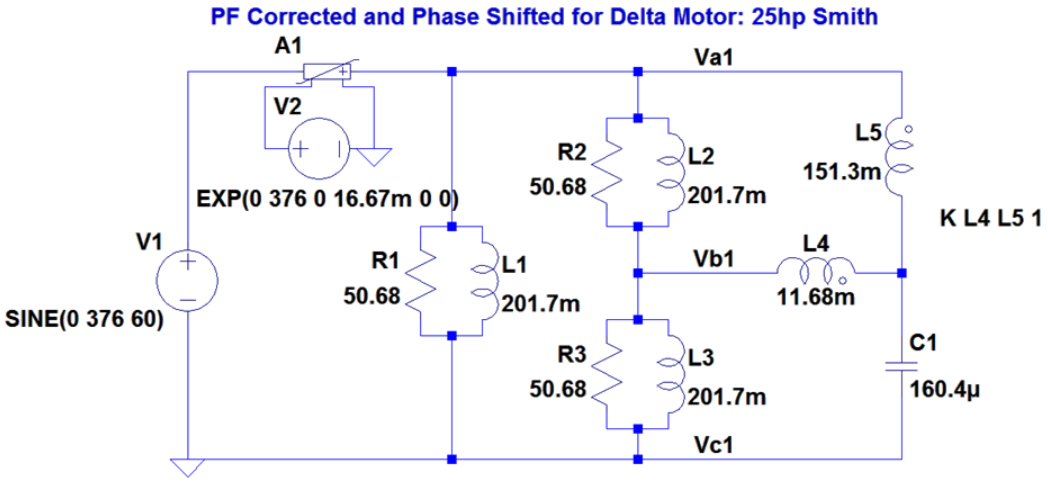

Figure 51: LTspice model of Smith converter with 25hp delta-connected motor with varistor

The exponential peak voltage controlling the varistor is equal to the source at 376V and the time constant it set to 16.67ms corresponding to one period of the input

voltage. The addition of the varistor results in th source current waveform shown in Figure 52 below, and is equivalent to the waveform from the original circuit but with the reference set at 0A. The amplitude balance and phase shift of the three-phase current through the motor also remains unaffected by the varistor.

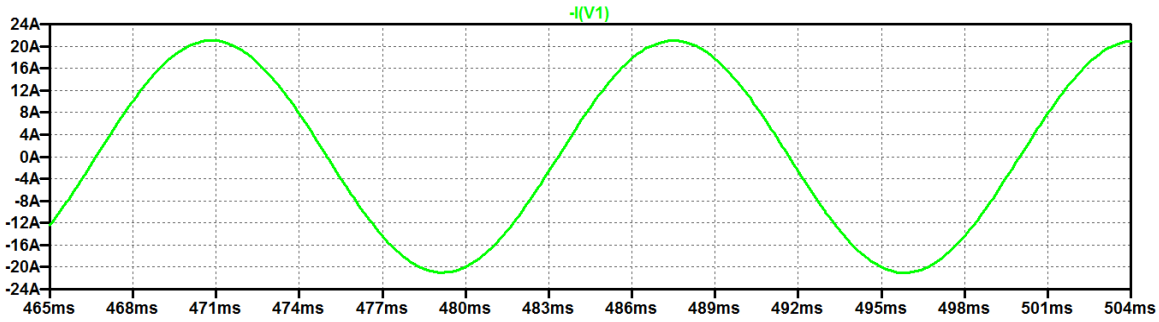

Figure 52: Source current with Smith converter and 25HP delta-connected motor with varistor

Figure 50 is the three-phase current from the converter. The green waveform is the current through resistor R1, the blue waveform is the current through resistor R2, and the red waveform is the current through resistor R3, all with the amplitude of 7.43A.

The nominal current through the motor without the conversion network ran by a three-phase source, like in Figure 3, is approximately 12.85A. The difference between the current provided from the converter is a factor of √3. This is because of the connection of the motor with the single-phase source and the conversion network. The current supplied to the motor is phase current which is √3 times smaller than line current supplied by a three-phase wye-connected source. The single-phase voltage source connected to the converter creates a three-phase delta-connected source. The converter equally divides the single-phase source current into three currents with amplitudes of 7.43A and shifts them out of phase by 120˚.

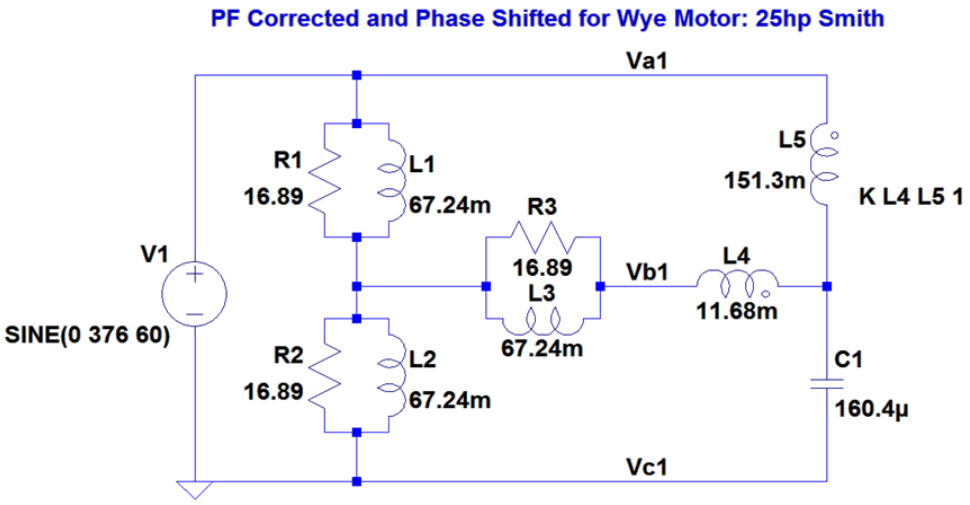

Figure 53: LTspice model of Smith converter with 25hp wye-connected motor

Figure 54 displays the voltage from the single-phase source driving the Smith converter and the 25HP wye-connected motor. This waveform is also the reference voltage in Figure 55 with peak amplitude of 376V. Figure 55 displays the three-phase voltage delivered from the converter to the motor in Figure 53. The green waveform is the reference voltage with a phase of 0˚, the blue waveform is the voltage between the top and middle line of the system shifted by +120˚, and the red waveform is the voltage between the middle and bottom line shifted by -120˚, all with the amplitude of 376V.

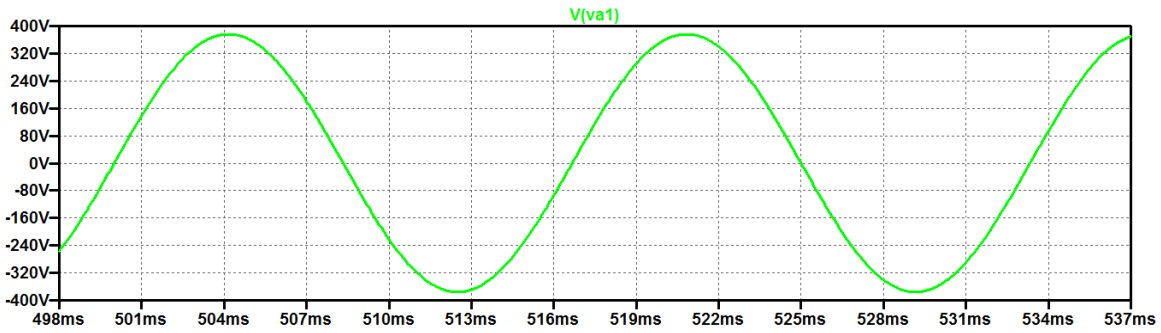

Figure 54: Single-phase source voltage with Smith converter and 25HP wye-connected motor

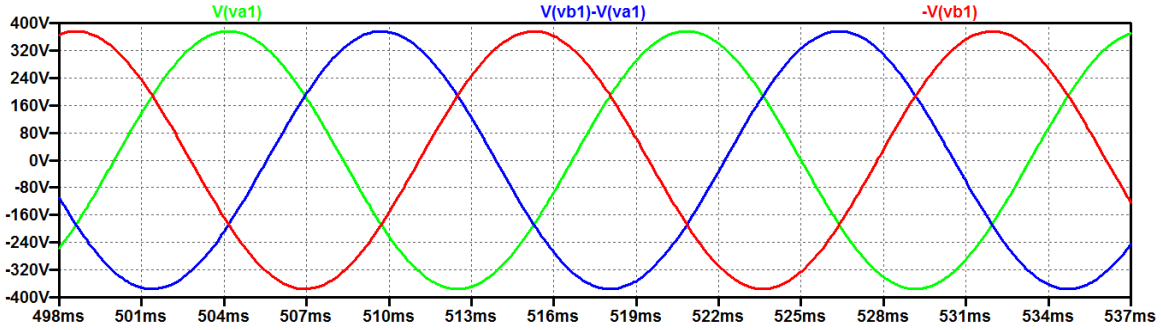

Figure 55: Three-phase voltage delivered from Smith converter to 25HP wye-connected motor

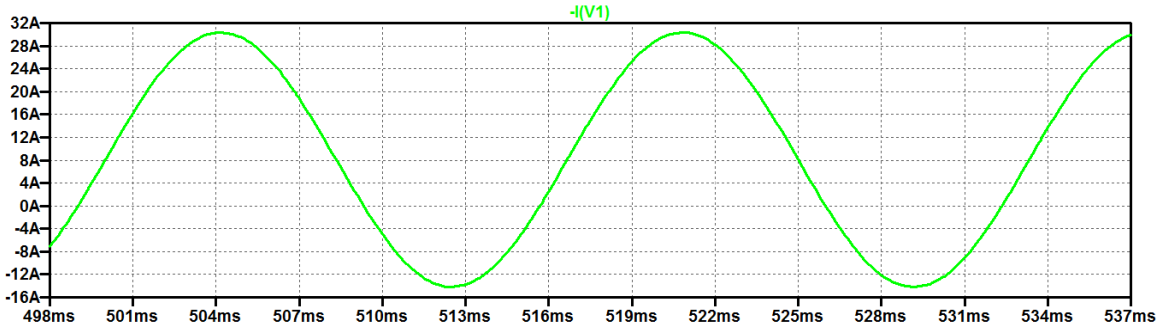

Figure 56: Single-phase source current with Smith converter and 25HP wye-connected motor

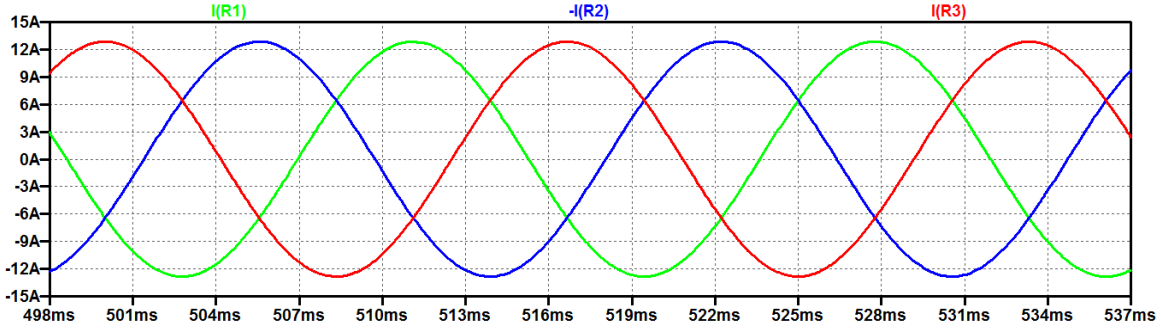

Figure 57: Three-phase current delivered from Smith converter to 25HP wye-connected motor

Figure 56 displays the current from the single-phase source driving the Smith converter and the 25HP wye-connected motor. Its amplitude is 22.26A with an offset of 8.11A, increasing the peak current to 30.37A. This is due to the same reason as the other systems. The current is not initialized to zero by the simulation settings. Therefore, we will incorporate a varistor into the network to initialize the voltage and the current. This is shown in Figure 58, below.

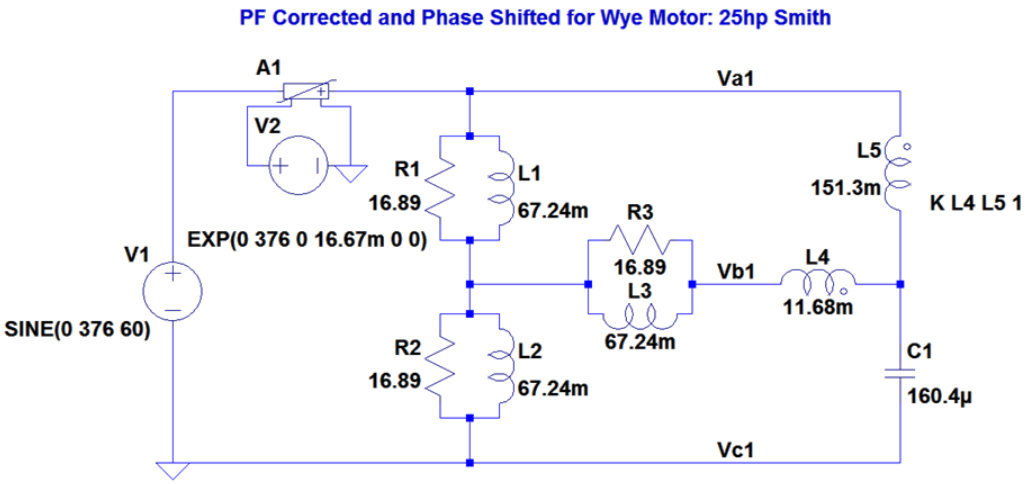

Figure 58: LTspice model of Smith converter with 25hp wye-connected motor with varistor

The exponential peak voltage controlling the varistor is equal to the source at 376V and the time constant it set to 16.67ms corresponding to one period of the input voltage. The addition of the varistor results in the source current waveform shown in Figure 59 below, and is equivalent to the original waveform but with the reference set at 0A. The amplitude balance and phase shift of the three-phase current in the motor also remains unaffected.

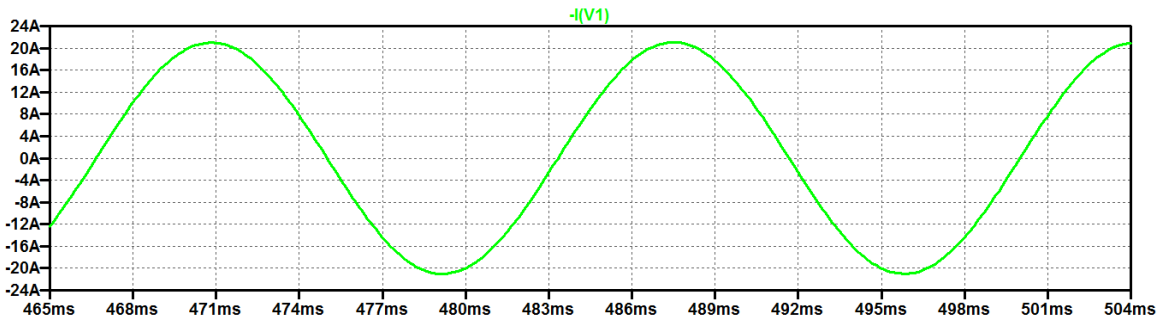

Figure 59: Source current with Smith converter and 25HP wye-connected motor with varistor

Figure 57 is the three-phase current from the converter. The green waveform is the current through resistor R1, the blue waveform is the current through resistor R2, and the red waveform is the current through resistor R3, all with the amplitude of 12.87A. The nominal current of the above wye-connected motor run by three-phase source is 22.30A. The single-phase voltage source connected to the converter creates a three-phase delta-connected source. The converter equally divides the single-phase source current into three currents for a delta-connected source with amplitudes of 7.43A, equivalent to the 12.85A current through the wye-connected motor, and shifts them out of phase by 120˚.

Since the theory behind the higher horsepower motor has been proved, let's go back and explore the effects of power factor. Returning back to the 25hp motor data in Table 3, the range of power factors for the system is listed for the range of slip. Similar to the results collected from the 1/3hp power motor, the desired components of the Smith converter are only derivable when the power factor is above around 0.7. To study further into this theory a series of tests, including no load, DC and locked rotor, were performed on the original 1/3hp three-phase induction motor. With the data from those tests, the equivalent circuit is derived for the range of slip values and is shown in Figure 60.

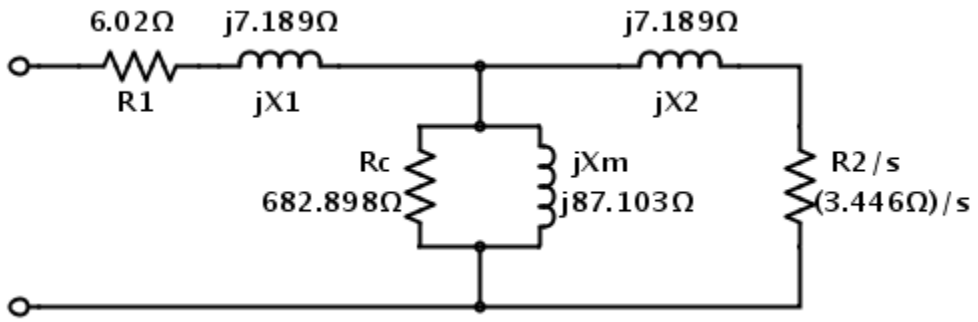

Figure 60: IEEE standard equivalent circuit of 1/3hp three-phase induction motor

Calculations are made for the slip incrementing by 1%, starting from zero up to the maximum slip. At 3%, the resulting components were two capacitors and one inductor. But when the slip increased to 4%, the derivation provided the desired two inductors and one capacitor, while still providing the proper components for the Marinus/Malengret converter. This verifies the theory behind the power factor. To examine closer at what power factor value the transition takes place, the calculations are done for increment of 0.01% in slip from 3.9% to 4%. Table 4 contains the reactance values of the conversion components of that slip range for both Marinus/Malengret converter and Smith converter, with the inductors uncoupled.

Table 4: Component results of Marinus/Malengret and uncoupled Smith converter with 1/3hp motor

		Marinus/Malengret			Smith (Uncoupled)		
s	**PF**	**$X_{Lmm}(\Omega)$**	**$X_{Cmm1}(\Omega)$**	**$X_{Cmm2}(\Omega)$**	**$X_{LC1}(\Omega)$**	**$X_{LC2}(\Omega)$**	**$X_{C12}(\Omega)$**
0.0390	0.7057	383.34	-102.03	-278.07	-12071.0	-32898.1	8756.1
0.0391	0.7063	381.78	101.89	-277.97	-20254.3	-55255.3	14746.8
0.0392	0.7069	380.23	-101.75	-277.86	62903.0	-171773.9	45967.9
0.0393	0.7074	378.70	-101.62	-277.76	56879.8	155478.5	-41719.0
0.0394	0.7079	377.18	-101.48	-277.65	19583.8	53583.9	-14416.4
0.0395	0.7085	375.67	-101.34	-277.55	11827.7	32393.7	-8738.4
0.0396	0.7090	374.18	-101.20	-277.44	8472.0	23225.9	-6281.8
0.0397	0.7096	372.70	-101.07	-277.34	6599.6	18110.1	-4911.0
0.0398	0.7101	371.23	-100.93	-277.23	5404.9	14846.1	-4036.3
0.0399	0.7106	369.78	-100.79	-277.13	4576.4	12582.6	-3429.8
0.0400	0.7112	368.34	-100.66	-277.02	3968.1	10920.6	-2984.4

The transition occurs at a power factor of 0.7074. The component values derived at that power factor are too large, so the values for a slip of 4% is chosen since the reactance values of the inductors decrease and still remains under the recommended 5% slip. Following the same procedure as with the 25hp motor, the inductors are coupled together and negative mutual inductance is combined with the capacitance to create the conversion network in Figure 61.

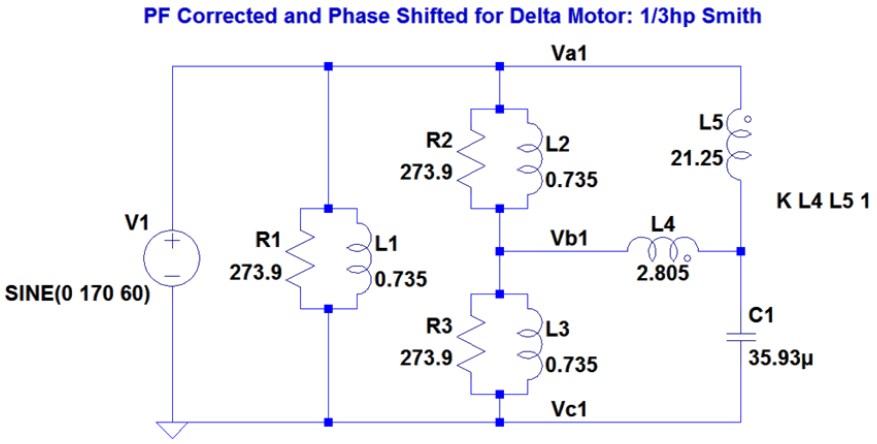

Figure 61: LTspice model of Smith converter with 1/3hp delta-connected motor

Figure 62 displays the voltage from the single-phase source driving the Smith converter and the 1/3HP delta-connected motor. This waveform is also the reference voltage in Figure 63 with peak amplitude of 170V. Figure 63 displays the three-phase voltage delivered from the converter to the motor. The green waveform is the reference voltage with a phase of 0˚, the blue waveform is the voltage between the top and middle line of the system shifted by +120˚, and the red waveform is the voltage between the middle and bottom line shifted by -120˚, all with the amplitude of 170V. Figure 64 displays the current from the single-phase source driving the Smith converter and the 1/3HP delta-connected motor. Its amplitude is 1.862A with an offset of 0.922A, increasing the peak current to 2.784A.

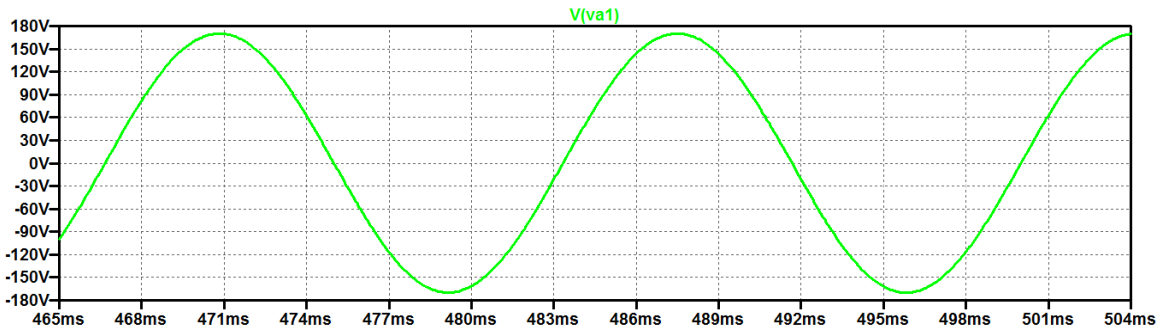

Figure 62: Single-phase source voltage with Smith converter and 1/3HP delta-connected motor

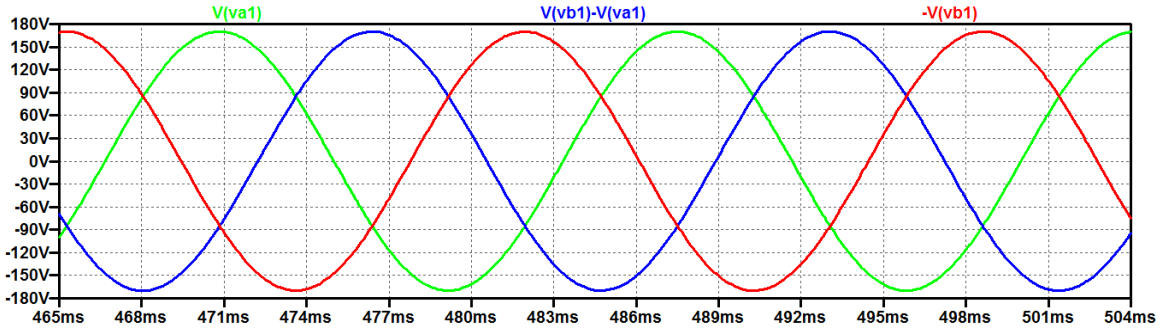

Figure 63: Three-phase voltage delivered from Smith converter to 1/3HP delta-connected motor

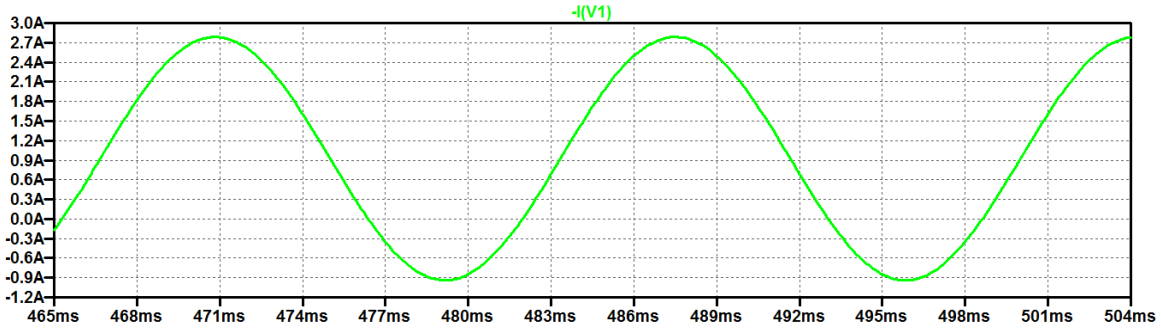

Figure 64: Single-phase source current with Smith converter and 1/3HP delta-connected motor

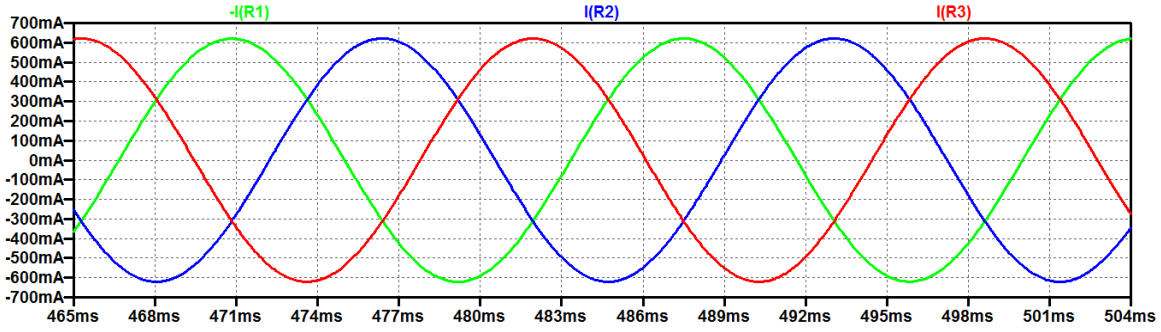

Figure 65: Three-phase current delivered from Smith converter to 1/3HP delta-connected motor

The source current offset is due to the same reason as the other systems. The current is not initialized to zero by the simulation settings. Therefore, we will incorporate the varistor into the network to initialize the voltage and the current. This is shown in Figure 66, below.

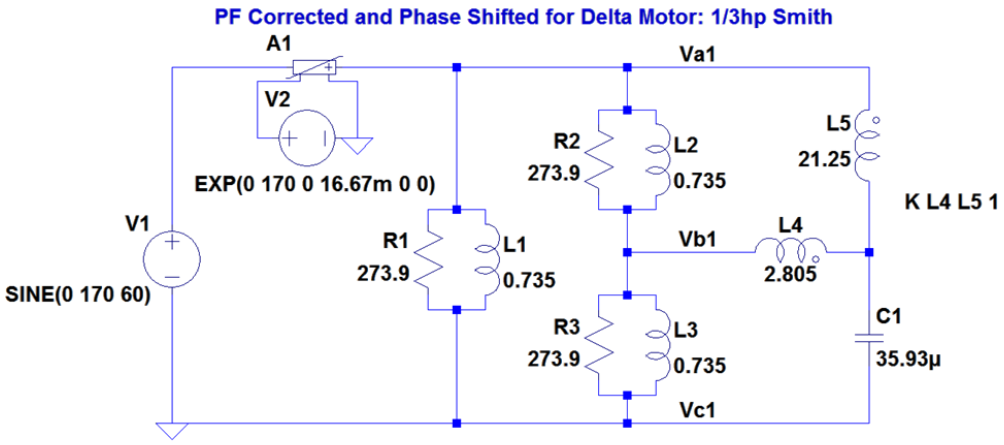

Figure 66: LTspice model of Smith converter with 1/3hp delta-connected motor with varistor

The exponential peak voltage controlling the varistor is equal to the source at 170V and the time constant it set to 16.67ms corresponding to one period of the input voltage. The addition of the varistor results in the source current waveform shown in Figure 67 below, and is equivalent to the original waveform but with the reference set at 0A. The amplitude balance and shift of the three-phase current through the motor also remains unaffected by the varistor.

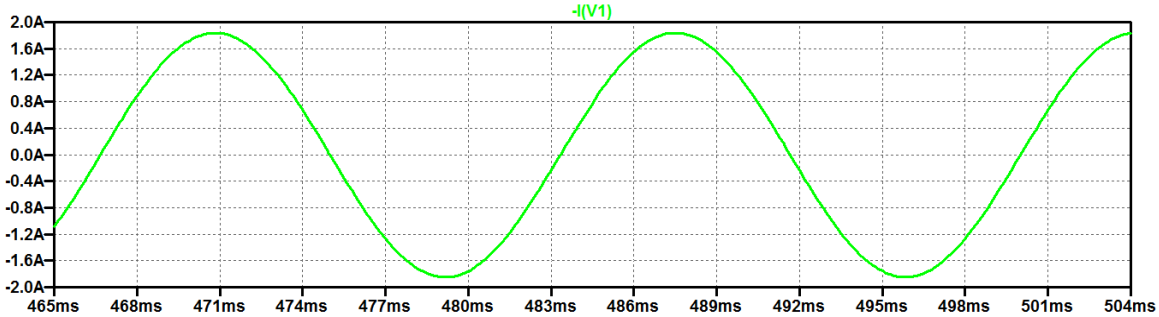

Figure 67: Source current with Smith converter and 1/3HP delta-connected motor with varistor

Figure 65 is the three-phase current from the converter. The green waveform is the current through resistor R1, the blue waveform is the current through resistor R2, and the red waveform is the current through resistor R3, all with the amplitude of 620.6mA. The nominal current of the above delta-connected motor run by three-phase source is 1.075A. This is √3 times larger than the simulated value, due to wye-to-delta transformation. The difference between the source current and the motor current is also due to the delta-connected source created by the converter.

To verify that the design is valid for both motors, the system consisting of the Smith converter and the wye-connected 1/3hp motor rated for 4% slip is simulated. The schematic of the system is shown in Figure 68. Figure 69 throughFigure 72 display the single-phase source voltage and current, and three-phase voltage and current of the motor windings.

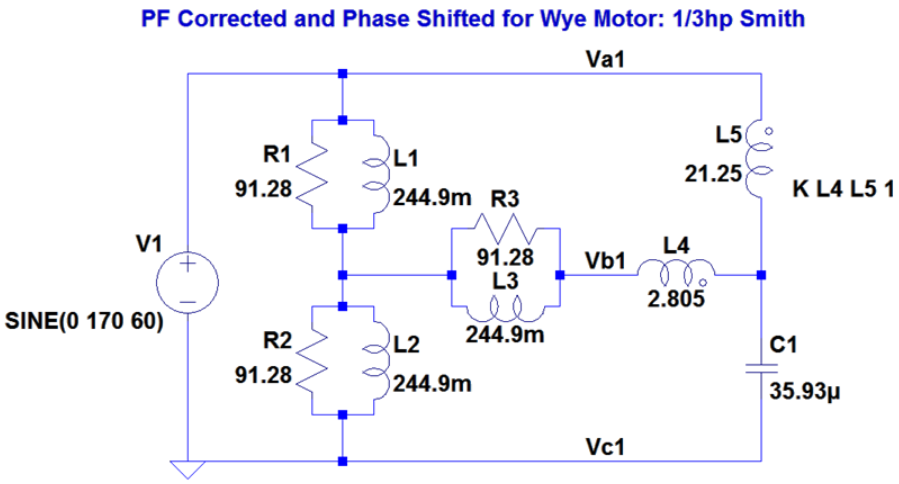

Figure 68: LTspice model of Smith converter with 1/3hp wye-connected motor

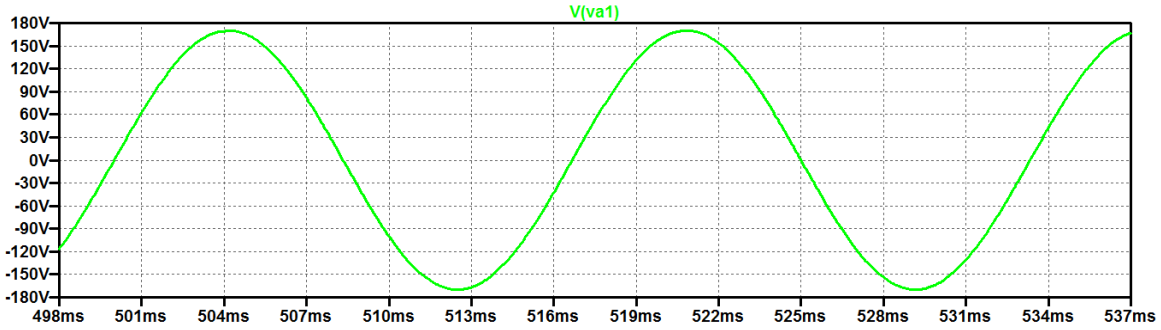

Figure 69: Single-phase source voltage with Smith converter and 1/3HP wye-connected motor

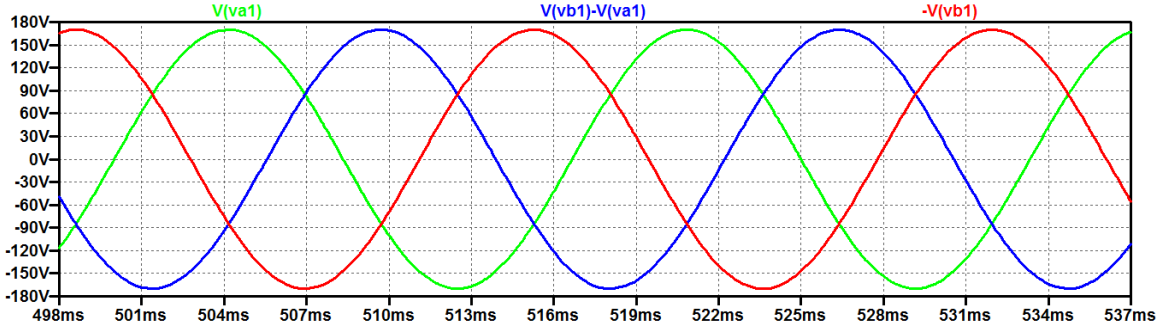

Figure 70: Three-phase voltage delivered from Smith converter to 1/3HP wye-connected motor

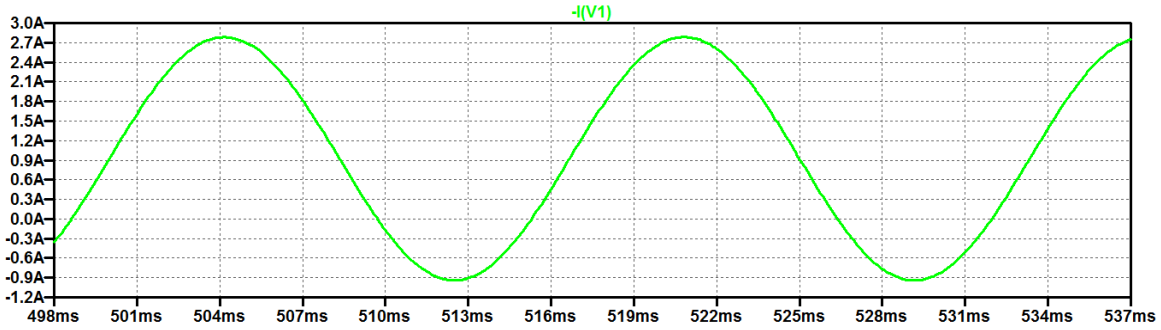

Figure 71: Single-phase source current with Smith converter and 1/3HP wye-connected motor

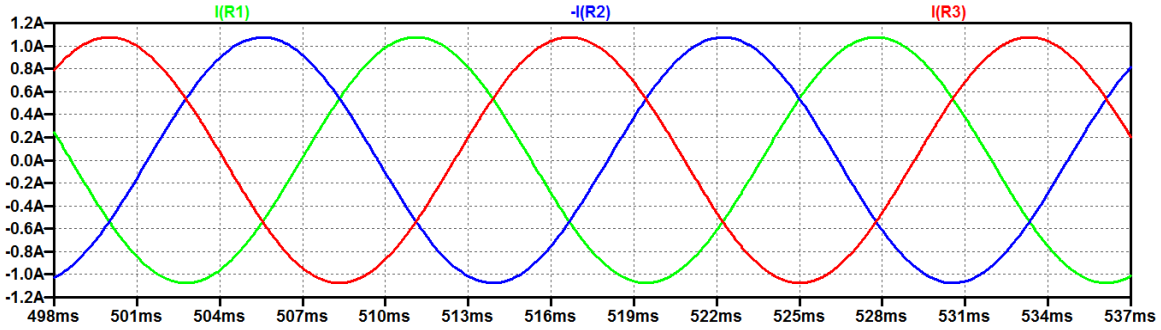

Figure 72: Three-phase current delivered from Smith converter to 1/3HP wye-connected motor

Figure 69 displays the voltage from the single-phase source driving the Smith converter and the 1/3HP delta-connected motor. This waveform is also the reference voltage in Figure 70 with peak amplitude of 170V. Figure 70 displays the three-phase voltage delivered from the converter to the motor. The green waveform is the reference voltage with a phase of 0˚, the blue waveform is the voltage between the top and middle line of the system shifted by +120˚, and the red waveform is the voltage between the middle and bottom line shifted by -120˚, all with the amplitude of 170V.

Figure 71 displays the current from the single-phase source driving the Smith converter and the 1/3HP delta-connected motor. Its amplitude is 1.862A with an offset of 0.922A, increasing the peak current to 2.784A. The source current offset is due to the same reason as the other systems. The current is not initialized to zero by the simulation settings. Therefore, we incorporate the varistor into the network to initialize the voltage and the current. This is shown in Figure 73, below.

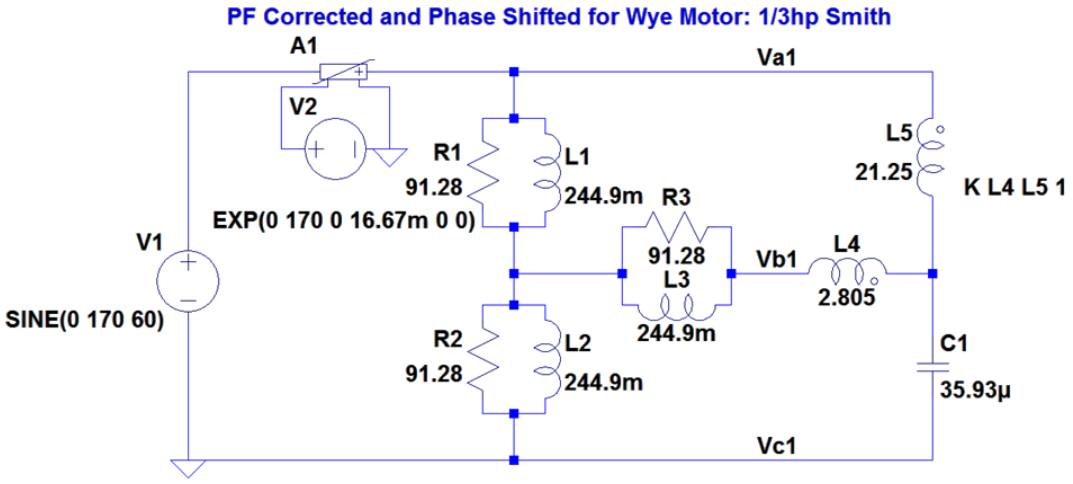

Figure 73: LTspice model of Smith converter with 1/3hp wye-connected motor with varistor

The exponential peak voltage controlling the varistor is equal to the source at 170V and the time constant it set to 16.67ms corresponding to one period of the input voltage. The addition of the varistor results in the source current waveform shown in Figure 74 below, and is equivalent to the original waveform but with the reference set at 0A. The amplitude balance and shift of the three-phase current through the motor also remains unaffected by the varistor.

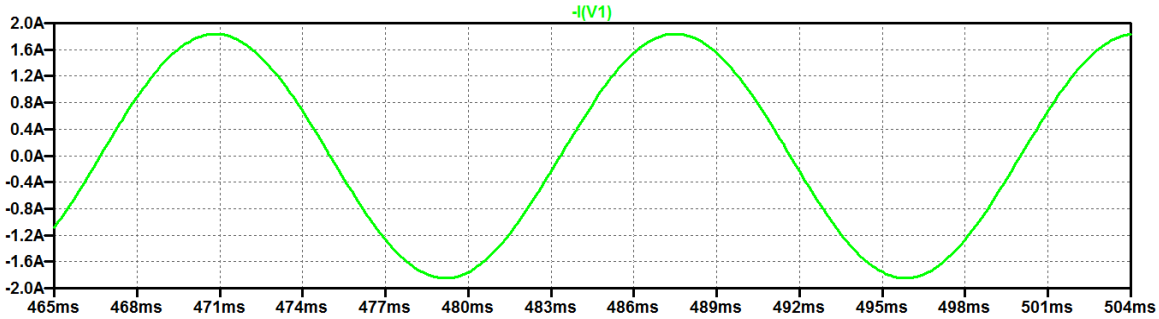

Figure 74: Source current with Smith converter and 1/3HP wye-connected motor with varistor

Figure 72 displays the current from the single-phase source. The green waveform is the current through resistor R1, the blue waveform is the current through resistor R2, and the red waveform is the current through resistor R3, all with the amplitude of 1.075A. The nominal current of the above wye-connected motor run by three-phase source is 1.862A. This is $\sqrt{3}$ times larger than the simulated value, due to wye-to-delta transformation. The difference between the source current and the motor current is also due to the delta-connected source created by the converter.

Since the results for both the 1/3hp and 25hp motors provide the desired Smith converter components for motors operating at a power factor of 0.707 and above, it can be concluded that the power factor is what controls the outcome of the converter derivations. Due to the relationship that higher horsepower motors experience higher power factors, a second conclusion can be made that using a higher horsepower motor is

recommended to better achieve the power factor value. Running a smaller horsepower motor with a larger slip will introduce more current into the system, decreasing the efficiency and heating up the motor that could eventually damage the system if it is run for a long period of time. But it is not required to use a larger horsepower motor, since the Smith converter can be derived using the 1/3hp motor.

Now that the derivations have been verified for the Marinus/Malengret and Smith single to three-phase conversion networks, it is important to look at the sensitivity of each system. There are two factors that can cause the system to function out of the bounds of ideality. These factors consist of the variation of the torque within the motor and the variation of the components within the conversion networks.

3.1 Measurement Procedure

The measurement method used for the sensitivity analysis is a form Error Vector Magnitude (EVM). EVM is usually used for complex communication systems to measure modulation accuracy. It considers all of the potential phase and amplitude distortions as well as noise and provides a single comprehensive measurement figure for determining the quality of a circuit or product [13]. This study can use the same form of analysis since we want to measure the phase and amplitude distortions due to variation in the torque of the motor and the values of the components in the conversion network.

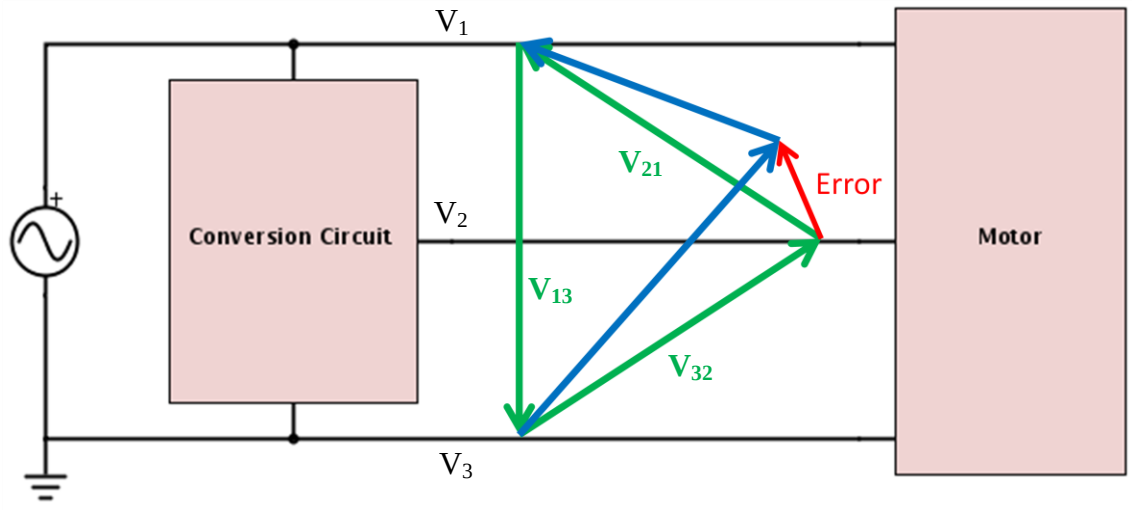

Figure 75: Block diagram of Error Vector Magnitude (EVM) measurement method

Figure 75, depicts our EVM method for the sensitivity analysis. The green vectors represent the phasor voltage for the system with components of nominal value and the blue vectors represent the phasor voltage for the system with components of varying values. For the two conversion networks and the two motor winding configurations there are three connection points between the conversion network and the motor. The top line of the conversion circuit, coming from the input source is the same potential as the top line connected to the motor. The bottom line connected to the conversion circuit, attached to the same ground as the source is also the same potential as the bottom line connected to the motor. Therefore in all different cases, the middle line is the only voltage that is changing.

The connection of the top and bottom line across the source causes vector voltage $\mathbf{V}_{13}$ remain constant in magnitude and phase, as long as the source does not change. That leaves two varying vector voltages, $\mathbf{V}_{32}$ and $\mathbf{V}_{21}$. Due to Kirchhoff's Voltage Law (KVL), which says that the sum of all the voltages in a loop equals zero, the sum of the voltage vectors must close the vector triangle. This means that along with variations in the converter and the motor, the connected tip of the two varying vectors is moving with relation to the nominal position, making the magnitude and phase of the varying voltages change together. With this relationship, we can subtract the potential vector of the nominal system (green) from the potential vector of the varied system (blue) to obtain the error vector. The relationship between the two changing vectors is shown in Figure 76.

The change in one of the vectors causes an equal and opposite reaction in the other. The closed vector triangle, shown on the left in Figure 76, translates into the imaginary versus real plot on the right, which properly shows the 120˚ phase difference

between each voltage and the error relationship. This error vector causes $\mathbf{V}_{32}$ to increase in magnitude and phase, and equally decrease $\mathbf{V}_{21}$ in magnitude and phase.

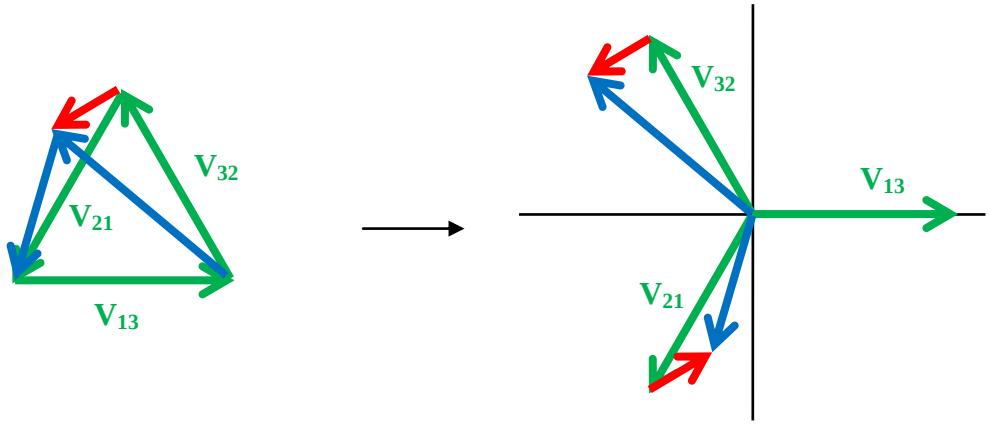

Figure 76: Closed triangle vector form to phasor plot representation of three-phase voltage

This method of measurement is a good technique for lab experimentation on systems of this nature, since the connections of the motor windings and conversion circuitry would be enclosed and would not always be easily accessible. As long as there are connection points, the voltage can always be probed, making this method easy to perform. To verify the accuracy of this measurement method, analysis will also be done on the current through the windings.

3.2 Torque Variation

The first set of sensitivity analysis is done on the torque variation of the motor. As discussed previously in Section 1.1.1, when modeling the resistance and inductance of the motor windings in parallel, the change in torque can be modeled as the change in resistance within the winding. From the results in Figure 13, the inductance value stays relatively the same and the resistance decreases as the torque increases. Therefore, we can model and simulate the sensitivity to torque variation as the change in resistance of the motor windings using LTspice. A variation of ±15% was chosen to analyze the

characteristics of the system with the torque varying around the operating point of the motor. Due to the extrapolation of data to acquire the winding resistance there is some margin of difference for the ±15% torque variation by ±0.5%.

3.2.1 Induction Motor with Marinus/Malengret Converter

Figure 77 displays the result for varying the torque by ±15% for both the wye and delta-connected motors. The voltage vectors resulting in the negative quadrant are due to the +15% change in torque and the vectors in the positive quadrant are due to the -15% change in torque. The relationship between the change in error vector as the torque shows that the system is more sensitive to the decrease in torque versus the increase. The rectangular form dimensions of the vector are in terms of percentage of voltage, therefore the polar form of the vector has a magnitude of percent peak nominal voltage and the phase error in degrees.

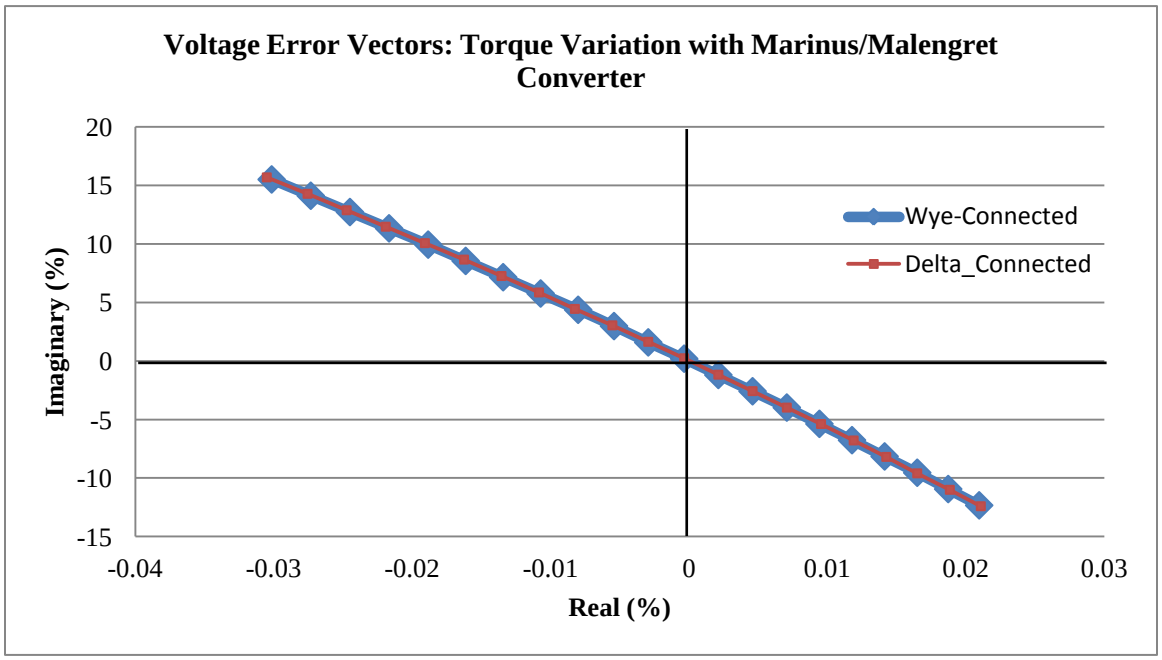

Figure 77: Voltage error vector results of ±15% torque variation on motor with MM converter

The variation in toque causes the same error vector results for both the wye and delta-connected motors. The magnitude of the error voltage vector changes by roughly 15% and 13% for the -15% and +15% changes in torque, respectively. Both error vectors move along the imaginary axis and deviate from normal by 0.1˚. This means that the connecting point of V_{21} and V_{32} changes vertically together and will cause the magnitudes and phase to change at the same rate, with some difference due to the slight phase difference of the error vector caused by the phase converter. This relationship is shown in Figure 78.

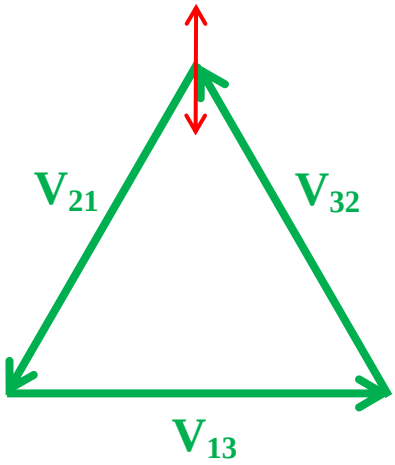

Figure 78: Closed three-phase vector triangle (green) with error vectors (red)

To further examine the effects of torque variation on both motors for the Marinus/Malengret converter, below are the figures that display the variation of the current in the time domain. Figure 79 throughFigure 82 display the nominal current waveforms in a delta-connected motor from a three-phase source for the converter at nominal, +15% and -15% torque.

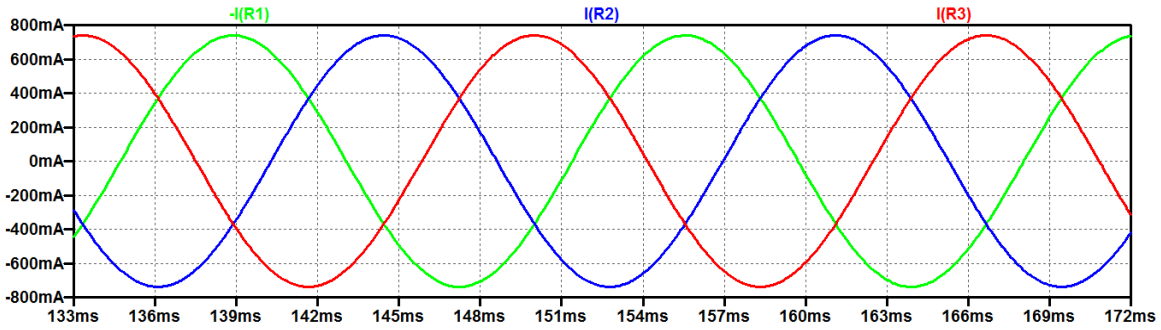

Figure 79: Three-phase current of 1/3HP delta-connected motor driven by three-phase source

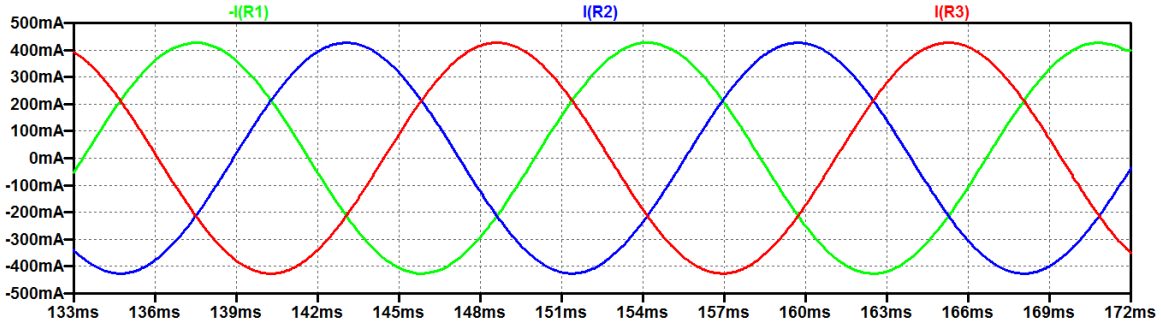

Figure 80: Three-phase current from MM converter to 1/3HP delta-connected motor at nominal torque

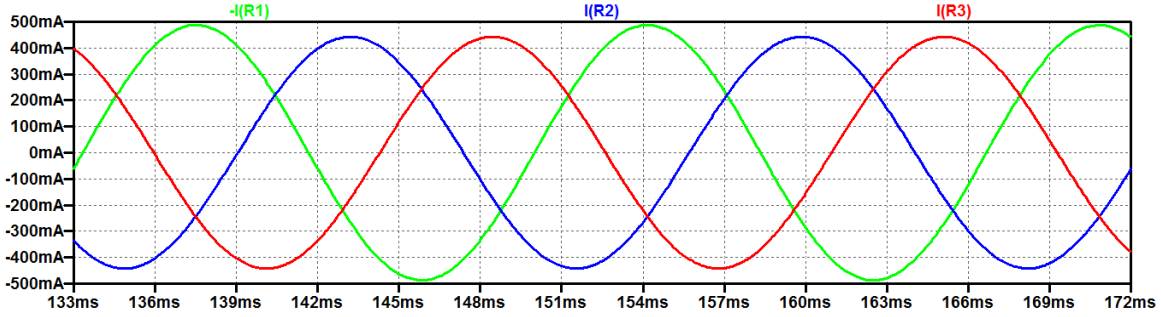

Figure 81: Three-phase current from MM converter to 1/3HP delta-connected motor at +15% torque

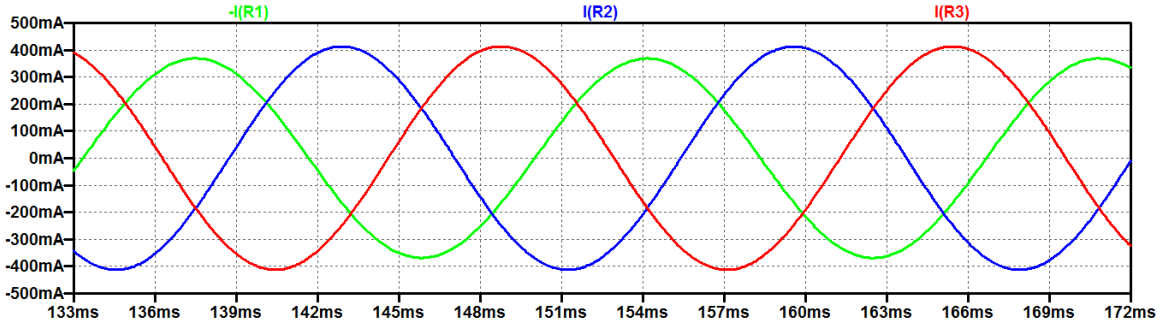

Figure 82: Three-phase current from MM converter to 1/3HP delta-connected motor at -15% torque

The connection of the conversion network across the other two windings causes an equal effect on amplitude and phase. The -15% and +15% torque changes causes a 3.2% and 3.7% amplitude error, respectively, in both R_2 and R_3. The currents experience a phase change equivalent in value but in opposite directions. Both angles decrease to ±116.4˚, moving in toward the reference current for the -15% change in torque. For the +15% change in torque, both current phases increase to ±123.4˚, moving away from the reference current. The phase errors for the current waveforms are 3% and 2.8% for the -15% and +15% torque variation, respectively.

Figure 83 throughFigure 86 display the effects of the torque on the single-phase source current compared to the source voltage. The current phases for the nominal, +15% and -15% torque change are 0.008˚, 0.004˚ and 0.13˚, respectively. The current magnitudes for the nominal, +15% and -15% torque change are 1.280A, 1.291A and 1.293A, respectively. The ±15% torque variation causes a maximum current and phase increase of 1.02% and 0.072%, respectively.

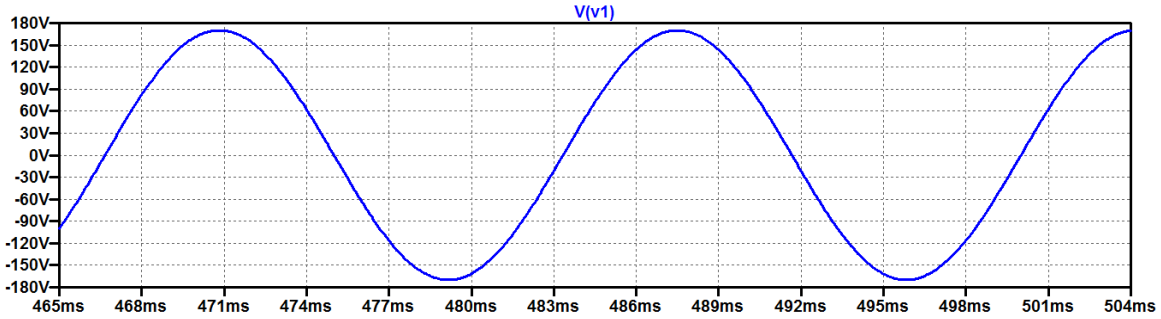

Figure 83: Single-phase source voltage with MM converter and 1/3HP delta-connected motor

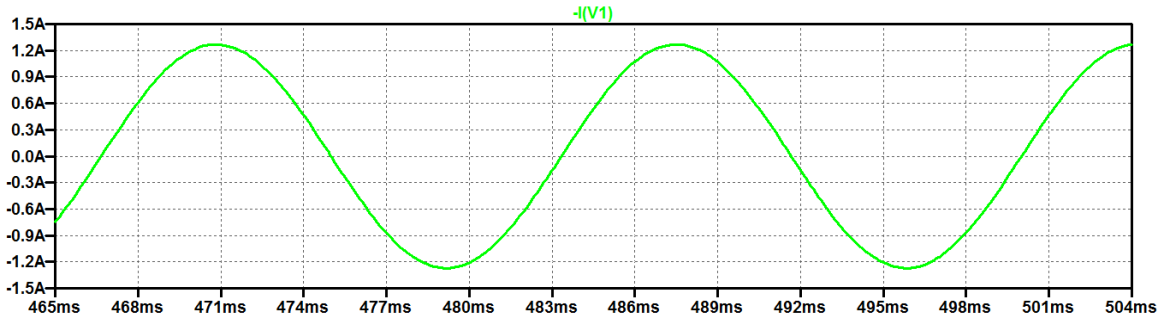

Figure 84: Source current with MM converter and 1/3HP delta-connected motor at nominal torque

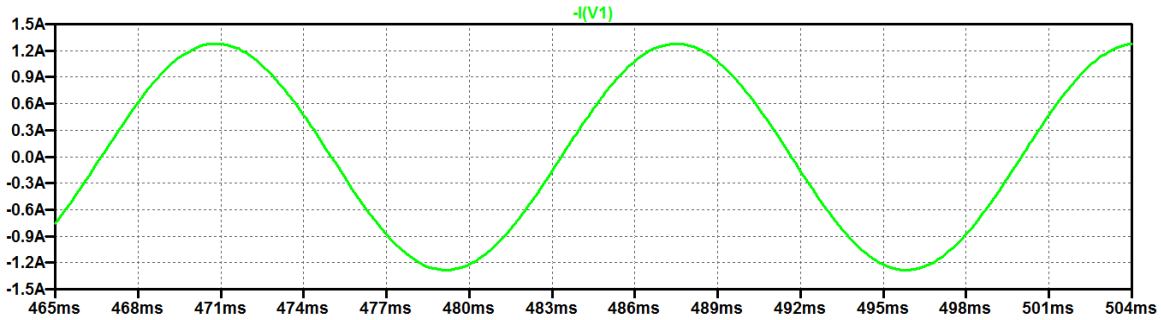

Figure 85: Source current with MM converter and 1/3HP delta-connected motor at +15% torque

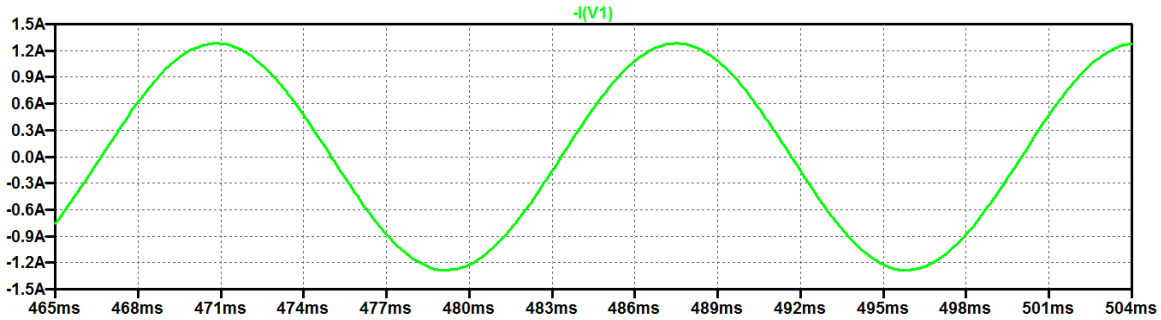

Figure 86: Source current with MM converter and 1/3HP delta-connected motor at -15% torque

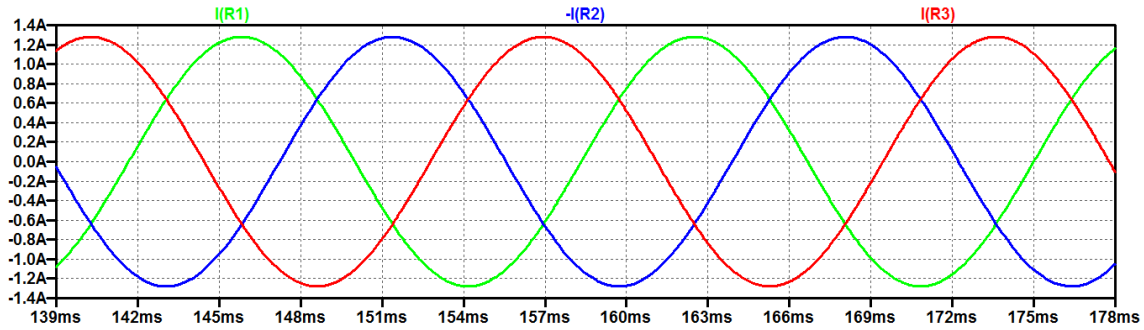

Figure 87: Three-phase current of 1/3HP wye-connected motor driven by three-phase source

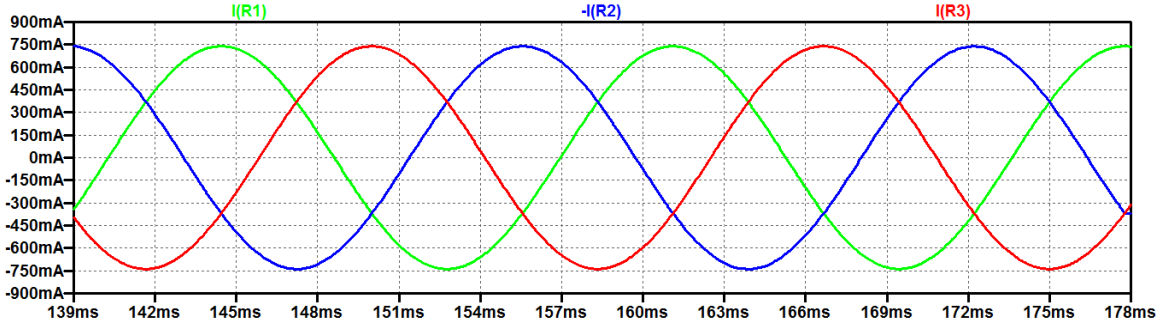

Figure 88: Three-phase current from MM converter to 1/3HP wye-connected motor at nominal torque

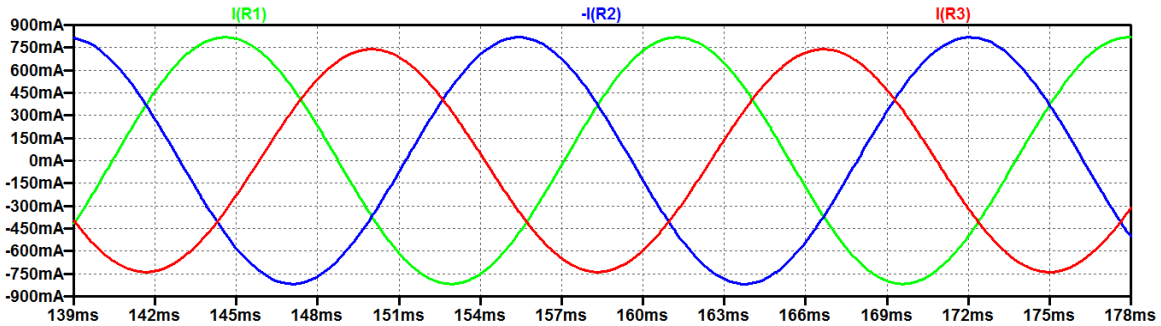

Figure 89: Three-phase current from MM converter to 1/3HP wye-connected motor at +15% torque

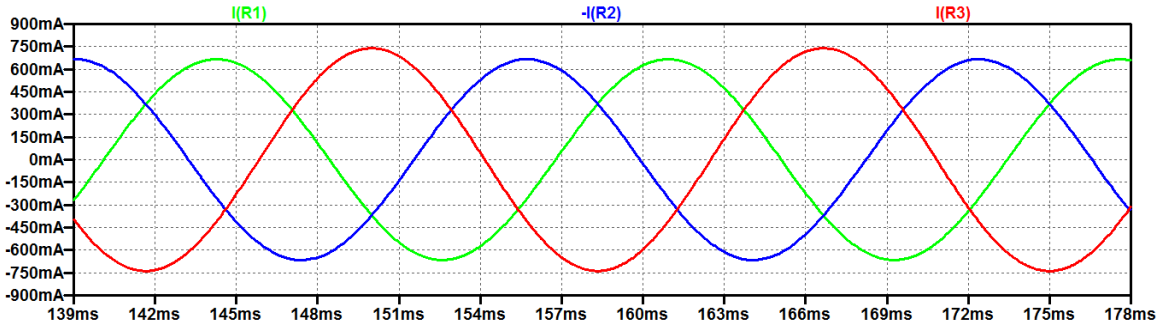

Figure 90: Three-phase current from MM converter to 1/3HP wye-connected motor at -15% torque

Figure 87 displays the current in the 1/3HP wye-connected motor operating from a three-phase source, each waveform resulting in a peak value of 1.28A. Figure 88 displays the current at nominal torque, with the same peak values of 738.9mA. Figure 89 displays the current at +15% change in torque with peak values of about 818.0mA for R_1 and R_2, and 738.9mA for R_3. Figure 90 displays the current at -15% change in torque with peak values of about 665.7mA for both R_1 and R_2, and 738.9mA for R_3. The current through R_3 remains the same no matter the change in torque. The connection of R_3 to the conversion network holds the value steady as it causes the rest of the circuit that is parallel to it to vary. This could be due to an H-bridge relationship

The connection of the conversion network across the other two windings causes an equal effect on the amplitude and phase. The -15% and +15% torque changes cause a 9.9% and 10.7% amplitude error, respectively, in both R_1 and R_2. The currents experience a phase change equivalent in values but in opposite directions. Both angles decrease to ±116.8˚ moving in towards the reference current for the -15% change in torque. For the +15% change in torque, both current phases increase to ±123.7˚, moving away from the reference current. The phase errors for the current waveforms are 2.7% and 3.1% for the -15% and +15% torque variation, respectively.

Figure 91 through Figure 94 display the effects of the torque on the single-phase source current compared to the source voltage. The current phases for the nominal, +15% and -15% torque change are 0.008˚, 0.004˚ and 0.13˚, respectively. The current magnitudes for the nominal, +15% and -15% torque change are 1.280A, 1.290A and 1.293. The ±15% torque variation causes a maximum current and phase increase of 1.02% and 0.072%, respectively, like in the delta-connected motor.

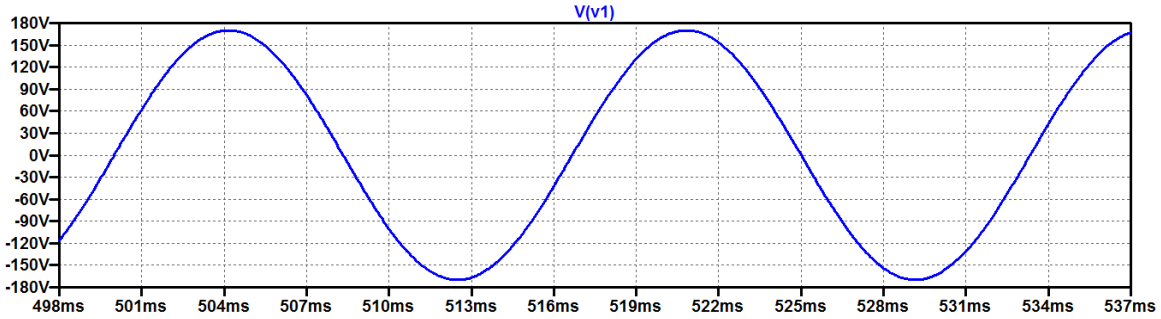

Figure 91: Single-phase source voltage with MM converter and 1/3HP wye-connected motor

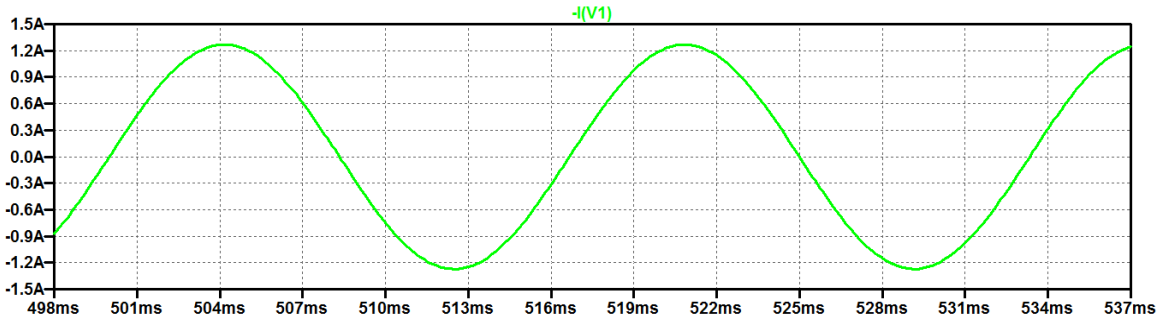

Figure 92: Source current with MM converter and 1/3HP wye-connected motor at nominal torque

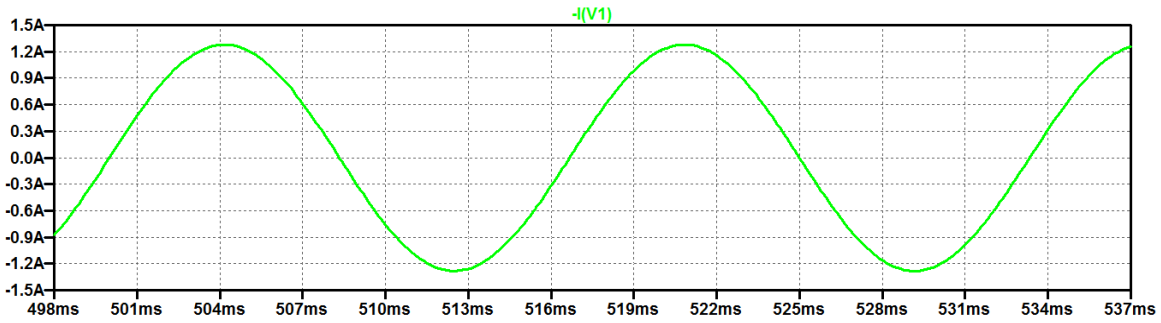

Figure 93: Source current with MM converter and 1/3HP wye-connected motor at +15% torque

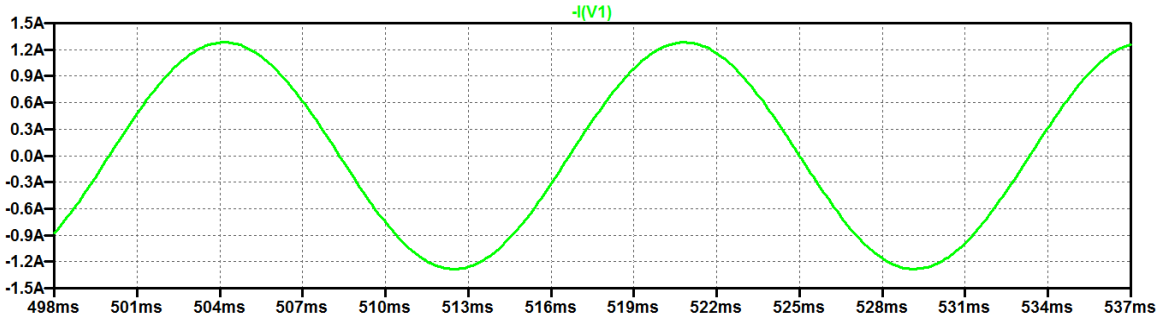

Figure 94: Source current with MM converter and 1/3HP wye-connected motor at -15% torque

3.2.2 Induction Motor with Smith Converter

Figure 95 displays the result for the torque variation of the wye and delta-connected motors, represented by the variation of the motor winding resistance, when connected to the Smith converter. The voltage vectors resulting in the negative quadrant are due to the +15% change torque and the vectors in the positive quadrant are due to the -15% change in torque. The relationship between the change in error vector as the torque shows that the system is more sensitive to the decrease in torque versus the increase. The rectangular form dimensions of the vector are in terms of percent voltage, therefore the polar form of the vector have a magnitude of percent peak nominal voltage and the phase error in degrees.

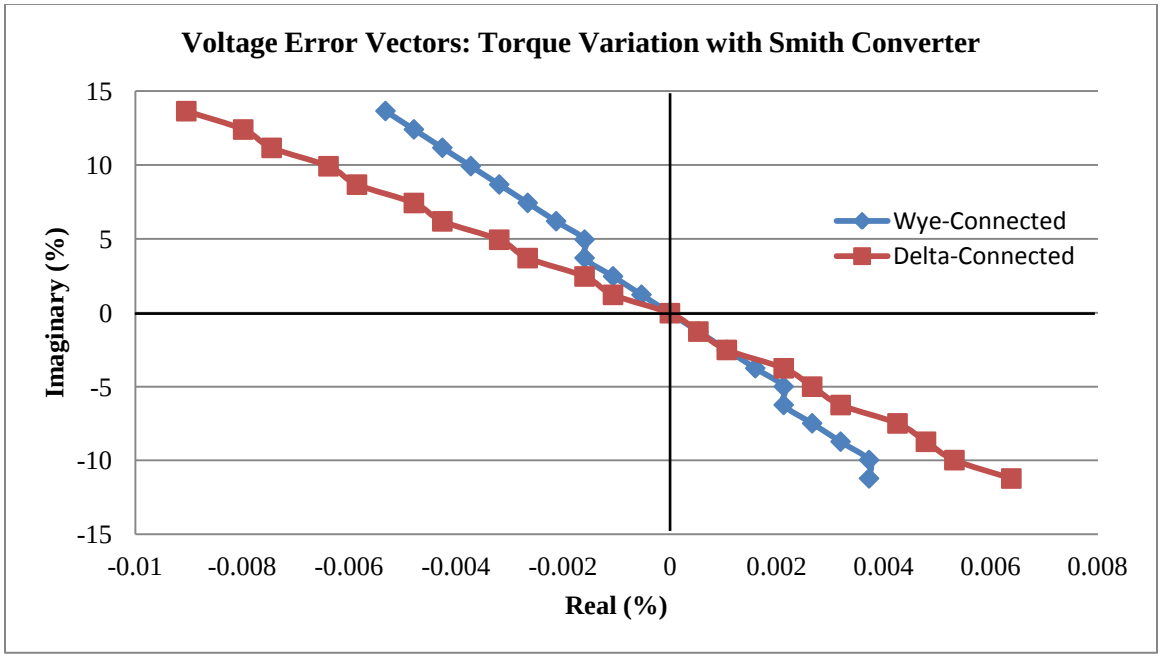

Figure 95: Voltage error vector results from ±15% torque variation on wye and delta-connected induction motor with Smith converter

The error voltage magnitudes change by approximately 13.6% and 11.2% for the +15% and -15% torque change, respectively. The error vectors move along the imaginary axis and deviate from the normal by 0.02˚ and 0.04˚ for the wye and delta-connected

motors, respectively, allowing the assumption that it's along the imaginary axis. This means the connection point of V_{21} and V_{32} in Figure 78, changes vertically together and causes the magnitudes and phase to change at the same rate, with less phase error than the Marinus/Malengret converter. To further examine the effects of torque variation, the current is simulated in the time domain for the Smith converter.

Figure 96 displays the current in the 25HP delta-connected motor operating from a three-phase source with each waveform resulting in a peak value of 12.85A. Figure 97 displays the current at nominal torque, with a peak current value of 7.42A. Figure 98 displays the current at +15% change in torque with peak current values of 8.35A for R_1 and 7.66A for both R_2 and R_3. Figure 99 displays the current at -15% change in torque with peak current values of 6.53A for R_1 and 7.20A for both R_2 and R_3. The current through R_1 only changes in magnitude because that is the winding that is connected across the source and since the phase and magnitude of the voltage is held constant. The difference of the peak current through R_1 is 12.5% and 12.0% for the +15% and -15% torque change, respectively. The connection of the conversion network across the other two windings causes an equal effect on amplitude and phase. The +15% and -15% torque changes causes a 3.2% and 3.0% amplitude error, respectively, in both R_2 and R_3. The currents experience a phase change equivalent in value but in opposite directions. Both angles decrease ±116.93˚ moving in toward the reference current for the -15% change in torque. For the +15% change in torque, both current phases increase to ±123.04˚, moving away from the reference current. The phase errors for the current waveforms are 2.6% and 2.5% for the -15% and +15% torque variation, respectively.

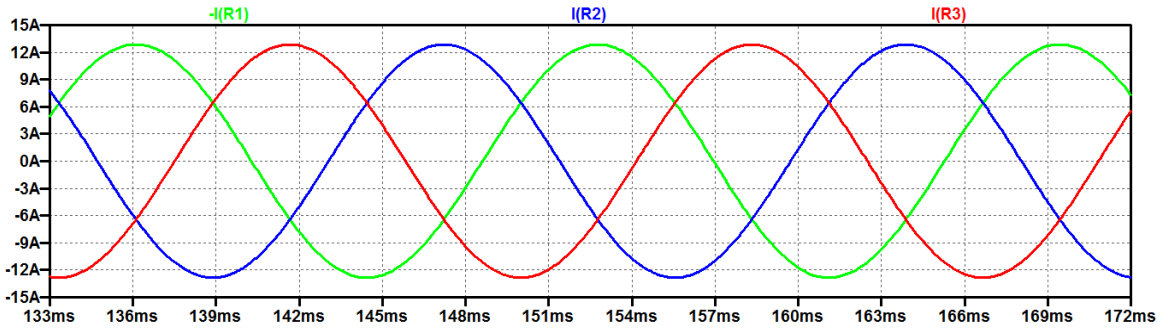

Figure 96: Three-phase current of 25HP delta-connected motor driven by three-phase source

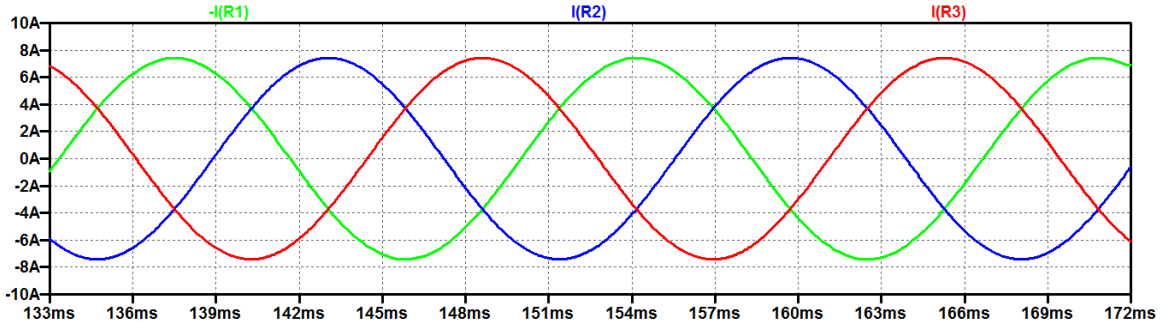

Figure 97: Three-phase current from Smith converter to 25HP delta-connected motor (nominal torque)

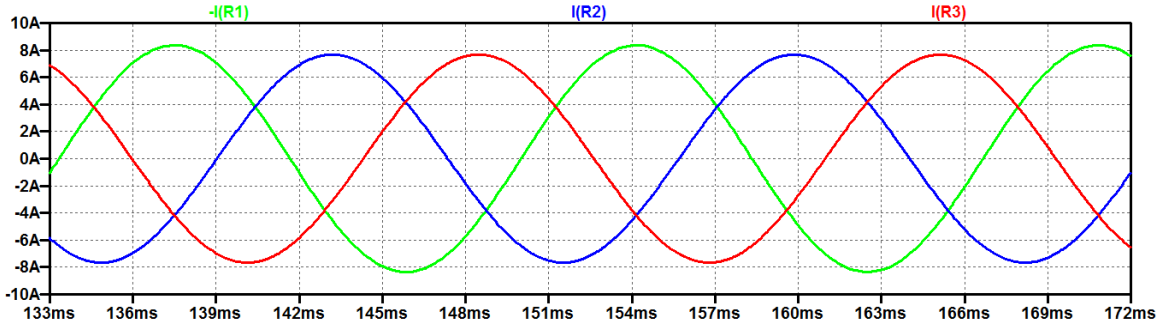

Figure 98: Three-phase current from Smith converter to 25HP delta-connected motor (+15% torque)

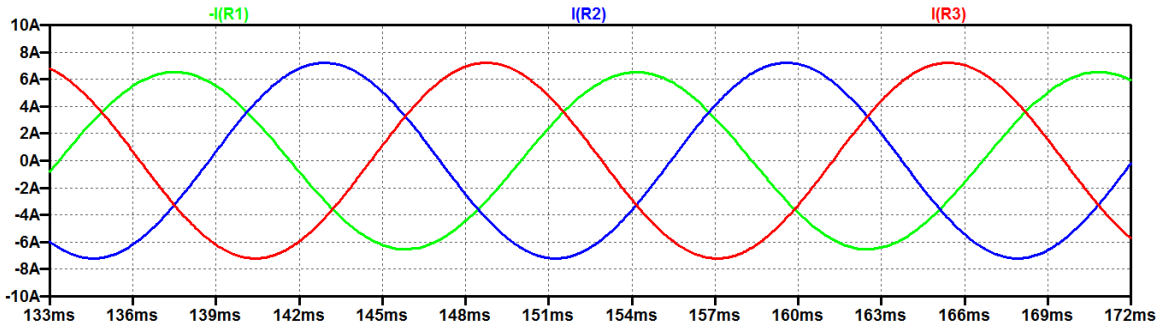

Figure 99: Three-phase current from Smith converter to 25HP delta-connected motor (-15% torque)

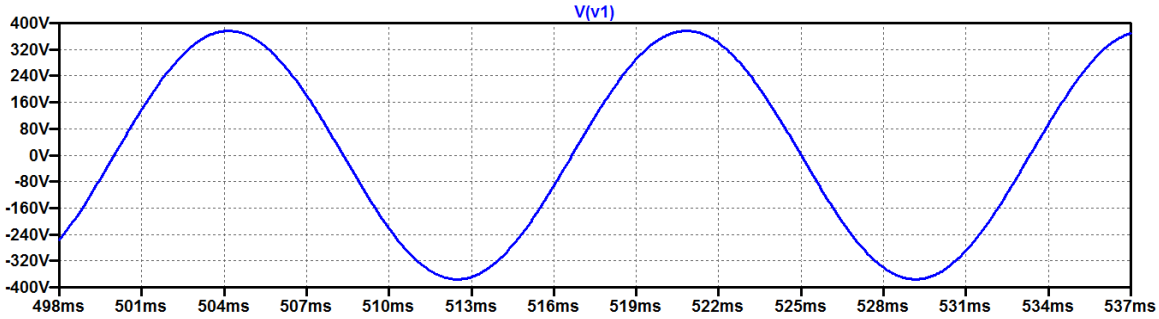

Figure 100: Single-phase source voltage with Smith converter and 25HP delta-connected motor

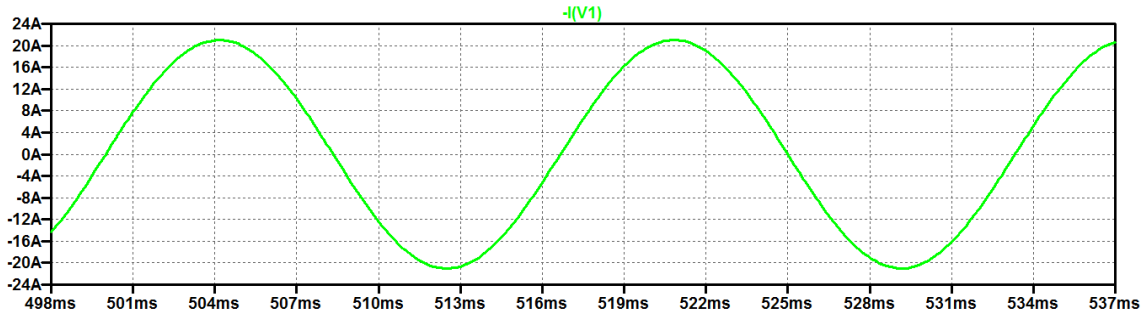

Figure 101: Source current with Smith converter and 25HP delta-connected motor at nominal torque

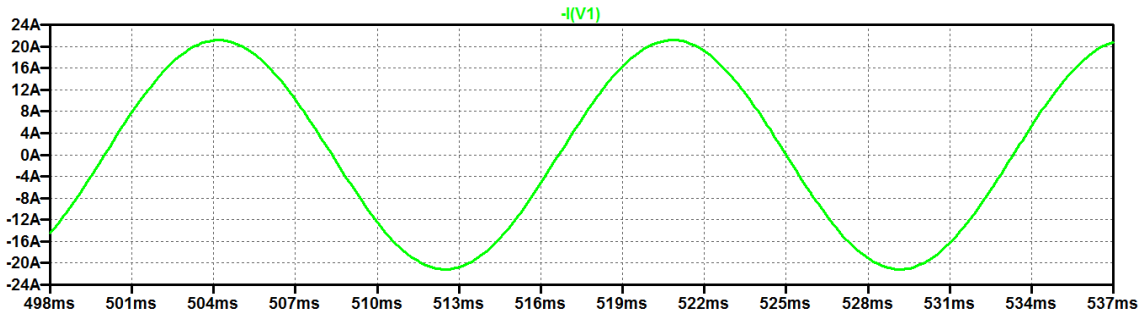

Figure 102: Source current with Smith converter and 25HP delta-connected motor at +15% torque

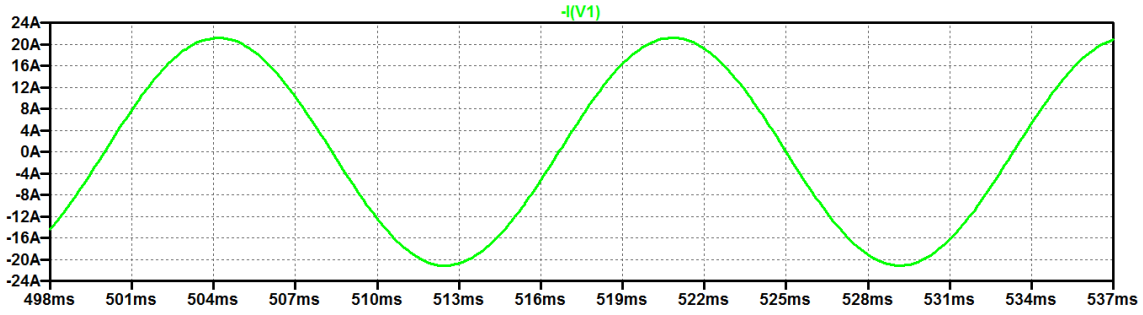

Figure 103: Source current with Smith converter and 25HP delta-connected motor at -15% torque

Figure 100 throughFigure 103 display the effects of the torque on the single-phase source current compared to the source voltage. Due to the offset issue previously discovered, a varistor added to the network to gradually increase the source to initialize the voltage and current to zero resulting in the elimination of the offset. The current phases for the nominal, +15% and -15% torque change are 0˚, 0˚ and 0.002˚, respectively. The current magnitudes for the nominal, +15% and -15% torque change are 22.26A, 22.39A and 22.41A, respectively. The ±15% torque variation causes a maximum current and phase increase of 0.76% and 0.001%, respectively.

Figure 104 displays the current in the 25HP wye-connected motor operating from a three-phase source with each waveform resulting in a peak value of 22.26A. Figure 105 displays the current at nominal torque, with the peak current of 12.85A. Figure 106 displays the current at +15% change in torque with peak current values of about 14.09A for both R_1 and R_2, and 12.85A for R_3. Figure 107 displays the current at -15% change in torque with peak current values of about 11.71A for R_1 and R_2, and 12.85A for R_3. The current through R_3 remains the same no matter the change in torque.

The connection of the conversion network across the other two windings causes an equal effect on the amplitude and phase. The -15% and +15% torque changes causes an 8.9% and 9.6% amplitude error, respectively, in both R_1 and R_2. The currents experience a phase change equivalent in values but in opposite directions. Both angles decrease to ±117.13˚ moving in towards the reference current for the -15% change in torque. For the +15% change in torque, both current phases increase to ±123.26˚, moving away from the reference current. The phase errors for the current waveforms are 2.3% and 2.7% for the -15% and +15% torque variation, respectively.

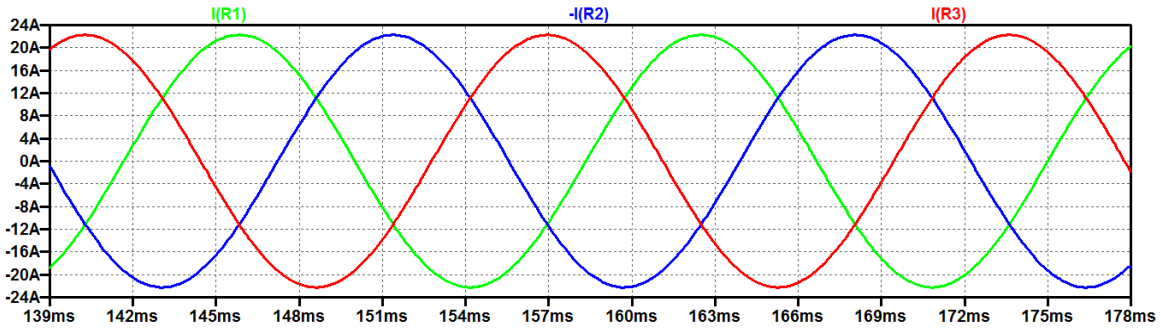

Figure 104: Three-phase current of 25HP wye-connected motor driven by three-phase source

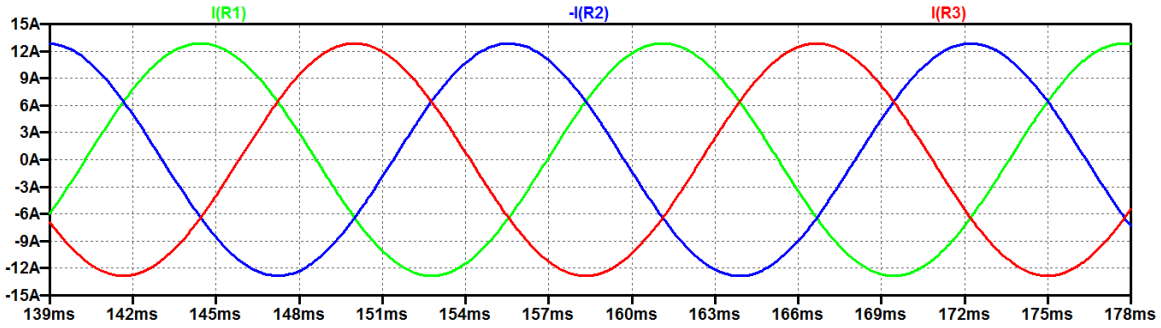

Figure 105: Three-phase current from Smith converter to 25HP wye-connected motor (nominal torque)

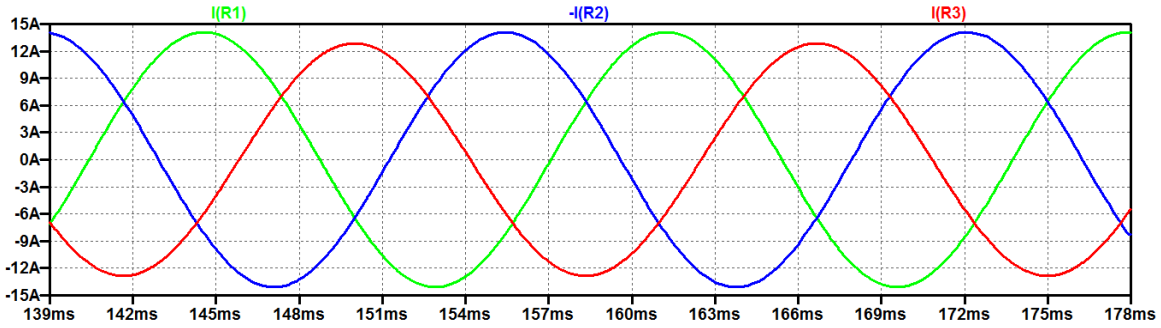

Figure 106: Three-phase current from Smith converter to 25HP wye-connected motor (+15% torque)

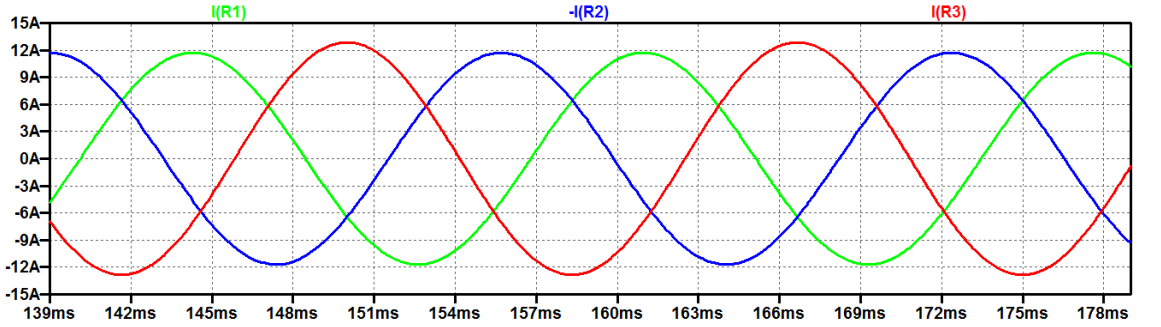

Figure 107: Three-phase current from Smith converter to 25HP wye-connected motor (-15% torque)

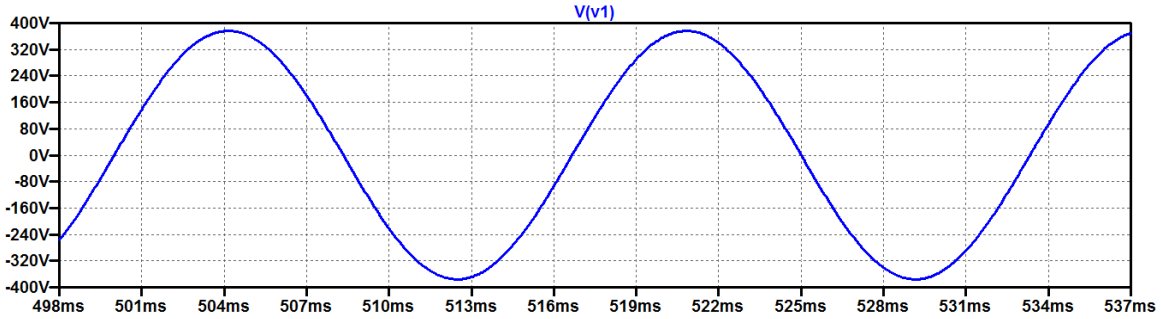

Figure 108: Single-phase source voltage with Smith converter and 25HP wye-connected motor

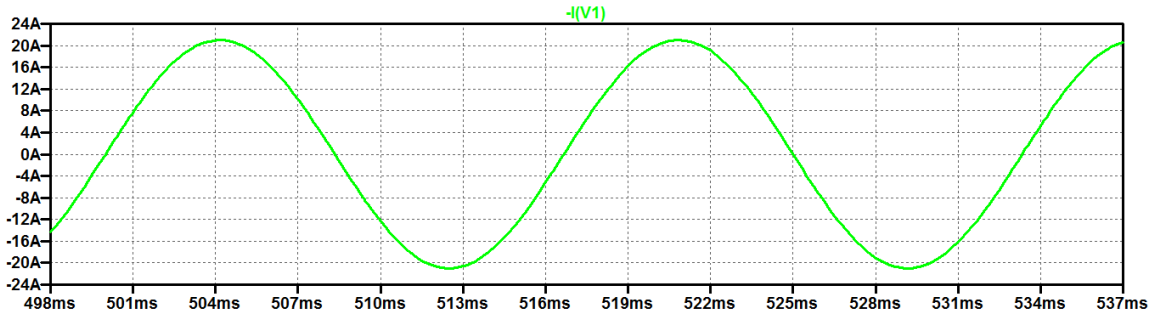

Figure 109: Source current with Smith converter and 25HP wye-connected motor at nominal torque

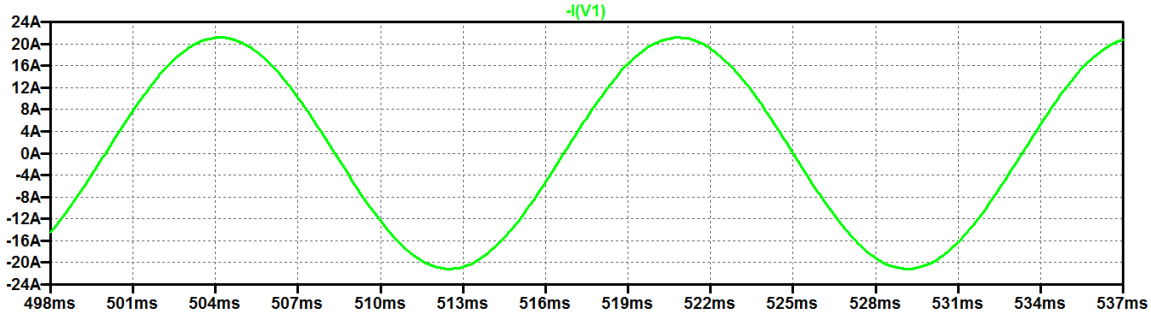

Figure 110: Source current with Smith converter and 25HP wye-connected motor at +15% torque

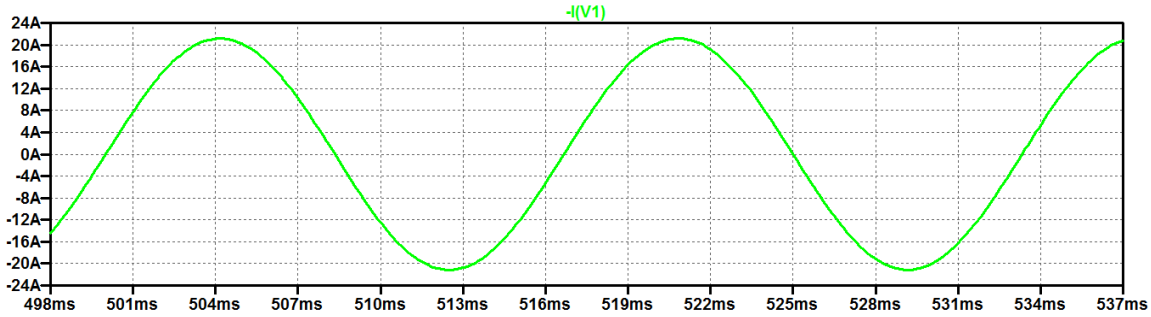

Figure 111: Source current with Smith converter and 25HP wye-connected motor at -15% torque

Figure 108 through Figure 111 display the effects of the torque on the single-phase source current compared to the source voltage. Due to the offset issue previously discovered, a varistor added to the network to gradually increase the source to initialize the voltage and current to zero resulting in the elimination of the offset. The current phases for the nominal, +15% and -15% torque change are 0˚, 0˚ and 0.002˚, respectively. The current magnitudes for the nominal, +15% and -15% torque change are 22.26A, 22.39A and 22.41A, respectively. The ±15% torque variation causes a maximum current and phase increase of 0.76% and 0.001%, respectively, like with the delta-connected motor.

Overall, the variation in torque doesn't have too much effect on the phase of each system. With the ±15% change in torque, two of the three phases change between 2% and 3%. The converter that experienced the smallest phase change was the Smith converter. The wye-connected motor experiences amplitude variation for two of the three phases, whereas the delta-connected motor network experiences amplitude variation in all three but mostly in only one. The input source current amplitude doesn't vary more 0.46% and 0.59% for the Marinus/Malnegret and Smith converters, respectively. The phase changes by 0.002% and 0.14%. Therefore, the change in source current is minimal.

As a total, the systems are more sensitive to the decrease in torque versus the increase. This is due to the stability of the conversion network. The single to three-phase converters are designed for a certain resistance of the motor winding and when the resistance is increased in the parallel winding, making the system more inductive and capacitive, larger transients are introduced. When analyzing the data for both motors, the

Smith converter proves to be less sensitive in both amplitude and phase change. This could be due to the coupling of the inductors.

3.3 Conversion Circuit Component Variation

Another factor that could contribute to the sensitivity of the three-phase system is the tolerance of each component within the conversion network. Monte Carlo analysis is performed to study the effects due the component variation. The way this method works is that the simulation randomly selects component values within a specified tolerance range about the nominal value. The number of random values is set to obtain a desired number of events. From this, a trend is formulated to specify the worst possible outcome. The parameters of this study include tolerances of ±5% and ±10%, and 500 random events. The percentages are based on tolerances of components that are currently available on market. The number of events is based on how many it takes to achieve the full trend shape but not have too many of the individual points overlapping. The number of events that were initially studied was 100, 300, 500 and 1000. From those, the parameter of 500 events was chosen.

3.3.1 Marinus/Malengret Converter Component Variation

Figure 112 and Figure 113 display plots of voltage error vectors for both wye and delta-connected motors run by the Marinus/Malengret converter. The origin of the plot represents zero voltage error and extends from the origin to each blue data point in each plot. The vertical and horizontal axes represent the imaginary coefficient of the rectangular form of the error vector the real coefficient. Both coefficients are the normalized so that in the polar form, the vector magnitude is the percent voltage error in reference to the nominal voltage and the phase is the direction the connecting point of the

two varying vectors is moving, like in Figure 78 from the previous section. Each plot exhibits close to a linear relationship through the origin of the real-imaginary axis. The top right quadrant displays the +5% and +10% component variation whereas the bottom left quadrant displays the -5% and -10% component variation.

When the wye and delta-connected motors are run by the Marinus/Malangret converter, the voltage error is evenly distributed along an angle of about 15˚ and 205˚ from the origin for both component variations. The error vectors can experience a direction of any angle but due to the trend in data, it is more likely for the vector to point along the 15˚ and 205˚ direction to the opposite ends of the rectangular shaped plot trend. These vectors represent the maximum error of 14% and 28% magnitude voltage and can rotate to the outer most corners by ±5˚ and ±10˚, with a ±1% and ±2% change in magnitude for the ±5% and ±10% component variation, respectively. The width of the rectangular trend is approximately 2% and 4% magnitude voltage for ±5% and ±10% component variation, respectively.

The vectors that formulate around the origin of the plot cause less of an error since the magnitude is less that 5% magnitude voltage even though the angle is varying between 0˚ and 360˚. In referencing Figure 78, we can visualize that the small magnitude of the error vector rotating around the origin in a circular motion will cause a small error in the two voltage vectors V_{32} and V_{21}. The vectors that reach outer most corners of the trend will cause a larger error of V_{32} and V_{21} due to the larger vector magnitude.

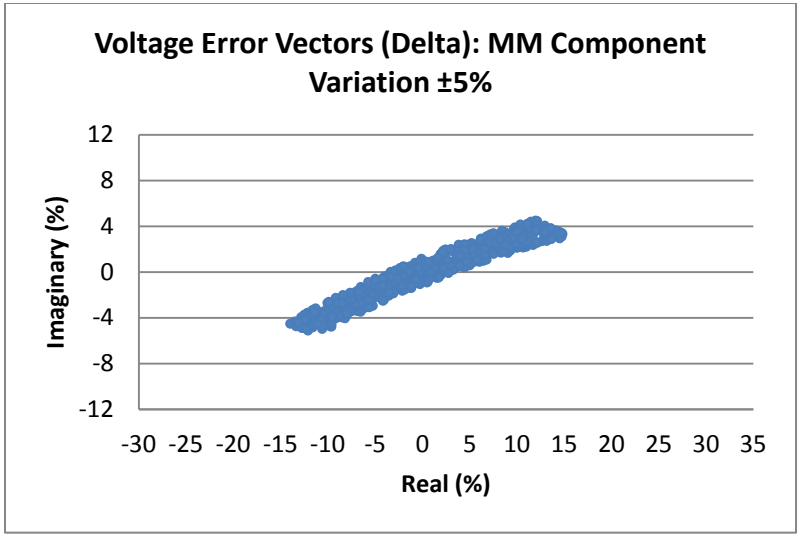

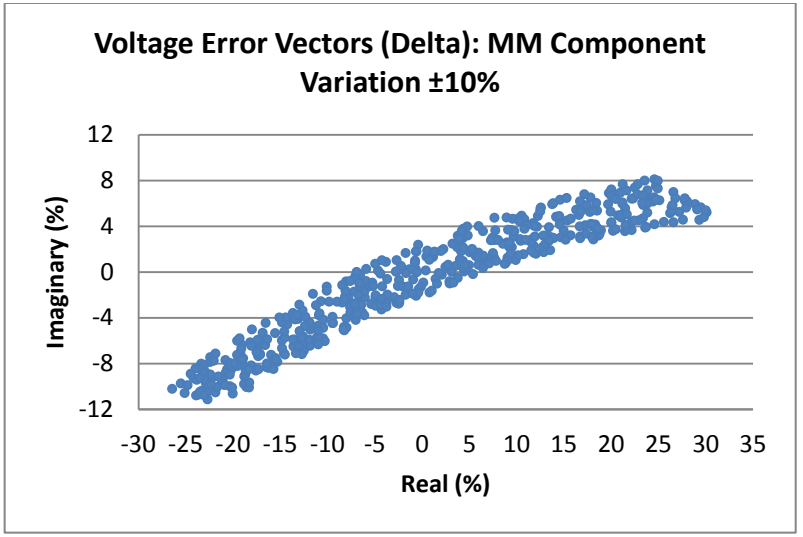

Figure 112: Error vector plot of ±5%/ ±10% component variation Monte Carlo in Marinus/Malengret converter with delta-connected motor

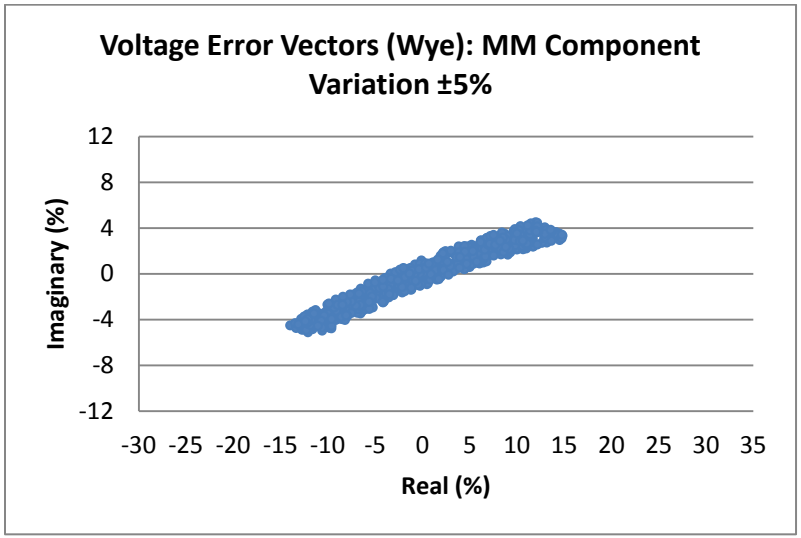

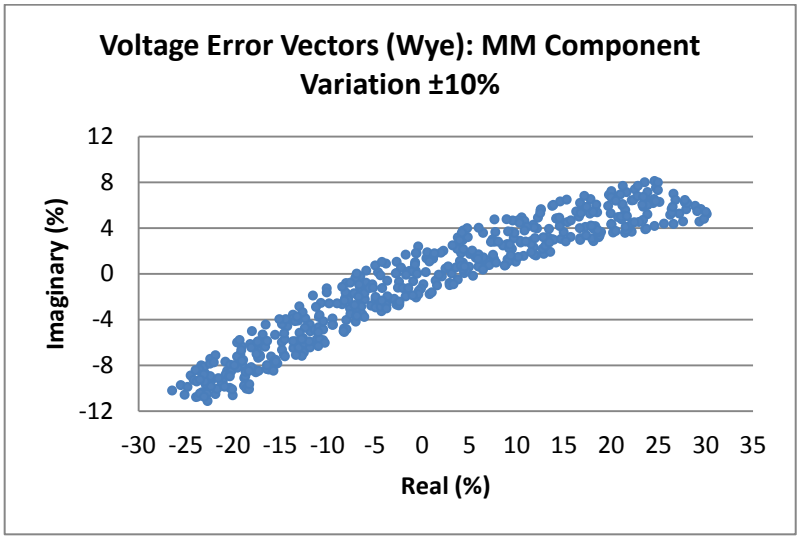

Figure 113: Error vector plot of ±5%/±10% component variation Monte Carlo in Marinus/Malengret converter with wye-connected motor

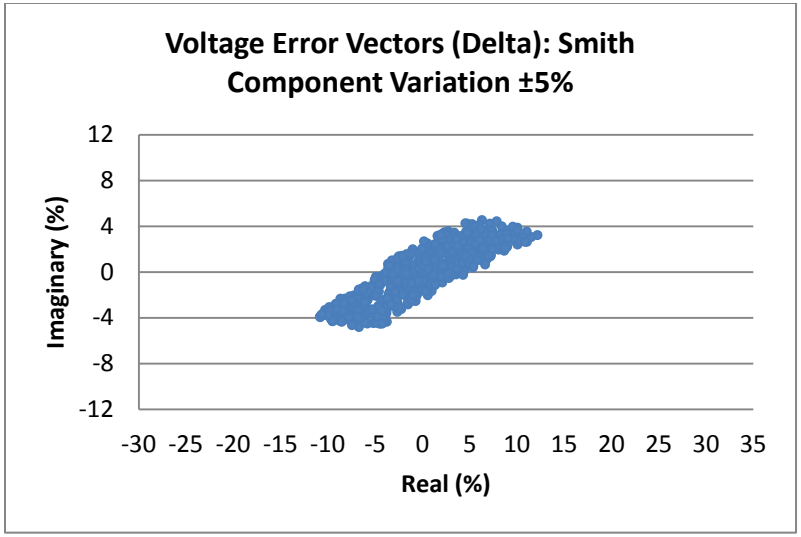

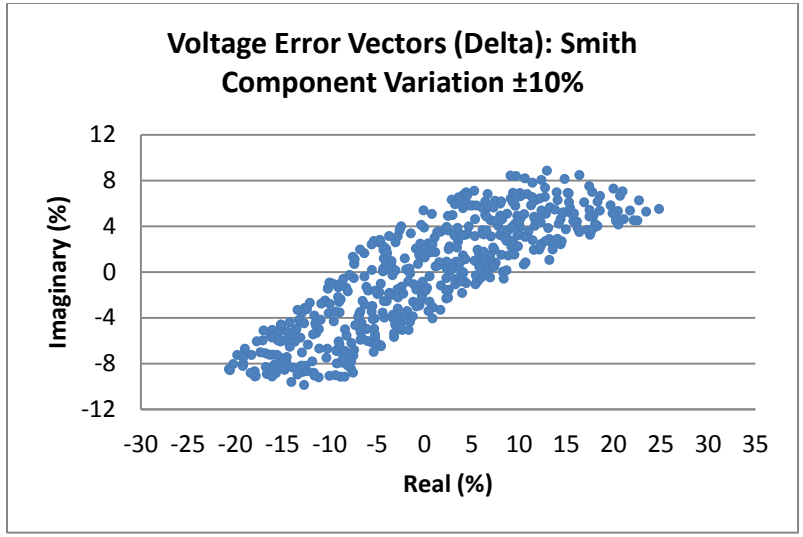

Figure 114: Error vector plot of ±5% and ±10% component variation Monte Carlo in Smith converter with delta-connected motor

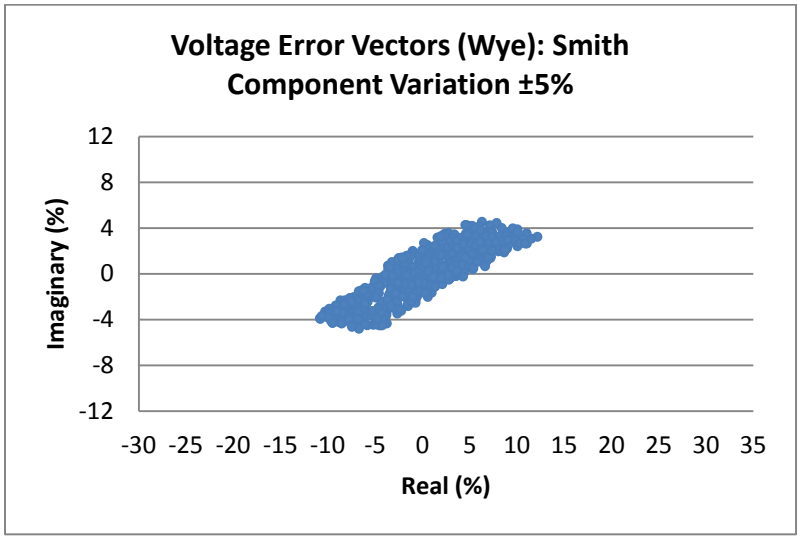

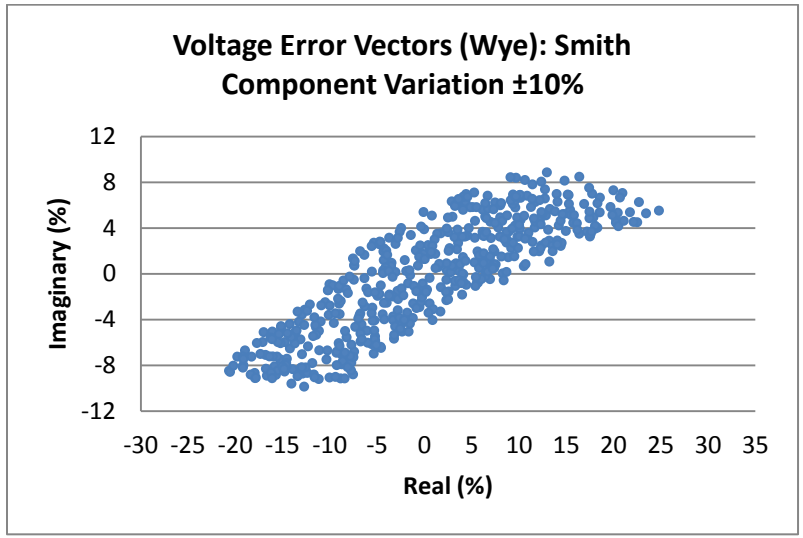

Figure 115: Error vector plot of ±5% and ±10% component variation Monte Carlo in Smith converter with wye-connected motor

3.3.2 Smith Converter Component Variation

Figure 114 and Figure 115 display the data collected for both wye and delta-connected motors run by the Smith converter. The data is displayed using the same parameters as the Marinus/Malengret component variation data. Like the previous section, the top right quadrant displays the +5% and +10% component variation whereas the bottom left quadrant displays the -5% and -10% component variation. The vector magnitude is the percent voltage error in reference to the nominal voltage and the phase is the direction the connecting point of the two varying vectors is moving, like in Figure 78.

When the wye and delta-connected motors are run by the Smith converter, the voltage error is evenly distributed along an angle of about 25˚ and 210˚ from the origin for both component variations. The error vectors can experience a direction of any angle but due to the trend in data, it is more likely for the vector to point along the 25˚ and 210˚ direction to the opposite ends of the rectangular shaped plot trend. These vectors represent the percent voltage error along the trend line of 10% and 18% magnitude voltage and can rotate to the outer most corners by ±13˚ for both ±5% and ±10% component variation, with a ±5% and ±7% change in magnitude, respectively. The width of the rectangular trend is approximately 4% and 8% magnitude voltage for ±5% and ±10% component variation, respectively.

Like the previous system, the vectors that formulate around the origin of the plot cause less of an error since the magnitude is less that 5% magnitude voltage even though the angle is varying between 0˚ and 360˚. In referencing Figure 78, we can visualize that the small magnitude of the error vector rotating around the origin in a circular motion

will cause a small error in the two voltage vectors V_{32} and V_{21}. The vectors that reach outer most corners of the trend will cause a larger error of V_{32} and V_{21} due to the larger vector magnitude.

The results of this testing concludes an overall trend that the component variation causes an even trade of magnitude and phase of the two branch voltages. As V_{21} decreases in magnitude and phase, V_{32} will increase as a result. If V_{21} increases in magnitude and phase, then V_{32} will decrease. There are some instances where the error voltage vectors are along the imaginary axis causing an equal change in magnitude and phase in V_{21} and V_{32}, but those occurrences are less likely to happen.

There are a few similarities and differences between the three conversion networks and their connections to the motors and the source. From the top level perspective, the Marinus/Malengret and Smith converters consist of three connections, shown in Figure 116. Two of the three connections are across the source so the potential of those lines remain constant as long as the source voltage remains constant. These two lines also connect to the motor, meaning there is only one line between the converter and the motor that is varying. The three-phase voltage comes from measuring between the lines meaning that the input voltage to the motor is line-to-line. Both wye and delta-connected motors can run off of this converted power.

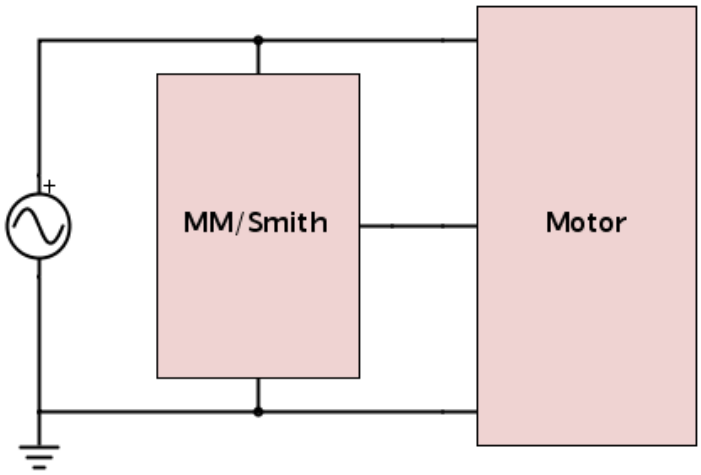

Figure 116: Block diagram of Marinus/Malengret and Smith converter connection to source and motor

Figure 117 displays the top level diagram for the Cal Poly converter and induction motor connection. The Cal Poly converter consists of four connection lines, with two connected across the source also leading to the motor like in the previous system. This means that there are two varying voltages between the converter and the motor. The

bottom of the four lines is connected to a neutral potential and the other three lines are measured with reference to that line. This means that the input voltage of the motor is phase voltage and line current. The only motor that can utilize the four connections of the converter is the wye-connected motor. For wye-connected motors, line current is $\sqrt{3}$ times larger than phase current allowing the converter to supply more power. This means that the Cal Poly converter can provide higher current for larger loads.

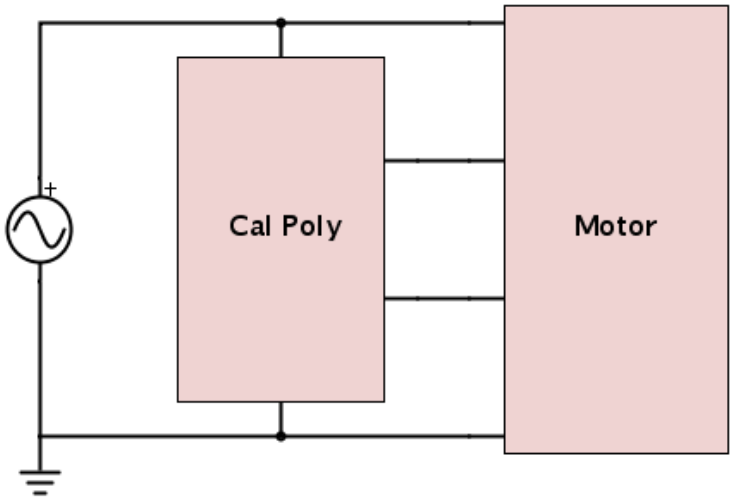

Figure 117: Block diagram of Cal Poly converter connection to source and motor

The observation of the four lines leading from the Cal Poly converter to the motor introduced a theory of a possible third motor configuration. If we take a delta connected motor and disconnect two of the windings, it creates an open-delta configuration as shown in Figure 118. This creates a motor that also consists of four winding connections like the wye-connected motor.

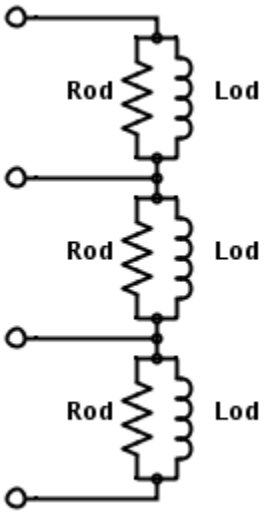

Figure 118: Open-delta motor configuration with parallel resistive and inductive windings

Due to the results of receiving the same three-phase power when connecting the wye and delta-connected motors to each of the Marinus/Malengret and Smith networks, the first step in verifying this theory is to test open-delta-connected motor with the Cal Poly converter.

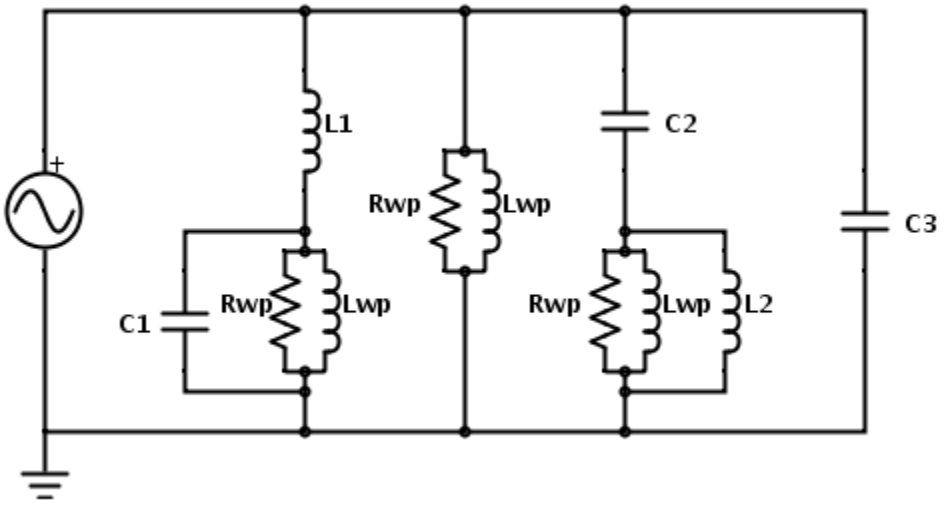

Figure 119: Cal Poly converter and wye-connected motor with common grounded

To do so, we start with the Cal Poly converter system shown in Figure 119. The motor windings, parallel R_{wp} and L_{wp}, are connected in the wye configuration with the

common node connected to ground. The left branch with L_1 and C_1 introduces the -120˚ phase shift and the right conversion branch with C_2 and L_2 introduces the +120˚ phase shift.

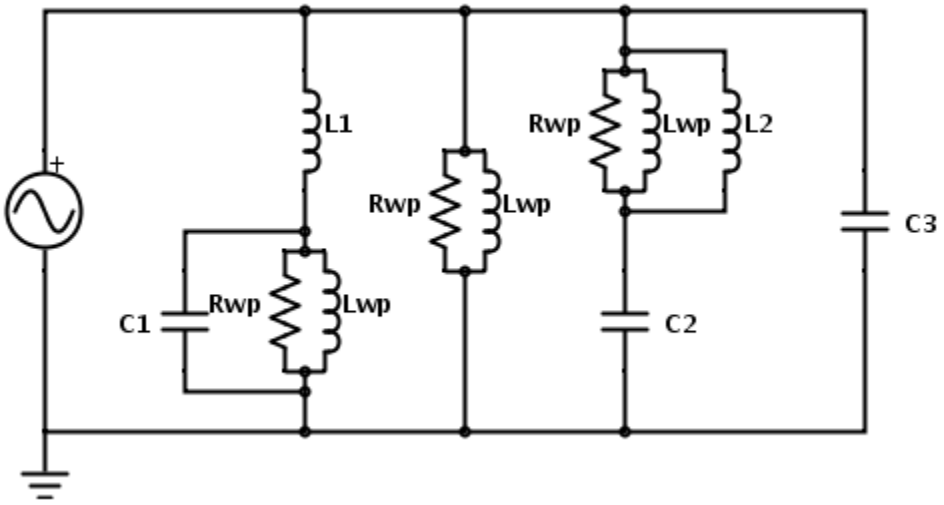

Figure 120: Wye-to-Open-delta transformation with Cal Poly converter

In Figure 120, the motor winding and L_2 are swapped with C_2, still producing a +120˚ phase shift. When deriving the transfer function of this branch, the same result occurs no matter if the capacitor is on top or on the bottom. The impedance that determines the output is still the winding in parallel with the inductor and the total impedance of the input voltage is still the impedance in the branch. By observation, from the component switch, we achieve the open delta motor configuration.

This is better seen in Figure 121 after rearranging the components. The source is connected across the two middle lines from Figure 118 and the conversion network connected across all four. From a top level perspective there are two lines between the source and the converter that run straight to the motor as well. There are two additional lines that vary depending on loading and conversion values. This matches with the Cal Poly top level diagram in Figure 117.

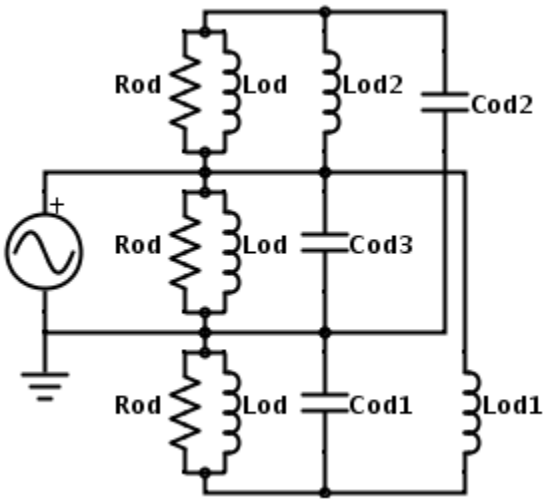

Figure 121: Open-delta motor configuration with Cal Poly converter

Figure 122 displays the LTspice model used to simulate the system. The open-delta motor winding values are equivalent to the wye-connected motor windings and the conversion components values are equivalent to the Cal Poly converter components. These are derived from the 1/3hp three-phase induction motor at a load of 12in-lbs, the same operating load used to derive the Marinus/Malengret converter. Simulation figures are captured starting at 1.483s.

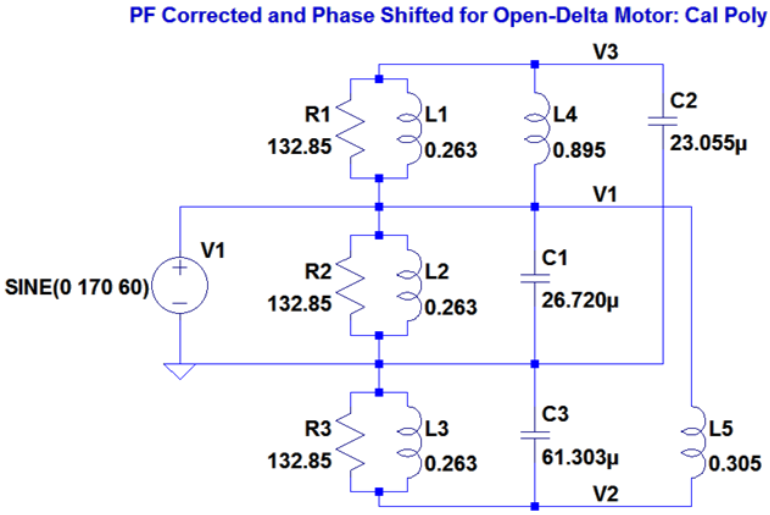

Figure 122: LTspice model of open-delta-connected motor and Cal Poly converter

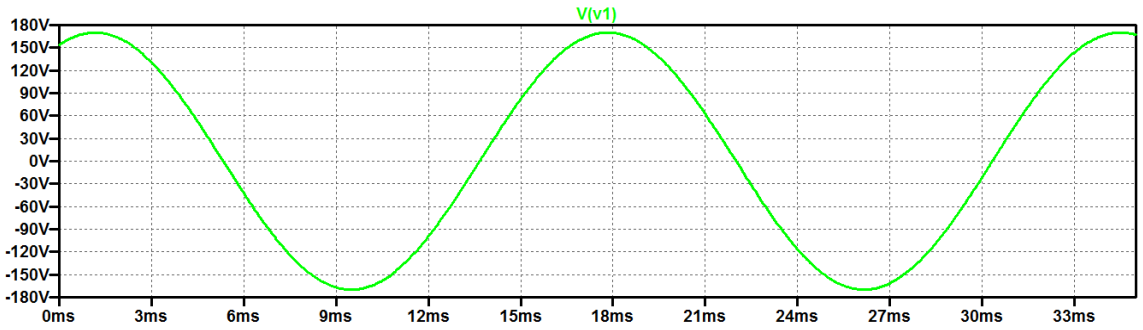

Figure 123: Single-phase source voltage with CP converter and 1/3HP open-delta-connected motor

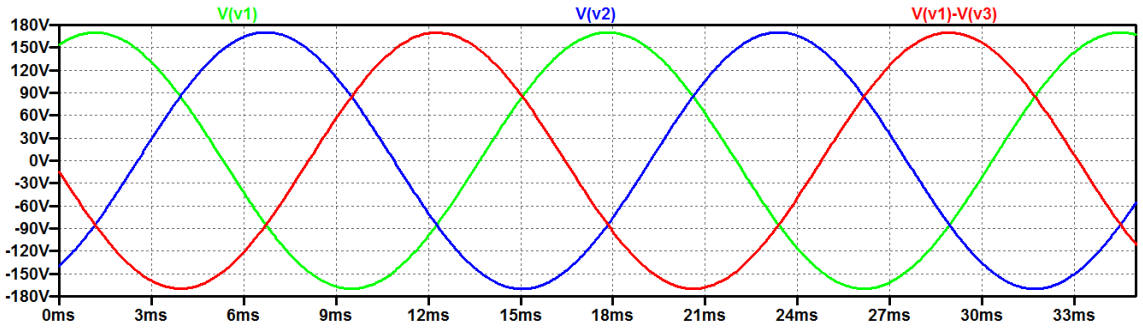

Figure 124: Three-phase voltage delivered from CP converter to 1/3HP open-delta-connected motor

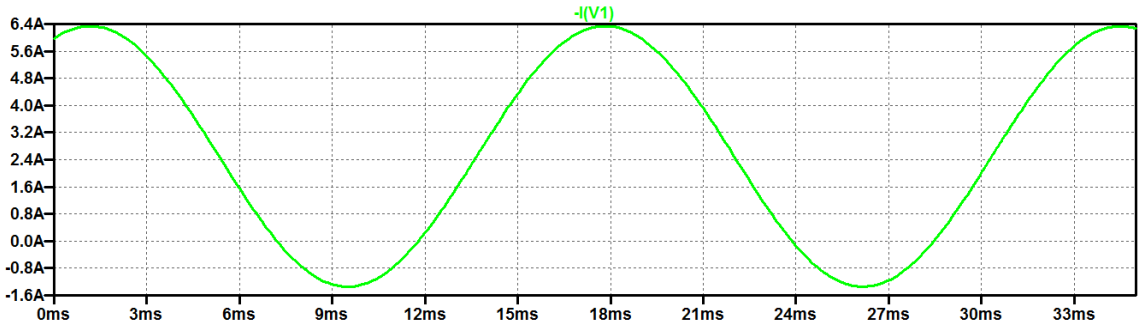

Figure 125: Single-phase source current with CP converter and 1/3HP open-delta-connected motor

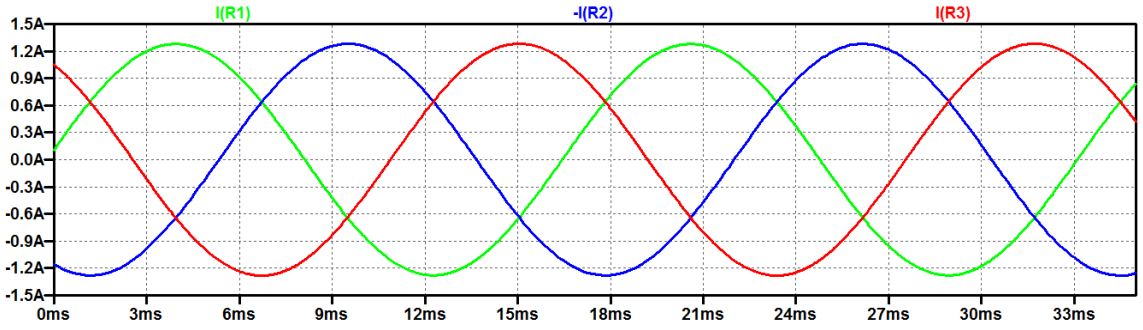

Figure 126: Three-phase current delivered from CP converter to 1/3HP open-delta-connected motor

Figure 123 displays the voltage from the single-phase source driving the Cal Poly converter and the 1/3HP open-delta-connected motor. This waveform is also the reference voltage in Figure 124 with peak amplitude of 170V. Figure 124 displays the three-phase voltage delivered from the converter to the motor. The green waveform is the reference voltage, V_2, with phase shift of 0˚. The blue waveform is the voltage across the top winding, R_1 and L_1, with a phase shift of +120˚, leading the reference voltage. The red waveform is the voltage across the bottom winding, R_3 and L_3, with a phase shift of -120˚, lagging the reference voltage.

Figure 125 displays the current from the single-phase source driving the Smith converter and the 1/3HP delta-connected motor. Its amplitude is 3.84A with an offset of 2.5A, increasing the peak current to 6.34A. The source current offset is due to the same reason as the other systems. The current is not initialized to zero by the simulation settings. Therefore, we incorporate the varistor into the network to initialize the voltage and the current, shown in Figure 127 below.

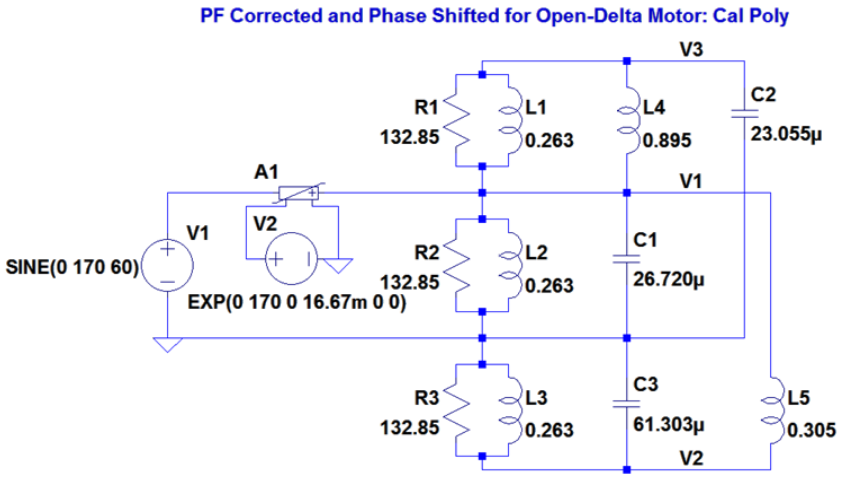

Figure 127: LTspice model of reduced Cal Poly converter and 1/3hp open-delta-connected motor with varistor

The exponential peak voltage controlling the varistor is equal to the source at 170V and the time constant it set to 16.67ms corresponding to one period of the input voltage. The result of the addition of the varistor is shown in Figure 128 below, displaying the original source current but with the reference set at 0A. The amplitude balance and shift of the three-phase current through the motor will also remain unaffected by the varistor.

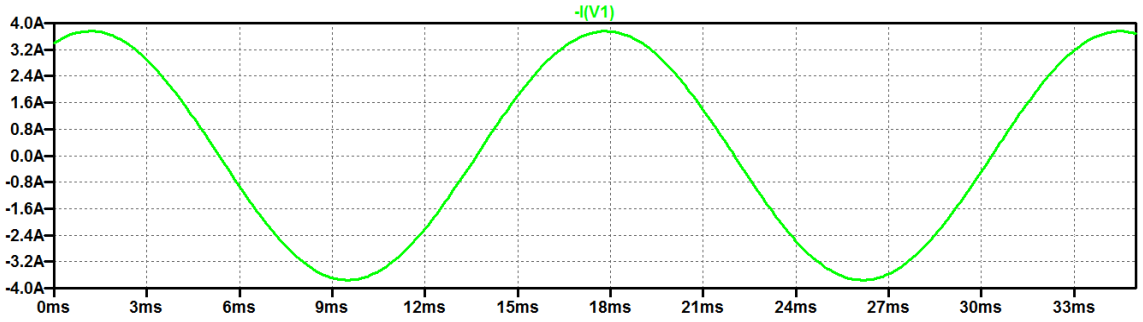

Figure 128: Source current with CP converter and 1/3HP OD-connected motor with varistor

Figure 126 is the simulation results of the current going through resistance of the windings from Figure 122. The green, blue and red waveforms are the current flowing through resistors R_1, R_2 and R_3, respectively. The peak value for each current is 1.28A which is 1/3 the source current. This is because the converter evenly distributes the single-phase source current into three currents of amplitude 1.28A, all out of phase by 120˚.

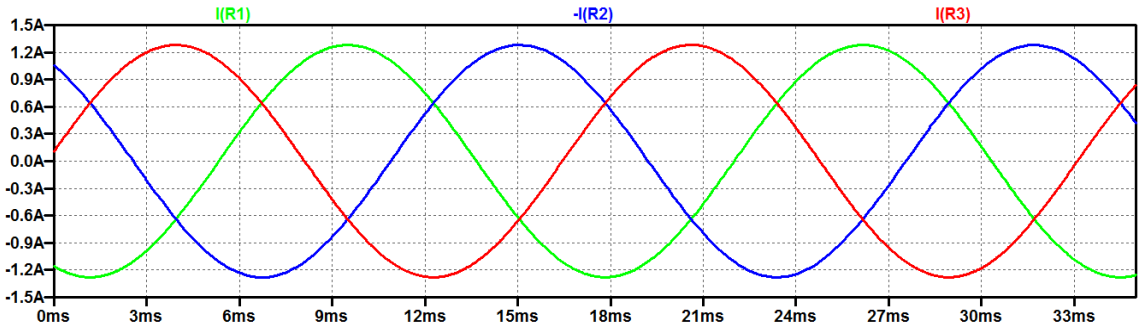

Figure 129: Three-phase current of 1/3HP open-delta-connected motor driven by three-phase source

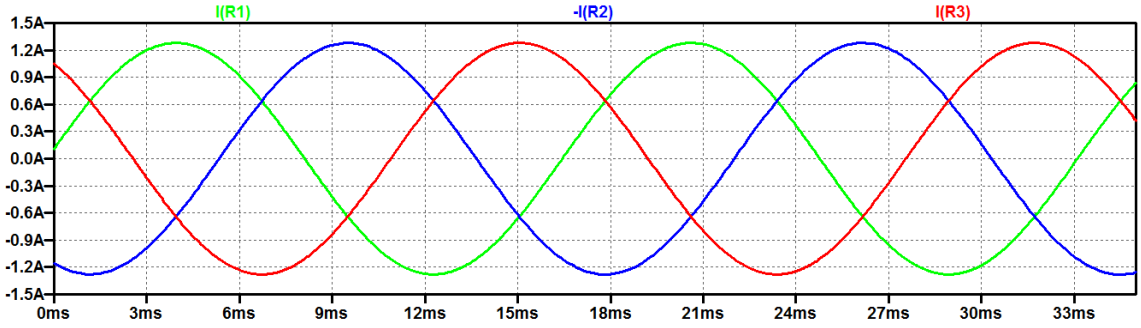

Figure 130: Three-phase current from CP converter to 1/3HP OD-connected motor at nominal torque

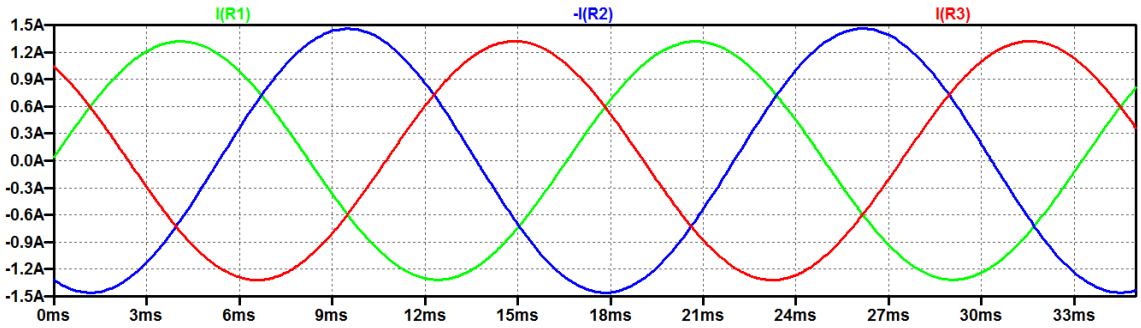

Figure 131: Three-phase current from CP converter to 1/3HP OD-connected motor at +15% torque

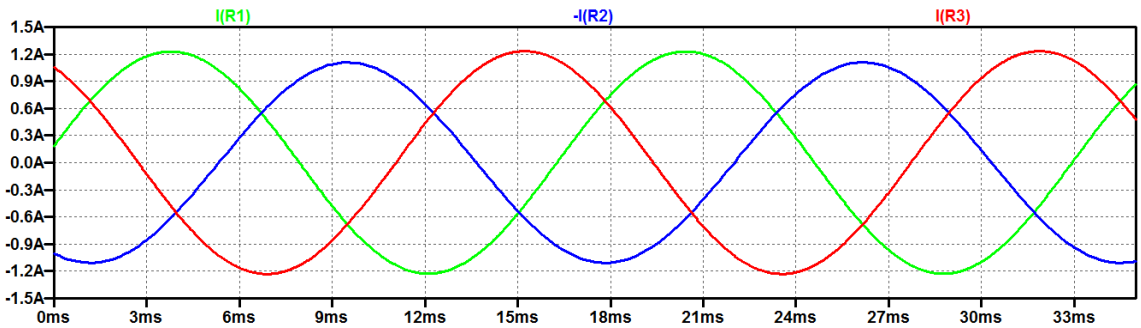

Figure 132: Three-phase current from CP converter to 1/3HP OD-connected motor at -15% torque

Next is the torque variation analysis for the system. Figure 130 represents the current at nominal torque, with a peak current value of 1.28A. The Figure 131 represents the current at +15% change in torque with peak current values of 1.32A for R_1 and R_3, and 1.46A for both R_2. Figure 132 represents the current at -15% change in torque with peak current values of 1.23A for R_1 and R_3, and 1.11A for R_2. The current through R_2 only changes in magnitude because of the connection across the constant source. The difference of the peak current through R_2 is 14.1% and 13.2% for the +15% and -15% torque change, respectively.

The connection of the conversion network across the other two windings causes approximately an equal effect on amplitude and phase. The +15% and -15% torque change causes a 3.9% and 3.1% amplitude error, respectively, for both R_1 and R_3. Both angles decrease approximately ±116.8˚ moving in toward the reference current for the +15% change in torque. For the -15% change in torque, both current phases increase to approximately ±123.6˚, moving away from the reference current. The phase error for the current waveforms are 2.6% and 3.0% for the +15% and -15% torque variation, respectively.

The amplitude and phase change for R_1 and R_3 are comparable to the Marinus/Malengret and Smith converters with the wye and delta-connected motors. The amplitude change of current through R_2 is the highest out of all three making this system the most sensitive to torque variation.

In attempts to test these conversion networks, the systems experienced large transients at the start-up of the motor. This is because at start-up there exists little to no resistance within the winding, only inductance. The reduction in resistance causes the transients of the system to spike and can cause damage to the conversion components and the motor. To be able to use the converters, a start-up network must be incorporated. One suggestion is to add resistance into the system so the conversion network can "see" the winding full load at which it is designed to operate and then to remove it when the load of the winding is high enough to not cause a spike in the voltage and current. Two ways this can be achieved is by adding resistors in series with the motor lines or in parallel with switch relays to either short them out or remove them from the system when start-up is done.

There are a few details to pay attention to in the design of the start-up network. First being the efficiency of the method. It should be analyzed as to attempt to not counteract the efficiency of the converter. If the start-up network would be used for a short period of time, there shouldn't be too much of a negative contribution. If the application requires frequent start-ups and introduces the network for longer periods of time, a start-up network with less power loss should be investigated. The next item to keep in mind is the load of the motor during the entire time it's operating. The start-up circuit may need to incorporate a sensor to add the resistance back into the system if the load drops too far below its operating value.

Through the analysis of each converter, we have discovered there are optimal applications in which each converter can be used. The Marinus/Malengret converter is

able to run motors with a power factor of 0.501 and above. The Smith converter is able to run motors with a power factor of 0.707 and above. Due to sensitivity results, the Smith converter would be the best option for both wye and delta-connected motors. But if the power factor is below 0.707, the Marinus/Malengret converter would have to be used.

Another approach in determining the more optimal converter to implement is analyzing the values of its derived components. As displayed in Table 3 and Table 4, the values of the reactances of the conversion components decrease as the power factor and horsepower of the motor increase. As the Marinus/Malengret and Smith converters approach their threshold power factors, the reactances increase substantially. The components that will be affected the most are the inductors. For most cases the value of the inductor is directly related to the actual size and weight of the component. The other factor to take into consideration is the inductors rated current. The rated current of on-market inductors is inversely proportional to its value. As the inductor value increases, the smaller the listed rated current becomes. This makes it hard to find the larger inductors at the higher current level needed. When they are found, in some cases the physical size of the component makes it unrealistic to implement the conversion network. This could prevent the use of passive conversion.

The values of inductors for the Marinus/Malengret converter in this study range from 50mH to 3H. The inductance values reduce as the power factor, horsepower and slip of the motor all increase. These relationships in some cases go hand-in-hand. To remain with a small scale surface-mount or through-hole package for an inductor, the inductance has to stay below 10mH. Therefore, the sizes of the inductors are going to be large and heavy. To define large and heavy, let’s take a look at the actual size of inductors needed

to build the Marinus/Malengret converter. To achieve the 50mH inductor design, the 25HP motor is run at a slip of 5%. The peak current flowing through it is 16A. A 50mH inductor with a current rating of 20A chosen from Hammond Manufacturing and exhibits a weight of 72lbs with length and width dimensions of 9 inches by 8.25 inches and a height of 7.5 inches [16]. The extreme size and weight is due to its current rating of the inductor, therefore running the motor at the higher slip to achieve a lower inductance value isn't a good idea. But by running the motor at a slip of 2.7% results in a 0.1H inductor that still has high current, with a peak value of 7.53A. This will also result in a large inductor. This may cause the Marinus/Malengret converter to be an impractical choice for a large horsepower motor.

If we look at the other end of the spectrum, when the 1/3HP motor is running with a slip of 2.7%, the 2.68H inductor has a peak current of 95mA. A 2.6H inductor with a current rating of 300mA from Hammond Manufacturing weighs 3.25lbs [16]. The length and width dimensions are 3.25 inches by 2.5 inches with a height of 3 inches. This is a more reasonable sized inductor, but it still depends of the application to determine if this is practical. Therefore, in determining the value of an inductor for the conversion network, it is important to pay attention to the relationship of the inductance value, the horsepower and the slip. The higher horsepower and slip will increase the amount of current through the inductor. If the inductance value is low and the horsepower and slip of the motor are high, then the size of the inductor will probably be extreme, possibly making it not available on-market. The cost of these inductors if bought individually is around $100 each [17].

Now, let's look at the capacitors used for the Marinus/Malengret converter. The power factor correction and conversion capacitors are available on-market in the 5-25μF range with maximum voltage ratings above $120V_{AC}$, and cost $5-$15 if bought individually. As the value of the capacitor increases toward the 100μF range, the cost depends more on the maximum voltage rating. The higher the voltage rating, the higher the cost will be for the capacitor [17].

Next is the cost and sizing analysis for the Smith converter. In this network we use an autotransformer or in a more simple case a two winding transformer. These transformers are harder to find on-market for our purposes since the winding values are very unique. They might have to be custom made to implement this converter. Transformers can cost anywhere from $20 to $200. The size is comparable to the inductors used for the Marinus/Malengret converter. The capacitors in the Smith converter follow the same scaling as the ones found in the Marinus/Malengret converter. In the previous study of the passive single to three-phase converters, an active single to three-phase motor drive made by Schneider Electric was purchased for energy efficiency comparison [8]. The converter costs approximately $400 but without variable speed, units can cost around $200. In reviewing the component pricing, the Marinus/Malengret and Smith converters can be implemented for comparable costs.

Due to the sensitivity to each system, it is suggested to design each converter at less than nominal torque of the motor. The sensitivity analysis shows that there is less effect on the amplitude of the transients as the torque is increased than when it is decreased. Motors can operate successfully within ±10% voltage amplitude error, so if the motor ends up operating at the load the converter was not designed for, the motor will

still run [14]. If the torque decreases and the converter was designed using a lower torque, the effect on the transients will be affected less than what they would be if it was designed for the nominal load.

One final detail to pay attention to during the design of the networks is the effects on the input source current. From this study, the maximum increase in current from the nominal is 1.02% when the torque was varied by ±15%. With the maximum peak current values of 2.193A and 22.41A for the 1/3HP motor and 25HP motor, respectively, the 1/3HP motor is well under the 15A/20A current ratings of a residential outlet whereas the 25HP is not [18]. The 25HP motor would not be able to be implemented due to the current rating, but also because it requires a 460V input source. From these observations, the choice of motor size depends on its nominal input current ratings which should not exceed the 15A/20A residential current rating. In addition to the nominal and ±15% torque variation analysis, it is important to study the effects of source current when the torque is decreased below the -15% torque variation due to the greater sensitivity to the decrease in torque.

Chapter 6: Conclusion/Future Works

Single to three-phase power conversion is possible using passive networks for both wye and connected motors. The equivalency between the Marinus/Malengret converter and Smith converter allows the user to choose which network better suits the needs of their applications. The Marinus/Malengret converter enables the use of motors with low power factors (PF > 0.5), but is more sensitive to torque variation. The Smith converter is less sensitive to torque variation but requires a motor with a power factor larger than 0.7.

The Cal Poly converter operates a wye-connected motor providing neutral line making it possible to ground the common connection of the motor for a return current path. The Cal Poly converter can also provide the three-phase power to the proposed third motor configuration described as open-delta. This configuration with the Cal Poly converter has the same characteristics of delta-connected motor with the Marinus/Malengret and Smith converters when the torque is varied. The magnitude and phase of the current in the windings not across the single-phase source change at the same rate as with the other two converters, but the amplitude of the current in the winding across the source varies by a larger percentage. The amplitude of the current is equivalent to that of the wye-connected motor, therefore eliminating the $\sqrt{3}$ scaling reduction of the current in the delta-connected motor.

All converters and motor configurations experience voltage and current sensitivity due to the torque variation of the motor and the component variation of the conversion networks. The characteristics can be analyzed using the parallel winding model to simulate both motor configurations with the converters in computer simulation software.

To simulate the system successfully, it is necessary to initialize the current and voltage of the single phase source by gradually increasing the source from zero to its nominal amplitude. The sensitivities of the system lead to the necessity of a start-up circuit and suggested off-nominal conversion component values.

To successfully implement the passive single to three-phase conversion networks, future work must be performed. These include designing a start-up circuit and research into the parameters of the inductors and autotransformers within the conversion networks to reduce the cost and physical size, and improve the overall system performance. The start-up circuit would need to be an efficient implementation as to not introduce an excessive amount of power loss. Due to the applications of the motors, like in air conditioners, the system might need to start frequently. The start-up network would need to be able to sense these instances and provide the necessary load to reduce the transients.

Next, there needs to be further research done on the parameters of the inductors and autotransformers within the converters. The main issue with these components is their physical size. The physical size of the component is due to the value of the inductor and the amount of current flowing through it. Since these parameters are inversely related to each other, there must be an operating point of the motor at which the component values and currents are optimal when compared to what is available on-market. The quality factor is also an important factor to keep in mind when optimizing the values and currents. The quality factor will determine the overall efficiency of the system. The higher the quality factor, the higher the efficiency will be.

With the data provided in this paper and the resulting circuits, costs and previous data studying efficiencies, passive single to three-phase power conversion has the opportunity to be an alternate solution for power conversion. In comparison of the total cost of an active converter and the components necessary to implement a passive converter, the amounts are comparable. In the previous study, the power efficiencies of the passive networks utilizing components with low quality factor were measured [8]. The results were compared with an on-market active converter, and the passive converter came within 1%. With further work done on the start-up network and optimizing for smaller, less expensive, energy efficient conversion components, the passive single to three-phase converter could meet or beat the cost and efficiency of an active converter and provide comparable performance.

References

[1] O. J. M. Smith, "High-efficiency single-phase motor," Energy Conversion, IEEE Transactions on,vol.7, no.3, pp.560-569, Sep 1992

[2] E. Cipriano, C.B. Jacobina, E.R.C. da Silva, N. Rocha, "Single-Phase to Three-Phase Power Converters: State of the Art," *Power Electronics, IEEE Transactions*, vol.27, no.5, pp.2437-2452, May 2012

[3] Industrial Electronics Information for Manufacturing Applications *(February 2015), Basic Polyphase Devices* [Online], Available: http://www.industrial-electronics.com/polyphase-devices/Basic-Polyphase-devices.html

[4] S. J. Chapman, "Induction Motors," in Electric Machinery Fundamentals, 5th ed. United States of America: McGraw-Hill Co., 2011, Ch. 6, pp. 311–396.

[5] Tripp-Lite *(February 2015), Single-Phase vs 3-Phase Power* [Online], Available: http://www.tripplite.com/products/single-vs3-phase

[6] J. P. Donohoe (*September 2013), Three Phase Power* [Online], Mississippi State University, Available: http://www.ece.msstate.edu/~donohoe/ece3614three_phase_power.pdf

[7] IEEE Power and Engineering Society, "112: IEEE Standard Test Procedure for Polyphase Induction Motors and Generators," 2004

[8] T. Davenport, H. Homer, J. Marroquin, "Cal Poly High-E AC, Energy Efficiency Air-Conditioner," *Max Tech and Beyond Design Competition for Ultra-Low-Energy-Use*, June 2014

[9] Pharos University in Alexandria *(February 2015), Chapter 2: Induction, or Asynchronous Machines* [Online], Available: http://www.pua.edu.eg/PUASite/uploads/file/Engineering/courses/Fall%202013/EE%20380/Induction%20Motors-Chapter%282%29.pdf

[10] C. K. Alexander, M. N. O. Sadiku. Fundamentals of Electric Circuits, 4th ed. United States of America: McGraw-Hill Co., 2009.

[11] S. Marinus, M. Malengret, "Using passive elements and control to implement single-to three-phase conversion," *Africon, 1999 IEEE,* vol.2, no., pp.611-614 vol.2, 1999

[12] O. J. M. Smith, "Three phase motor operated from a single phase power supply and phase converter," U.S. Patent 5 545 965, August 13, 1996.

[13] Electronic Design *(February 2015), Understanding Error Vector Magnitude* [Online], Available: http://electronicdesign.com/engineering-essentials/understanding-error-vector-magnitude

[14] A. H. Bonnett, R. Boteler, *(2001)* "*The Impact That Voltage Variations Have on AC Induction Motor Performance* [Online], ACEEE, Available: http://www.aceee.org/files/proceedings/2001/data/papers/SS01_Panel2_Paper27.pdf

[15] National Electrical Manufacturers Association (NEMA) *(2011), American National Standard Motors and Generators* [Online], Available: https://www.nema.org/Standards/ComplimentaryDocuments/Contents%20and%20Forward%20MG%201.pdf

[16] Hammond Manufacturing *(2015)*, Transformers [Online], Available: https://www.hammfg.com/

[17] Mouser Electronics *(2015)*, Products [Online], Available: http://www.mouser.com/

[18] Minnesota Department of Labor and Industry *(2011)*, ELI Inspection and Checklist [Online], Available: http://www.dli.mn.gov/ccld/pdf/eli_inspection_checklist.pdf